UTS UNIVERSITY OF TECHNOLOGY SYDNEY

Adsorption-desorption of arsenic species in river sediment, water and associated microplastics

by Kien Thanh Nguyen

Thesis submitted in fulfilment of the requirements for the degree of **Doctor of Philosophy**

under the supervision of Professor John Zhou

University of Technology Sydney
Faculty of Engineering and Information Technology

June 2022

CERTIFICATE OF ORIGINAL AUTHORSHIP

I, Kien Thanh Nguyen declare that this thesis, is submitted in fulfilment of the requirements for the award of Doctor of Philosophy, in the School of Civil and Environmental Engineering/Faculty of Engineering and Information Technology at the University of Technology Sydney.

This thesis is wholly my own work unless otherwise referenced or acknowledged. In addition, I certify that all information sources and literature used are indicated in the thesis.

This document has not been submitted for qualifications at any other academic institution.

This research is supported by the Australian Government Research Training Program.

Signature: Production Note:
Signature removed prior to publication.

Date: 06/06/2022

ACKNOWLEDGEMENT

First and foremost, I would like to thank my principal supervisor, Professor John Zhou, for his constant guidance, encouragement, and patience throughout my PhD study. His guidance helped me in the research, publications and this thesis. This thesis would not be possible without his help, exceptional supervision, and valuable contributions. In the last semester, I appreciated his support to obtain the tuition fee scholarship so that I could fully focus on study. I also would like to thank my co-supervisor, Doctor Yuhan Huang for his support, insightful comments and revisions on my publications and thesis. He provided significantly useful and practical help whenever I needed.

I would like to thank Doctor Mohammed Johir and Nirenkumar Pathak for their help in various laboratory work, including the interruption period due to COVID-19 pandemic. I also would like to thank Ms Van Le and UTS Graduate Research School for their help in administration matters. I would like to thank Professor David McGloin and GRS for their support to obtain the UTS Scholarship for the Research Session 2 2021. I would like to thank all my friends, who encouraged and helped me over the time. I also appreciate Dr. Youngwoo Choo at University of Technology Sydney, Dr. Bin Gong and Dr. Songyan Yin at the University of New South Wales to help in analysing samples. Finally, I would like to acknowledge my family (my parents and, especially my wife Nguyet Tran and my daughter Chi Nguyen), who have worked hard and stayed with me through one of the toughest times of my life.

CONTENTS

LIST OF FIGURES

LIST OF TABLES

ABBREVIATIONS

α:	the Elovich initial adsorption rate
β:	the Elovich desorption constant
As:	Arsenic
As(III):	Inorganic arsenite
As(V):	Inorganic arsenate
BET:	Brunauer-Emmett-Teller
C_e:	the concentration in solution at the equilibrium time
C_o:	the concentration in solution at the initial time
C_t:	the concentration in solution at time t
DI water:	Deionized water
DOM:	Dissolved organic matter
Eh:	Redox potential
FTIR:	Fourier Transform Infrared Spectroscopy
HDPE:	High-density polyethylene
K_F:	the Freundlich constant
K_L:	the Langmuir bonding energy constant
K_p:	the solid-solution partition coefficient
Ks:	the Sips energy constant
LDPE:	Low-density polyethylene
LOI:	Loss-on-ignition
MPs:	Microplastics
OM:	organic matter
n:	the Freundlich exponent

n_s: the Sips exponential factor

PA: Polyamide

PCBs: Polychlorinated biphenyls

PE: Polyester

PET: Polyethylene terephthalate

PFO: Pseudo first-order

PP: Polyprolylene

PS: Polystyrene

PSO: Pseudo second-order

PTFE: Polytetraflouroethylene

PUR: Polyurethane

PVC: Polyvinyl chloride

q_e: the concentration in the adsorbent at the equilibrium time

q_o: the concentration in the adsorbent at the initial time of desorption

q_m: the maximum concentration in the adsorbent at the equilibrium time

q_t: the concentration in the adsorbent at time t

R_L: the equilibrium parameter

RS: River sediment

RW: River water

RS-NOM: River sediment without organic matter

SEM-EDS: Scanning electron microscopy ad energy dispersive X-ray spectroscopy

SOM: Soil organic matter

SSA: Specific surface area

TOC: Total organic carbon

UV: Ultraviolet

XPS: X-Ray Photoelectron Spectroscopy

XRD: X-ray powder diffraction

LIST OF PUBLICATIONS

Kien Thanh Nguyen, Hung Manh Nguyen, Cuong Kim Truong, Mohammad Boshir Ahmed, Yuhan Huang, John L. Zhou (2019) Chemical and microbiological risk assessment of urban river water quality in Vietnam. *Environmental Geochemistry and Health*, 41: 2559-2575. https://doi.org/10.1007/s10653-019-00302-w

Kien Thanh Nguyen, Mohammad Boshir Ahmed, Amin Mojiri, Yuhan Huang, John L. Zhou, Donghao Li (2021) Advances in Arsenic contamination and adsorption in soil for effective management. *Journal of Environmental Management*, 296: 113274. https://doi.org/10.1016/j.jenvman.2021.113274

Kien Thanh Nguyen, Yuhan Huang, John L. Zhou. Behaviour and mechanism of arsenite and arsenate interactions with river sediment and microplastics. *Journal of Environmental Management* (**Accepted on 6 June 2022**).

ABSTRACT

Arsenic (As) is a ubiquitous toxic metalloid, and its pollution has been reported in soil, surface water, groundwater and sediment worldwide. Additionally, micro-plastics (MPs) are an emerging organic pollutant widely detected in different environments. So far, studies on the interfacial behaviour of As in the river sediment-water were limited. This PhD research, therefore, aims to explore the adsorption and desorption processes and interfacial behaviour of As in the contaminated water-sediment system. The kinetic and isotherm sorption models are used to estimate the sorption behaviours of As(III) and As(V), while various surface characterisation methods are applied to understand the interactions between As species with adsorbent surface and the transformation among As species.

Firstly, the adsorption and desorption of As(III) on river sediment (RS) were investigated under various environmental conditions and sediment characteristics. Higher As(III) and As(V) adsorption on RS was found in acidic to neutral conditions and on smaller size fractions of sediment. The monolayer maximum surface adsorption (q_m) of As(V) (210.0 mg/kg) was higher than that of As(III) (201.7 mg/kg). The FTIR results showed the changes in surface functional groups of river sediment before and after adsorption, indicating that Fe–O/Fe–OH, Si(Al)–O, –OH and –COOH functional groups were predominantly involved in As(III) and As(V) adsorption on sediment surface.

Secondly, the adsorption of As(III) and As(V) on polystyrene (PS) and low-density polyethylene (LDPE) in deionized (DI) water and simulated river water (RW) conditions were investigated by using bead MPs. Physisorption was the main mechanism involved in the adsorption processes based on the isotherm modelling. Moreover, the interactions between As species and PS and LDPE mainly occurred on the carboxyl and hydroxyl groups of adsorbent

surfaces, whilst electrostatic force and non-covalent interaction played an important role in the adsorption mechanism of As(III) and As(V) on PS and LDPE.

Furthermore, the sorption behaviour of As(III) and As(V) was evaluated by using mixtures of sediment with PS or LDPE and DI water or RW. The amounts of As(III) and As(V) adsorbed in RW solution with the presence of PS and LDPE were lower than those in sediment only, suggesting that PS and LDPE may inhibit sediment adsorption of As(III) and As(V). The desorption process showed a positive impact of RW in the release of As(III) and As(V) into the water phase. This study provided valuable information on the sorption behaviour and mechanism of inorganic As species in the simulated river system.

CHAPTER ONE:

INTRODUCTION

1. CHAPTER ONE: INTRODUCTION

1.1. Background

Arsenic (As) received significantly higher concern than other metals because it is a notorious trace metalloid in the environment and can be toxic and carcinogenic for human health (Jiang et al., 2018). A substantial number of studies have investigated all aspects of As including the sources of As exposure, speciation, contamination, mobility and transport, exchanged ion, modelling, treatment methods and its toxic characteristics in terms of carcinogenic and non-carcinogenic effects for human health and environment (Smedley and Kinniburgh, 2002). The concentrations of As in contaminated groundwater varied between 0.5 and 5,000 μg/L (Ravenscroft et al., 2009), whilst the average of As concentration in polluted river water was 0.8 μg/L and ranged from 0.1 to 2.1 μg/L (Singh et al., 2015). For example, high As concentrations in water of Mole River, New South Wale, Australia was high as 13,900 μg/L due to mining activities (Ashley and Lottermoser, 1999). According to Stafilov et al. (2010), average As concentration in European soil was 7.0 mg/kg and reached to 18,100 mg/kg in lower Silesia, Southwestern Poland in soil of Au-enriched me-allogenic zones (Karczewska et al., 2007). As releasing to groundwater or surface water poses a major environmental problem (Dousova et al., 2012).

As derives from either natural source (e.g. rocks) or anthropogenic activities (e.g. industry and agriculture) (Patel et al., 2005). As can be released into the atmosphere via fossil fuel combustion, agricultural activities (e.g. spraying of pesticides and fertilizers), emissions associated with metallurgical activities, and tannery industries (Dousova et al., 2012). Anthropogenic activities were the main sources of elevated arsenic contamination in surface waters (Hao et al., 2018). Many countries such as Argentina, Chile, Mexico, China, Hungary, Bangladesh, India and Vietnam face with high As contaminated-groundwater for the purposes

of drinking and irrigation (Singh et al., 2015). As present in stream sediments can be derived from both natural and anthropogenic sources. Erosion process can provide As contamination in sediments from upper to lower streams (Polizzotto et al., 2008). However, mining activities causing the weathering of sulphide minerals are considered as the largest subsoil sources of As.

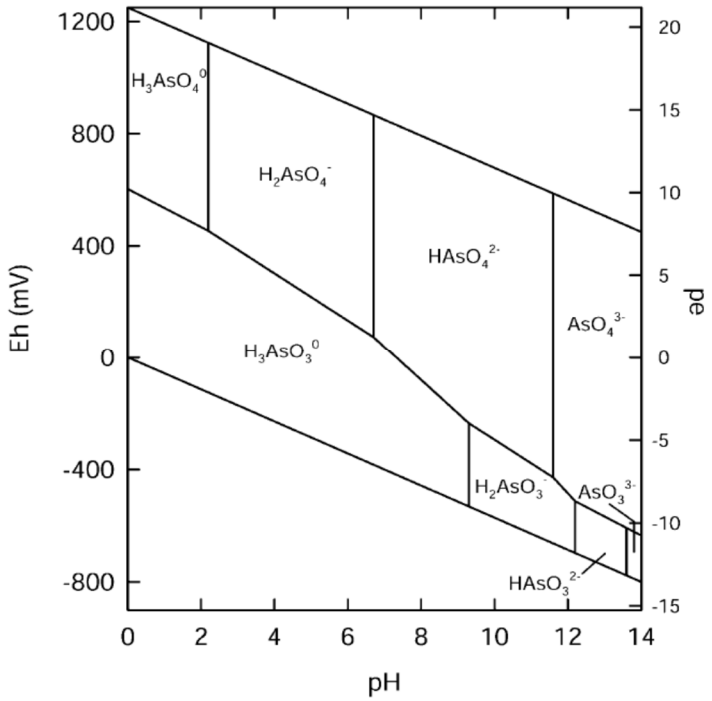

Figure 1.1. Forms of As species in Eh-pH diagram (Smedley and Kinniburgh, 2002).

Arsenic exists in various inorganic and organic forms (Carlin et al., 2016). Inorganic arsenite and arsenate are the major compounds in water bodies and sediments of rivers. As(V) is the most dominant form in water, whilst As(III) is predominant in reduced redox environment (Even et al., 2017; Gorny et al., 2018). As speciation are controlling by the important environmental factors of redox potential (Eh) and pH (Smedley and Kinniburgh, 2002). $HAsO_4^{2-}$ becomes dominant at pH ≥ 7, $H_2AsO_4^-$ is dominant at pH < 7, while H_3AsO_4 and AsO_4^{3-} occur in extremely conditions (**Figure 1.2**).

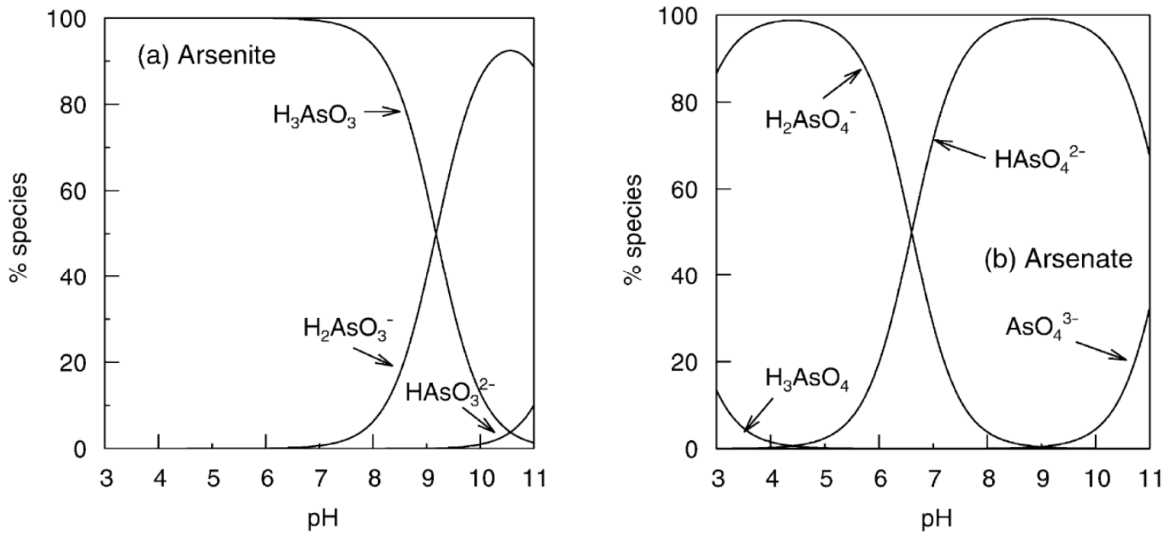

Figure 1.2. Effects of pH on As(III) and As(V) speciation (Smedley and Kinniburgh, 2002).

The extent of As contamination in soils, stream sediments, groundwater, surface water (rivers, lakes and estuaries) depends on its source, microbial activity and the physiochemical characteristics of solid-aqueous phases (Dousova et al., 2012; Smedley and Kinniburgh, 2002). Concentration of As in the stream sediments ranges from 1-15 mg/kg (Plant et al., 2005). Cullen and Reimer (1989) indicated that As(V) predominates in the oxic surface layer, whilst the less stable As(III) prevails in the anoxic zone. The variations of As concentrations depend on the changes in the surface layer of sediments, the level of stratification, temperature and flow dynamics of the overlying water column (Postma et al., 2010). Natural organic matter plays a key role in As mobility while redox conditions control the regulating arsenic dynamics in the aquatic systems (Dousova et al., 2012).

Recently, microplastics (MPs) have received increasing attention as they are considered not only as pollutants in aquatic systems but also as the adsorbents in terms of the association with As and other heavy metals. MPs are currently concerned as an emerging aquatic pollutant in freshwater systems due to high densities and ecological effects (Rodrigues et al., 2018; Shen et al., 2021). The presence and content of MP in the ecosystems such as marine, lake and river

waters and sediments have been widely investigated (Galafassi et al., 2019). MPs have been detected in river water bodies in various physical conditions including shapes (fragments, pellets, fibres, films and foam), colours (white, transparent, black, red, yellow, green) and types (primary and secondary). Polyethylene (PE), polypropylene (PP), polyvinyl chloride (PVC), polystyrene (PS) and polyethylene terephthalate (PET) were found as the major groups of MPs (Andrady and Neal, 2009). Mass abundance of MPs in river waters were reported as high as 152 mg/m^3 in Tamsui River, Taiwan (Wong et al., 2020), followed by Antuã River, Portugal and Dongjiang River, China, at 62 and 51.7 mg/m^3, respectively (Fan et al., 2019; Rodrigues et al., 2018). High mass contents of MPs in river sediments were found in Rhine River (Germany) 932 mg/kg (Klein et al., 2015), Tet River (France) 458 mg/kg (Constant et al., 2020) and Brisbane River (Australia) 129.2 mg/kg (He et al., 2020a). Another concern related to MPs is that they can adsorb and convey metal ions in river and marine systems. Significant concentrations of metals on natural and aged MPs were reported including Al, Cr, Cu, Fe, Mn, Ti and Zn (He et al., 2020b; Vedolin et al., 2018; Wang et al., 2017). Dong et al. (2019 and 2020) conducted the kinetic and isotherm adsorption of As(III) onto different types of MPs. Adsorption of As(III) on polytetrafluoroethylene (PTFE) and PS influenced by controlling factors including pH, temperature, interfering nitrate and phosphate ions. The effects of pH, SSA, NO_3^- and PO_4^{3-} on adsorption of As(III) on MPs were similar to soils and sediments. Polarity, morphology and organic polymer composition also enhanced heavy metals adsorption on MPs (Ahmed et al., 2021; Godoy et al., 2019). Adsorption of As(III) on MP surface primarily occurs via hydrogen bond of carboxyl group, while electrostatics forces and non-covalent are the main interactions of adsorption mechanisms (Dong et al., 2020). However, one question is concerning how As interacts with different adsorbents in environments such as sediments and MPs, in river water (RW) or seawater. Sediment is a vital compartment in river

systems, and works as a sink of metals, MPs and other pollutants (Jahan and Strezov, 2018; Nematollahi et al., 2021).

The interfacial behaviour of As (both As(V) and As(III)) in the stream sediments–water interface under different environmental factors (pH, MPs and sediment properties), including the sorption kinetics, isotherm and mechanisms should be studied to develop a better understanding. The research questions of this study are:

- Research question 1. What is the predominating adsorption behaviour of As in the river/sediment systems under various controlling factors?
- Research question 2. What is the As adsorption and desorption mechanism at the sediment-water system?
- Research question 3. How do the interactions among As, MPs and river sediment capture or release As in sediment-water system?

1.2. Research Objectives

This study principally aims to explore the adsorption and desorption processes and interfacial behaviour of arsenic in the contaminated river water-sediment systems. To achieve the overall aim, three specific objectives have been set out:

(i) Assess the adsorption and desorption processes and interfacial behaviour of inorganic As species in the water-sediment system, and the effects from environmental factors including pH, initial As concentrations in solution, sediment and river water characteristics.

(ii) Evaluate the adsorption behaviour and mechanism of inorganic As species on selected MPs.

(iii) Investigate the behaviour and mechanism of interactions among sediments, MPs with inorganic As species, in distilled water and river water systems.

1.3. Research significance

This research was to explore the sorption capacities of selected RS and MPs for As(III) and As(V) under various controlling factors including environmental parameters (pH, initial As concentrations, DI water, RW) and adsorbents characteristics (sediment organic matter and fraction sizes, different types of MPs). The study provided valuable information on the impacts of RS on sorption behaviour and mechanism of As(III) and As(V) in the simulated river system. PS and LDPE play significant roles in capturing As(III) and As(V), as well as how they worked with RS for sorption of As species were discussed for feasible management of As contaminated water-sediment in river. The results are valuable for assessing the long-term fate and management of As contaminated river systems.

RS, PS and LDPE play significant roles in the adsorbing or transporting As(III) and As(V) in the rivers. In contrast, RW enhanced As releasing into the water bodies, but had a negative impact on the adsorption of As(III). Among different batch essays studied in this work, DI water provides better adsorption affinity of adsorbents for As(III) and As(V) because it does not own any controlling element itself, while the effects of RW were still complicated.

1.4. Thesis Outline

This thesis consists of seven chapters as follows:

Chapter 1 is the introduction chapter, identifying the research problem and research objectives. The main tasks to achieve the objectives and scope of this research are also described in detail. Chapter 1 explains the PhD research's background and significance.

Chapter 2, named “literature review”, reviews the degrees of As contamination in soils and sediments, effects of controlling factors on arsenic adsorption/desorption behaviours are discussed. Additionally, the issues of MP contamination in river systems as well as how they

interact with arsenic are also reviewed. Subsequently, the key findings from the literature review are summarized and research direction is introduced.

Chapter 3, named "materials and methodologies", provides information about the main materials and methodologies used in this study.

Chapter 4, titled with "Adsorption-desorption of arsenic species on river sediments on the associated mechanism", examines the interactions of inorganic As species with river sediments under various controlling factors.

Chapter 5 explores "adsorption of arsenic species on distilled and river water". This chapter focussed on the behaviours of As(III) and As(V) adsorption on PS and LDPE pellets under different solutions.

Chapter 6 titled with "adsorption-desorption of arsenic species on river sediment and microplastics", discuss how arsenic adsorbs on or desorbs from sorbents in the presence of both river sediment and PS or LDPE with the assessment of sorption mechanisms.

Chapter 7 summarizes significant findings of this work for sorption behaviours and mechanisms of As(III) and As(V) by using sediment and MPs as the adsorbents, as well as recommendations for future study.

CHAPTER TWO:

LITERATURE REVIEW

2. CHAPTER TWO: LITERATURE REVIEW

2.1. As contamination and adsorption in soils and sediments

Section 2.1 covers the contents of a published review paper: **Kien Thanh Nguyen**, Mohammad Boshir Ahmed, Amin Mojiri, Yuhan Huang, John L. Zhou, Donghao Li (2021) Advances in Arsenic contamination and adsorption in soil for effective management. *Journal of Environmental Management*, 296: 113274.

2.1.1 Background

As contamination in soils, water and plants is widely reported (Selim, 2013). This notorious trace metalloid has received heightened concern than other heavy metals due to its toxicity and carcinogenicity to humans (Hayat et al., 2017; Johnston et al., 2020). Environmental problems related to As are caused by the mobilization under natural conditions as well as through a range of anthropogenic sources such as mining and agricultural activities, and fossil fuel combustion (Ungureanu et al., 2015). As a result, As pollution occurs widely in the environment including soil, surface water (e.g., lakes, rivers), groundwater and sediment worldwide (Nguyen et al., 2019).

There are four valence states of As in nature including -3, 0, +3 and +5 with both organic and inorganic species (Basu et al., 2014; Wang and Mulligan, 2006a). However, As(III) and As(V) commonly occur in natural sediment-water systems (Baviskar et al., 2015). As(III) contents varied from < 5% to 40% of total As in railway soils in South Australia, although the source of As(III) was not provided (Smith et al., 2006). As(V) is the most abundant form of As in soil under Eh > 200 and pH 5-8 conditions (Akter et al., 2006; Álvarez-Benedí et al., 2005). The main forms of As(V) species in solution are $H_2AsO_4^-$, $HAsO_4^{2-}$ and AsO_4^{3-}, while As(III)

is mainly dissociated (Álvarez-Benedí et al., 2005; Martin et al., 2014) and easily mobilize. The toxic level of As(III) is estimated as 100 times as As(V) (Akter et al., 2006; Maji et al., 2007), and occurs in solution as H_3AsO_3 and $H_2AsO_3^-$. The solution pH affects the dissociation hence the sorption rates of As species, with As(V) sorption decreasing while As(III) sorption increasing with pH increases (Álvarez-Benedí et al., 2005; Antelo et al., 2005). Methylated is the major species of organic forms and may contribute substantial amounts in soils (Alloway, 2012). **Table 2.1** summarizes the structures and the acid dissociation constant (p*Ka*) of inorganic and organic As species.

Table 2.1. Physiochemical properties of As species.

Arsenic species	Dissociation reaction and structure	pK_a
Inorganic arsenate	$H_3AsO_4 + H_2O = H_2AsO_4^- + H_3O^+$	pK_{a1} = 2.20[a]
(As(V))	$H_2AsO_4^- + H_2O = HAsO_4^{2-} + H_3O^+$	pK_{a2} = 6.97[a]
	$HAsO_4^{2-} + H_2O = AsO_4^{3-} + H_3O^+$	pK_{a3} = 11.53[a]
Inorganic arsenite	$H_3AsO_3 + H_2O = H_2AsO_3^- + H_3O^+$	pK_{a1} = 9.23[a]
(As(III))	$H_2AsO_3^- + H_2O = HAsO_3^{2-} + H_3O^+$	pK_{a2} = 12.13[a]
	$HAsO_3^{2-} + H_2O = AsO_3^{3-} + H_3O^+$	pK_{a3} = 13.40[a]
Dimethylarsinic acid	$As(CH_3)_2(OH)O + H_2O = As(CH_3)_2O_2^- + H_3O^+$	pK_a = 6.20[b]
(DMA)		
Monomethylarsonic	$As(CH_3)(OH)_2O + H_2O = As(CH_3)(OH)O_2^- + H_3O^+$	pK_{a1} = 4.10[b]
acid (MMA)	$As(CH_3)(OH)O_2^- + H_2O = As(CH_3)O_2^{2-} + H_3O^+$	pK_{a2} = 8.70[b]
Arsenobetaine	$(CH_3)_3CH_2AsO_2^-$	pK_a = 2.18[b]
(AsB)		

[a.] Wilson et al. (2010); [b.] Wilson et al. (2010).

Although there are several processes of As transportation in soil, adsorption is the predominant process regulating As transport in aqueous systems (Stollenwerk, 2005), including the mobility, fate and bioavailability (Dousova et al., 2012; Farrell, 2017; Gedik et

al., 2016; Luo et al., 2019). Adsorption process and its mechanisms can be well explained with different isotherm models although As adsorption is greatly influenced by many factors including soil properties, As concentrations, and environmental factors such as pH (Aksentijevíc et al., 2012; Foo and Hameed, 2010). Previous studies have summarized the influence of various parameters from both soil properties and environmental conditions on As adsorption. For instance, Akter et al. (2006) reviewed how As adsorption and desorption processes affected the biological availability of inorganic As species in soils. The sources, behaviour, distribution, toxicity and remediation technologies of As in natural water worldwide were summarised by Basu et al. (2014) and Smedley and Kinniburgh (2002), while Smith et al. (2003) reported sources of As in natural environments and the exposure pathways in Australia. Wilson et al. (2010) provided a summary of As adsorption on soils including the effects of clay minerals, oxides and hydroxides, organic matter as well as the adsorption mechanisms.

2.1.2. As concentrations in highly contaminated river waters, sediments and soils

Baseline concentrations of As in rivers varied from 0.1-2.0 µg/L (Smedley and Kinniburgh, 2002). **Figure 2.1a** shows the highest levels of As pollution in rivers/creeks for each selected country from previous studies. The mean concentrations of As in polluted rivers varied from 15.6 µg/L in Simav River, Turkey to 125.5 µg/L in Slate Creek, USA, while the minimum and maximum concentrations in these selected rivers ranged at 0.2-28 µg/L and 20.2-239 µg/L. The sources of As pollution were different among rivers. Urban rivers receiving domestic raw sewage, household waste and industrial waste were found in Korotoa River, Bangladesh and Nhue River, Vietnam (Islam et al., 2015; Nguyen et al., 2019). Agricultural activities were considered as the main source of pollution in Claromecó stream, Argentina (Sosa et al., 2019). Mining sites were dominant sources that caused the most serious pollution of As in rivers such

as Hengshi River (China), Bournac Creek (France), Simav River (Turkey), and Slate Creek (USA). High As concentrations in rivers also derived from multi-sources including urban, agricultural and industrial wastewater such as Korotoa River in Bangladesh (Islam et al., 2015) and Haraz River in Iran (Nasrabadi, 2015).

Sediments can be considered as both carriers and sinks for contaminants in aquatic environments (Singh et al., 2005; Zhou et al., 2018). Minimum, average and maximum concentrations of As in sediments ranged at 1.8-8820, 5.9-32600 and 12.44-275000 mg/kg, respectively (**Figure 2.1b**). A wide range of sources contributed to high As contamination in river sediments such as urban wastewater (Karnaphuli River, Korotoa River in Bangladesh and Zarringol River in Iran) (Ali et al., 2016; Islam et al., 2015; Malvandi, 2017), industrial activities at Liaohe River (Ke et al., 2018) and Yangtze River (Yang et al., 2009), mining activities (Mole River in Australia, Bournac Creek and Presa River in France, mining Endeavour Inlet in New Zealand, Zlata Idka in Slovakia, Tigris River in Turkey, and Slate Creek in USA) (Casiot et al., 2007; Rapant et al., 2006; Ritchie et al., 2013; Varol and Şen, 2012; Wilson et al., 2004) or multi-sources of urban and agricultural activities, industrial and mining sites (Zhaosu River in China, Danube River in Europe, Gironde Estuary in France, Dokai Bay in Japan, Tisza River in Serbia, and To Lich River in Vietnam) (Gao, 2018; Kadokami et al., 2013; Larrose et al., 2010; Nguyen et al., 2016; Štrbac et al., 2017; Thuong et al., 2013; Woitke et al., 2003).

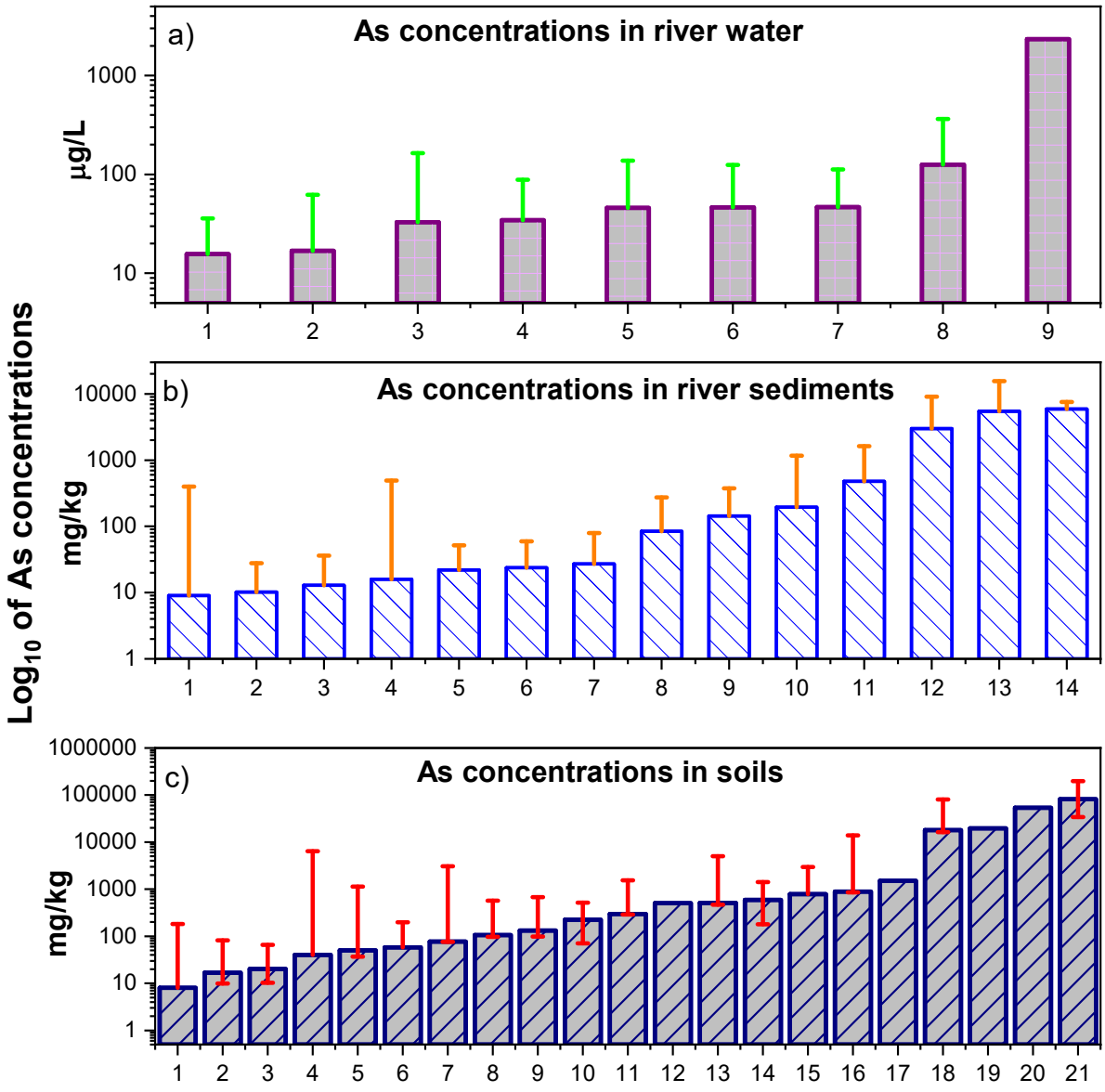

Figure 2.1. The mean As concentrations in contaminated river waters (a), river sediments (b) and soils (c). worldwide.

The background concentration of As in natural uncontaminated soils varies from 5.0 mg/kg to 7.5 mg/kg (Zhang et al., 2006) and from 42 mg/kg to 4530 mg/kg for polluted soils, while the earth's crust has the average concentration of As at 1.8 mg/kg (Wang and Mulligan, 2006a). In comparison, the average As concentrations in soil ranged between 8 mg/kg and 82000 mg/kg in contaminated soils, although concentrations as high as 116000 mg/kg were

also reported (**Figure 2.1c**). The lowest mean concentrations of As (**Figure 2.1c**) from the soil in the United States varies in the range of 0-174 mg/kg (Masri et al., 2021). The concentrations of As in agricultural soils, China was high as 6402 mg/kg (Jia et al., 2021), and were reported at 153-294 mg/kg in the mining soils from China. Overall, these Chinese soils were considered as slightly to moderately polluted by As compared to background concentration of As globally (Zhang et al., 2006) as well as exceeding the risk screening values in China at 40 mg/kg (Cao et al., 2021). The agricultural soils in Bangladesh were slightly polluted by As, being at 20.3 mg/kg of average As concentration (**Figure 2.1c**). The natural activities were again found as the main sources of As pollution in South America, with the mean concentration being 34 mg/kg (Tapia et al., 2019). The repeated applications of herbicides in a large area in South Australia were the reason leading to high level of As contamination in soils (35-545 mg/kg, mean = 133 mg/kg) (Smith et al., 2006), with a correlation between high concentrations of both As and iron (Fe) oxide content in soils ($r^2 = 0.57$), and As(III) contributed to 40% of the total As concentration in soils. As concentration in the Austrian Central Alps varied in the range 1-3000 mg/kg with the mean concentration of 77.1 mg/kg caused by mining, smelter activities and geogenic mineralization (Wenzel et al., 2002). The mine soils from the European countries were reported with mean As contaminations reaching over 500 mg/kg including Ouche mine soil in France (593 mg/kg), Losacio mine soil in Spain (508.5 mg/kg), and up to 892.7 mg/kg for Zlata Idka village in Slovakia (Rapant et al., 2006). In contrast, As concentrations in soils from the Turkonu Hg mine in Turkey were low at 6.9-65.2 mg/kg (Gemici and Tarcan, 2007), compared to other soils polluted by mining activities. The highest degree of As in contaminated soils was reported by Osuna-Martínez et al. (2021), with average As concentration of 82000 mg/kg in Aurora Chihuahua soils, followed by subsoils (54000 mg/kg) in Iran (Gerdelidani et al., 2021) and Aurora mine (18046) in Mexico (Carrillo-Chávez et al., 2014) due to mining activities. Consequently, different soils studied in those reports can be defined as slightly

polluted by As in Bangladesh, China, Czech Republic, Nigeria, South America, Turkey and United States, to moderately polluted in Australia, Austria and Belgium, and highly polluted in France, Iran, Mexico, Poland, Slovakia and Spain because their As concentrations all exceeded the level of uncontaminated soils at 6.0 mg/kg (Casado et al., 2007). It can also be concluded that the highest contamination of As in soils was caused by mining, followed by agricultural activities.

Table 2.2. Detailed information and references of As contamination in river waters, sediments and soils.

No.		Country /Region	Reference
	River water		
1	Simav River	Turkey	Gemici et al. (2008)
2	Hengshi River	China	Liao et al. (2017)
3	Nhue River	Vietnam	Nguyen et al. (2019)
4	Karnaphuli River	Bangladesh	Ali et al. (2016)
5	Korotoa River	Bangladesh	Islam et al. (2015)
6	Bournac Creek	France	Casiot et al. (2007)
7	Claromecó stream	Argenina	Sosa et al. (2019)
8	Slate Creek	USA	Ritchie et al. (2013)
9	Presa River	France	Culioli et al. (2009)
	River sediment		
1	Danube River	Europe	Woitke et al. (2003)
2	Liaohe River	China	Ke et al. (2018)
3	Dokai Bay	Japan	Kadokami et al. (2013)
4	Gironde Estuary	France	Larrose et al. (2010)
5	ZarrinGol River	Iran	Malvandi (2017)
6	Karnaphuli River	Bangladesh	Ali et al. (2016)
7	Korotoa River	Bangladesh	Islam et al. (2015)
8	Endeavour Inlet	New Zealand	Wilson et al. (2004)
9	Zhaosu River	China	Gao (2018)
10	Zlata Idka	Slovakia	Rapant et al. (2006)
11	Hengshi River	China	Liao et al. (2017)
12	Bournac creek	France	Casiot et al. (2007)
13	Slate Creek	USA	Ritchie et al. (2013)
14	Stream in Beydag	Turkey	Gemici et al. (2008)

No.		Country /Region	Reference
	Soils		
1	Seven land use	USA	Masri et al. (2021)
2	Mercury mine	Turkey	Gemici and Tarcan (2007)
3	Irrigated	Bangladesh	Bhuiyan et al. (2021)
4	Agricultural	China	Jia et al. (2021)
5	Contaminated	Belgium	De Brouwere et al. (2004)
6	Metal mining	Nigeria	Orosun (2021)
7	Central Alp	Austria	Wenzel et al. (2002)
8	Andes Volcanic	S. America	Tapia et al. (2019)
9	Former railway	Australia	Smith et al. (2006)
10	Mining	China	Cao et al. (2021)
11	Floodplain	Czech Republic	Kebonye et al. (2021)
12	Farmland	China	Dong et al. (2021)
13	Losacio mining	Spain	Casado et al. (2007)
14	Old mining	France	Jana et al. (2012)
15	Agriculture	Iran	Rezaei et al. (2019)
16	Mining waste	Slovakia	Rapant et al. (2006)
17	Former mining	France	Lebrun et al. (2021)
18	Mine waste	Mexico	Carrillo-Chávez et al. (2014)
19	Historical mining soils	Poland	Szopka et al. (2021)
20	Agricultural	Iran	Gerdelidani et al. (2021)
21	Mining zone	Mexico	Osuna-Martínez et al. (2021)

2.1.3. As adsorption by soils and sediments

Soils and sediments have received increasing attention as a natural sorbent in As sorption studies. The mobility, toxicity, fate and bioavailability of As in solid-water-plant systems are mainly controlled by the adsorption-desorption processes on soils or sediments. Soil/sediment properties would strongly affect the adsorption and desorption of As (Gedik et al., 2016; Huling et al., 2017; Selim, 2013; Xie et al., 2018b), whilst other parameters including ionic strength and competing anions (Williams et al., 2003), initial solute concentration of As, adsorbent dosage and reaction time (Matouq et al., 2015), and As speciation (Lombi and Holm, 2010) have also shown influence on As(V) adsorption.

2.1.3.1. Soil/sediment pH

Soil/sediment pH is considered as one of the most important parameters in As adsorption, and the relationship between solid pH values and As adsorption has been widely investigated (Arco-Lázaro et al., 2016; Campbell et al., 2014; Ma et al., 2015). Soil pH plays an important role in As adsorption due to its effect on As speciation and the charge of solid particle surfaces (Gitari and Mudzielwana, 2018; Huang et al., 2013). As(V) adsorption decreased significantly while As(III) adsorption increased with the pH increase on soils (Álvarez-Benedí et al., 2005; Deng et al., 2018; Fan et al., 2020). Adsorption of As(V) is extremely dependent on pH values (Williams et al., 2003), and increasing pH can cause an increase in repulsion of the soil surface to arsenate, resulting in the decrease in arsenate adsorption (Jiang et al., 2017). On the other hand, As(III) adsorption was highly favoured on positively charge sites in soil through electrostatic attraction under the acidic condition (Xu et al., 2009). It was suggested that As(V) adsorption exhibited a maximum adsorption around pH 6-7, and then decreased with further increase in solution pH (Goldberg et al., 2005). A study on the adsorption-desorption of As(V) in three Spanish soils showed that pH values slightly reduced during the As adsorption

experiments and pH was more important on As(V) sorption at high concentrations and for variations of several pH units (Álvarez-Benedí et al., 2005). **Figure 2.2a** illustrates the maximum adsorption of As(III) on a tropical soil increased from 150 mg/kg to 230 mg/kg when pH was increased from 3 to 7 (Goh and Lim, 2004), and reached the peak of 180.8 mg/kg at pH 7.09 for irrigated soil (Huang et al., 2013). The adsorption of As(V) on surface paddy soil (Jiang et al., 2017), in contrast, decreased from 1875 mg/kg (pH 3) to 1275 mg/kg (pH 5.5), or reached the maximum of 337 mg/kg at pH 4.5 for tropical soil (**Figure 2.2b**). The fact that soil surface positive charge density decreased with the increase in pH could be due to the increasing amount of the OH^- ions, resulting in decreasing adsorption (Goh and Lim, 2004). Moreover, Jeppu and Clement (2012) successfully incorporated sand pH value as a dependent variable of the modified Langmuir-Freundlich (MLF) isotherm equation for predicting As(V) adsorption onto pure goethite and goethite-coasted sand sorbents. On the other hand, pH may not be considered as a main factor affecting As sorption capacities (Alloway, 2012), and the impacts of soil pH on As adsorption were difficult to conclude (Jiang et al., 2005b). The adsorption capacity of As(V) on iron ore reached a maximum of 400 mg/kg at pH 4.5-6.5 (Zhang et al., 2004). Although Alloway (2012) suggested that pH had small influences on As(V) adsorption, **Figure 2.2(a and b)** indicated that soil pH had significant effects on the As(III) and As(V) adsorption on soils.

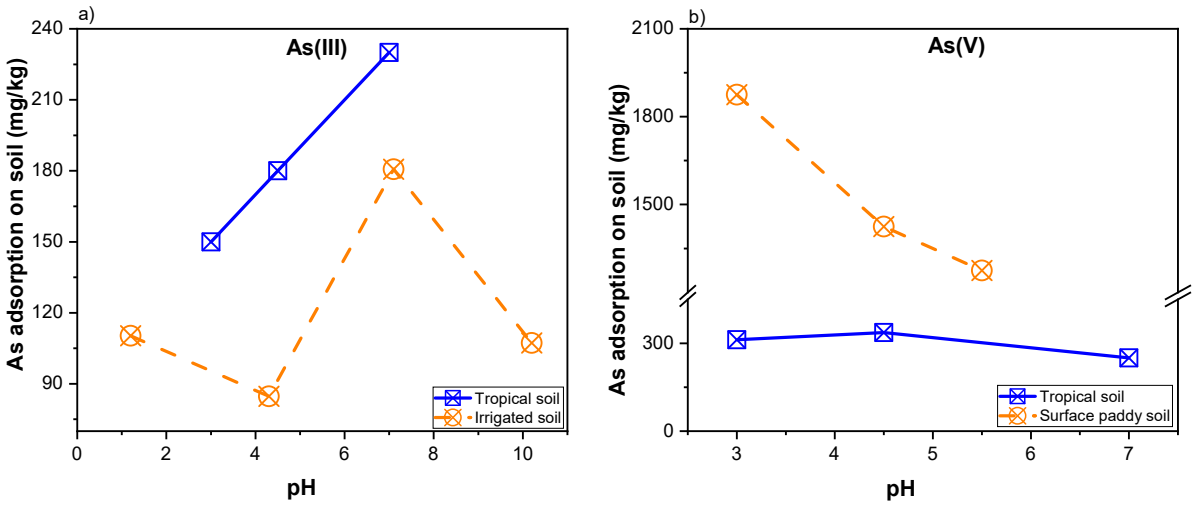

Figure 2.2. Effects of pH on (a) As(III) adsorption on tropical soil (Goh and Lim, 2004) and irrigated soil (Huang et al., 2013); b) As(V) adsorption on tropical soil (Goh and Lim, 2004) and surface paddy soil (Jiang et al., 2017).

2.1.3.2. Clay minerals

Clay minerals have a significant influence on As sorption in soils/sediments due to their unique physicochemical properties such as chemical and mechanical stability, large specific surface area, high charge density, layered structure and high cation exchange capacity (Gitari and Mudzielwana, 2018; Mukhopadhyay et al., 2017). The large total surface area is one essential property of clay minerals (Gitari and Mudzielwana, 2018) which represents the sum of external surface area and the internal surface area corresponding to the interlayer spaces (Jlassi et al., 2017), which allows clay minerals to adsorb water and environmental contaminants. Macht et al. (2011) expressed that the specific surface area of natural particles is an important factor in quantifying processes of sorptive interactions in soils. For example, the adsorption capacities of total As on three soils increased with an increase of soil surface area (**Figure 2.3**). Similarly, Xie et al. (2018b) found that As(III) and As(V) adsorption capacities decreased with the reduction of sediment clay content, with S_3 (45.5% clay) > S_2 (11.0% clay) > S_1 (7.2% clay), as shown in **Figure 2.4**. The role of clay content would enhance As(V) adsorption on the low-

energy surface because the behaviour of As on clay minerals is similar to that on the oxides (Goldberg, 2000), and large surface areas and active sites of clay minerals would provide a high capacity for As adsorption (Jiang et al., 2005b). Foroutan et al. (2019) reported the highest adsorption of As(V) on natural clay (~94%) at pH 3-4, which decreased to under 30% when pH was 9.0; the results were explained by the interactions between As(V) ions with hydroxyl ions in aqueous media. According to Gitari and Mudzielwana (2018), the adsorption of As(III) was via physisorption and occurred on the outer layer surface complex of the adsorbent while As(V) adsorption was via chemisorption and occurred in the inner layer surface complex of the adsorbent.

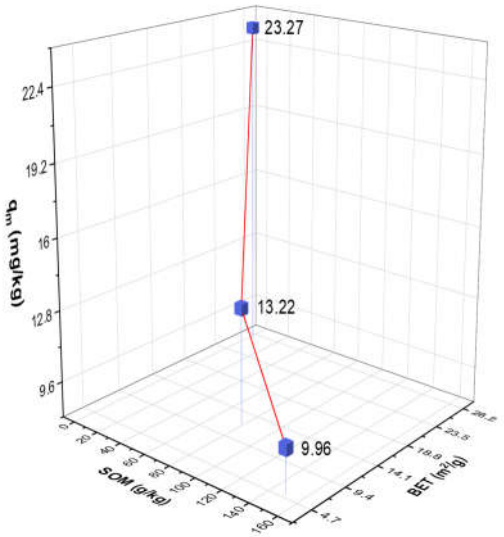

Figure 2.3. Effects of surface area of clay minerals and SOM on the adsorption of total As on soils (Feng et al., 2013).

The reaction of physical adsorption occurs rapidly on the surface of adsorbents with low enthalpy and creating multilayer formation. In contrast, chemical adsorption reacts slowly and irreversibly, having high enthalpy and monolayer formation. Similarly, Fan et al. (2020) suggested that the chemisorption process of As(V) adsorbed on the black soil occurs because

adsorbent and adsorbate share or exchange their electrons. Therefore, As adsorption will be favoured in terms of clay minerals in soils (Arco-Lázaro et al., 2016).

2.1.3.3. Soil organic matter (SOM)

The release of As from soils to the solution is mainly controlled by SOM (Wang and Mulligan, 2006a). SOM strongly interacts with As and affects its species and mobility in aquatic environments (Wang and Mulligan, 2006a). Varsányi and Kovács (2006) suggested that there was a correlation between total As and particulate organic carbon with low contents of extracted Fe (4.91 g/kg) and organic carbon in soil (0.04%), while no correlation was observed with higher concentration of extracted Fe (7.75 g/kg) and organic carbon content (0.09%). Jiang et al. (2005b) found that dissolved SOM reduced As(V) adsorption on both high- and low-energy surfaces of soil adsorption sites. It is postulated that dissolved organic matter competed with As for adsorption to mineral surfaces or formed complexes with As(V); however, the percentage of As retention on natural organic matter was low (Wilson et al., 2010). High stability of As in ionic solutions was due to the prevented aggregation of OM leading to the balanced distribution of surface charge, and expressed that As(V) released from soils was controlled by organic matter regardless of the adsorption mechanism (Grafe et al., 2011). Similarly, Feng et al. (2013) and Wang and Mulligan (2006b) pointed out that the content of SOM had great potential effects on As adsorption behaviour due to its interactions with mineral surfaces and/or with As itself. **Figure 2.3** shows that the total As maximum adsorption capacity (q_m) on three Chinese soils increased with a decrease of SOM. It was suggested that a portion of As was bound to SOM during As adsorption on humic acids through positively charged amine groups (Varsányi and Kovács, 2006), resulting the negative impact of SOM on As adsorbed on soils (Huang et al., 2013).

2.1.3.4. Bacteria

Bacteria can affect As adsorption because they can resist As(V) toxicity by reducing intracellular As(V) to As(III) (Wang and Mulligan, 2006b). Microbial redox cycling contributed to the acceleration of the kinetics of As(III) oxidizing or As(V) reducing reactions (Campbell et al., 2014), which affect the speciation of As in the environment. Furthermore, Wang and Mulligan (2006b) suggested As(V) can be used as an electron acceptor of anaerobic microorganisms for the oxidation of organic matter or H_2 gas. Xie et al. (2013) found that the rate of growth inhibition of bacteria increased with the increasing initial As(V) solution during 4-day reaction time (**Figure 2.4a**). They found that the highest inhibition rates occurred on the second day of exposure, being 24.5% and 40.8% with As(V) concentration of 800 and 1600 μg/L, respectively, which gradually decreased to 4.6% and 18.3% at the end of reaction. The authors suggested that the presence of As(V) deeply affected the growth of parts of bacterial cells till the second day of exposure, and then most of the organisms had been adapted to the As(V) stress environment, resulting in a decrease in the growth inhibition rates to their lowest levels (Xie et al., 2013). In turn, As adsorption on sediment particles was influenced by the presence of bacteria (Xie et al., 2018b). As shown from **Figure 2.4b**, the adsorption occurred rapidly during the first 7-days, and then gradually increased at the end of exposure. For instance, the estimated As(III) concentrations in these three soils were 12.5 mmol/kg, 17.1 mmol/kg and 18.5 mmol/kg at the first day, and reached 15.7 mmol/kg, 22.5 mmol/kg and 26.2 mmol/kg at 28 days for S_1, S_2 and S_3, respectively. The results for As(V) at the first day were 15.5 mmol/kg, 24.5 mmol/kg and 25.5 mmol/kg, and 28.1 mmol/kg, 44.3 mmol/kg and 51.3 mmol/kg at 28 days, respectively. It also can be found that amounts of As(III) and As(V) adsorption on the S_3 were significantly higher than those of S_1 and S_2 at any time of reaction time. It would be suggested that S_3 contained higher amount of clay content (45.5%) and Fe_2O_3 (4.68%), compared to S_1 (7.2% clay, 3.16% Fe_2O_3), and S_2 (11.0% clay, 3.95% Fe_2O_3). These

soil properties can enhance the adsorption of As on soil. Xie et al. (2013) suggested that bacteria can change their shape, activate detoxifying processes and strengthen antioxidant defence systems in order to adapt to an environment with high As contamination. It can be concluded that bacteria could reduce the adsorption affinity of As on soils because of the reduction from As(V) to As(III) under the impact of bacteria, then As(III) was released from solid phase into solution (Xie et al., 2018b).

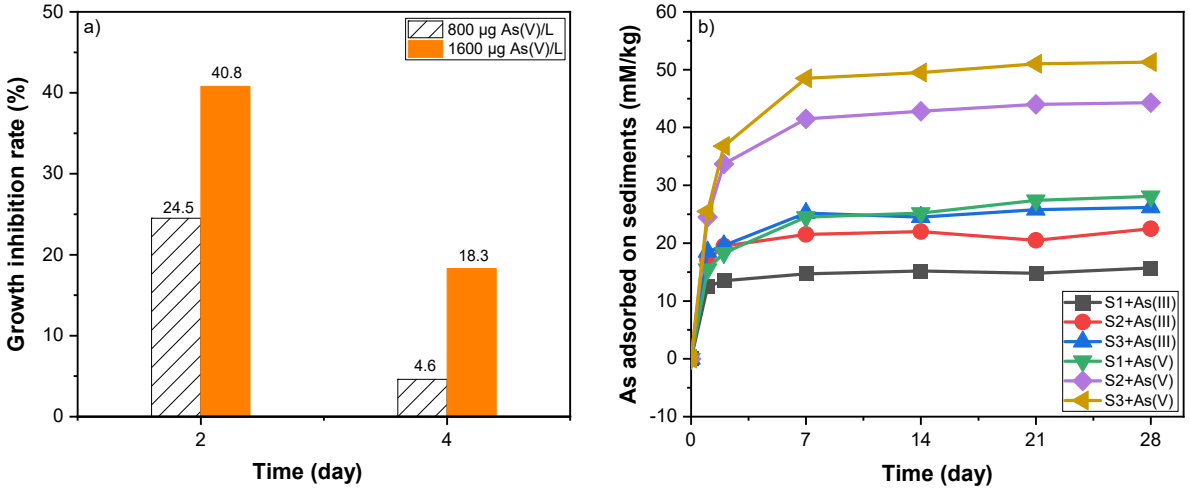

Figure 2.4. Interactions between bacteria and As adsorption. A) Effect of As(V) on the growth inhibition rate of bacteria (Xie et al., 2013); b) effect of bacteria on As(V) and As(III) adsorption, estimated and modified from the results of Xie et al. (2018b) study.

2.1.3.5. Ionic strength

The sorption of As on soils varies among inorganic As species under the effect of ionic strength. The adsorption of As(V) ions increased with increasing ionic strength at pH > 5.0, but was not significantly affected by ionic strength at pH < 5.0 (Antelo et al., 2015). In contrast, ionic strength had a relatively small effect on As adsorption (Li et al., 2019; Williams et al., 2003). Lower As(III) adsorption and higher As(V) adsorption and on the two soils investigated under acidic condition due to an increase in ionic strengths (Xu et al., 2009), whilst the amount of adsorbed As(III) increased in high pH solution. Antelo et al. (2015) reported that the presence

of Ca^{2+} ions at relatively high pH values (> 8) increased As(V) adsorption on ferrihydrite, while not influenced at pH < 8.0 due to the weak adsorption of this cation. The rate of As(V) adsorption increased by up to 30% when the concentration of Ca2+ was increased from 0.3 to 6.0 mM at pH 10.2.

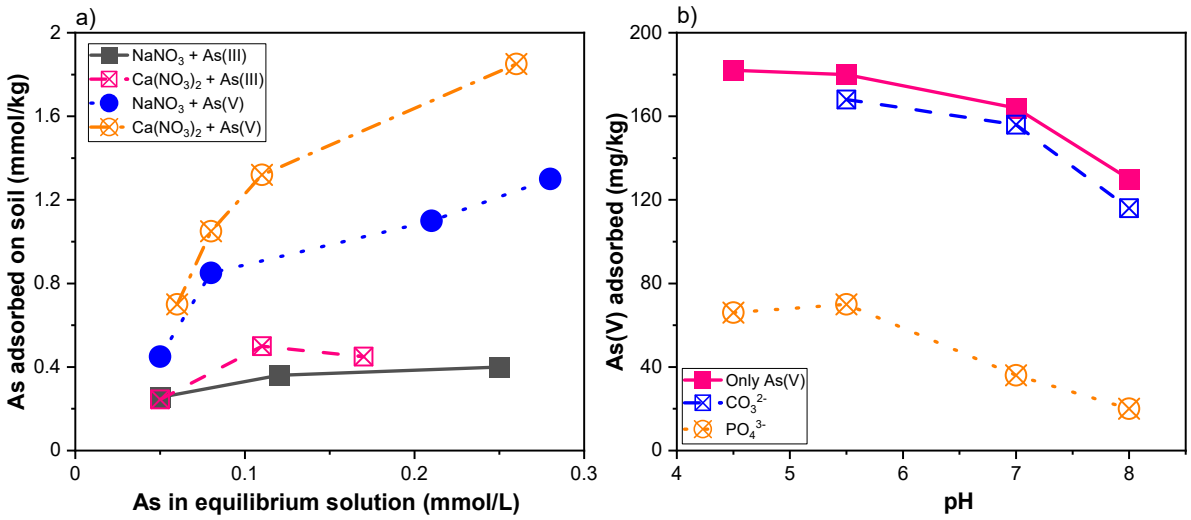

Figure 2.5. As(III) and As(V) adsorption onto soils. a) Effects of Na^{+} and Ca^{2+} (Smith et al., 2002); b) Effects of CO_3^{2-} and PO_4^{3-} (Williams et al., 2003).

As shown in **Figure 2.5a**, Smith et al. (2002) compared the effects of Ca^{2+} and Na^{+} on As(III) and As(V) adsorbed onto Alfisol soil, with Ca^{2+} having a greater influence on the adsorption of both As(III) and As(V) than Na^{+}. For example, the maximum adsorption of As(III) and As(V) in 0.1 mmol $Ca(NO_3)_2$ was 0.50 mmol/kg and 1.85 mmol/kg, higher than 0.40 mmol/kg and 1.30 mmol/kg in the presence of 0.1 mmol $NaNO_3$, respectively. In addition, **Figure 2.5b** pointed out the adsorption of As(V) was significantly higher than that of As(III). In general, the ionic strength had a marginally positive effect on As sorption on soils during both physisorption and chemisorption.

2.1.3.6. Anion competition

As adsorption generally decreased with the presence of anion competition (Alloway, 2012). Sharing the same chemical characteristics, the presence of PO_4^{3-} ions significantly decreased the adsorption of As(V) when both As(V) and PO_4^{3-} adsorption on minerals and soils (Selim, 2013; Williams et al., 2003) because soils and iron oxides have positively-charged surface (Jiang et al., 2017). As(V) adsorption on bulk soils greatly decreased within the pH range 3.0-4.5 with the presence of phosphate (Jiang et al., 2017). The similar effect of phosphate on As(III) sorption was found on the Alfisol and Oxisol soils in Australia (Smith et al., 2002), in the conditions of initial 0.2 mmol/L As(III) concentration and the presence of phosphate, amount of As(III) adsorption in soil decreased from 0.38 mmol/kg to 0.1 mmol/kg at equilibrium. The effect of phosphate on As adsorption varied in different soils. For example, at As concentration of 12.0 µg/L in solution, the adsorption of As(V) on soil from Beijing reduced from 1.75 mg/kg to 0.75 mg and from 1.16 mg/kg to 0.33 mg/kg for As(V) when phosphate exists in the solution (Feng et al., 2013). Phosphate had a significantly negative impact on adsorption of As while sulphate and chloride contents slightly enhanced the adsorption. However, the concentration of PO_4^{3-} exhibited less effect on As(V)/As(III) adsorption on soil from Hainan, China (Feng et al., 2013). Other anions presenting in soil solutions at higher concentrations such as CO_3^{2-}, Cl^-, SO_4^{2-}, NO_3^- had a relatively small effect on adsorption of As(V) (Álvarez-Benedí et al., 2005; Huang, 2018; Li et al., 2019; Williams et al., 2003). **Figure 2.5b** compares the effects of CO_3^{2-} and PO_4^{3-} due to the anion competition for As(V) adsorption onto soils (Williams et al., 2003). Of different anions, it was found that at the various pH degrees in soils, CO_3^{2-} slightly reduced the adsorption of As(V), while PO_4^{3-} had a significant impact on As(V) adsorption, reduced by 110-128 mg/kg in the pH 4.5-8.0. Such results were explained by Welch and Stollenwerk (2003) as due to sulphate adsorbed via electrostatic attraction acting as an outer-sphere complex in the presence of net positive surface

charge on soil. As a result, phosphate ions have shown strongly negative influence on As(III)/As(V) adsorption (Zeng et al., 2012) via chemisorption while other anions reduce As adsorption through physisorption.

2.1.3.7. Initial As concentration, adsorbent dosage and reaction time

Adsorption of As is influenced by the contents of As concentration, adsorbent dose and reaction (Matouq et al., 2015). In general, increasing initial concentration of As(V) or As(III) in solution leads to high rate of adsorption (Wang et al., 2018). The adsorption of As(V) on sediment in Wuhan, China was higher than that of As(III) at high initial As concentrations, particularly below 3.33 μmol/L As (Wang et al., 2018). However, Yolcubal and Akyol (2008) observed the opposite results that the degree of As(V) sorption in carbonate-rich soils at equilibrium in batch experiments decreased with increase in As(V) concentrations (0.1–200 mg/L). Regarding adsorbent dosage, efficiency of As(V) adsorption increased from 41.32% to 94.76% and from 47.27% to 98.82% with adsorbent concentration increasing from 0.25 to 2.0 g/L by using natural clay and clay/Fe-Mn composite, respectively (Foroutan et al., 2019), although no significant change of adsorption efficiency was observed with higher than 1.5 g/L of adsorbent dose. In addition, the residual As(V) concentration decreased from 1.0 mg/L to below detection limit when the amount of adsorbent (iron ore) was increased from 0 to 5.0 g/L (Zhang et al., 2004).

As adsorption from batch experiments displayed a strong time-dependent kinetic behaviour (Selim, 2013). Adsorption process exhibited a rapid rate at the initial stage, e.g. within the first 24 hours (Guo et al., 2007; Zhang et al., 2004), 48 hours (Williams et al., 2003) or seven days (Xie et al., 2018b), followed by a slower or stable rate over the next several weeks (Williams et al., 2003). Based on the laboratory batch experiments, As adsorption reached 99.0% and 98.7% for soils from Beijing and Hainan, but only 34.0% for soils from

Jilin, China after two hours of reaction. In comparison, Feng et al. (2013) and Guo et al. (2007) showed that adsorption capacity of As(III) was 386 mg/kg and 458 mg/kg for As(V) at 194 hours. The adsorption amount of As(III) on irrigated soils achieved 33% within the first hour of contact, while further adsorption was only 9.4% in the following 23 h (Huang et al., 2013).

2.1.3.8. Soil/sediment textures

Guo et al. (2007) reported that As adsorption on the fine grains (0.10-0.25 mm) of natural siderite was higher than on the coarse ones due to their greater surface areas. A study by Álvarez-Benedí et al. (2005) also showed that the amount of As adsorbed in the sandy clay loam soil was significantly higher than in the loamy sand soil as a result of greater adsorption surface of the sandy clay loam soil. In addition, the grain size also influenced the adsorption of As species (Guo et al., 2007). For instance, greater As(III) adsorption occurred with the grain size fractions between 0.04-0.08 mm and 0.25-0.50 mm than that of As(V) while the opposite trend happened with the grain size fraction of < 0.04 mm. According to Xie et al. (2018b), the adsorption capacity decreased in accordance with particulate texture, i.e. clay loam > loamy sand > silty sand and As(III) had less adsorption affinity than As(V) with the activity of bacteria. As concentrations on the selected soils in South Australia decreased from 256-1389 mg/kg on clay fraction (0-2 μm) to 170-675 mg/kg on sand fraction (250-2000 μm) (Smith et al., 2006). However, Jiang et al. (2005a, 2005b) did not observe any relationship between the changes of clay contents and As(V) adsorption on 16 soils in China. In addition, there was no significant correlation between the proportion of particulate grain size and total As content in the study of Varsányi and Kovács (2006). However, total As concentrations increased markedly with decreasing particle size with sand < silt < clay, with increasing As concentration generally correlated with increasing Fe concentrations ($r^2 = 0.57$) (Smith et al., 2006). Hence,

more proportion of clay fraction would enhance more adsorption of As on to soils and sediments.

2.1.3.9. As speciation

As adsorption rates are influenced by its speciation, with faster rate for As(V) than, normally at lower pH, and slower and similar rate to As(III) adsorption at a higher pH of 9 were reported (Welch and Stollenwerk, 2003). The adsorption of As(V) on Olivier loam and Windsor sand soils was higher than As(III) adsorption under varying conditions of ionic strength, As concentration and pH (Mohan and Pittman, 2007). As(III) adsorption on tropical soils and goethite was less than that of As(V) (Goh and Lim, 2004; Huang, 2018). Goh and Lim (2004) reported that the percentages of As(III) adsorbed on the tropical soil increased from 50% after 8h to 58% at 24h, while the figures for As(V) were 83% and 92%, respectively. Regarding As species, pH and redox conditions (Eh) in soil and water influenced the concentrations of As(III) and As(V) (Wang and Mulligan, 2006b). As(V) is dominating under the Eh > 200 mV and pH 5-8 (Violante and Pigna, 2002), while As(III) mainly occurs in reducing conditions (Wang and Mulligan, 2006a). Goldberge et al. (2005) pointed out that the oxidizing redox state As(V) was stable in soils, and as a result, As(V) species has been widely investigated in adsorption on soils (Álvarez-Benedí et al., 2005; Arco-Lázaro et al., 2016; Fan et al., 2020; Farrell, 2017; Gedik et al., 2016; Goldberg and Suarez, 2013; Jiang et al., 2017, 2005b, 2005a; Li et al., 2019; Luo et al., 2019; Williams et al., 2003; Yolcubal and Akyol, 2008; Zhang and Selim, 2005). The adsorption-desorption mechanisms of As(III) and As(V) under different controlling factors have been evaluated (Deng et al., 2018; Dousova et al., 2012; Feng et al., 2013; Guo et al., 2007; Mishra and Ramaprabhu, 2012; Qiu et al., 2018; Wang et al., 2018; Xu et al., 2009), although only a few studies focused on As(III) sorption (Caporale et al., 2013; Huang et al., 2013). The mechanism for adsorption of solute by a solid surface can be used to explain the

difference of As speciation adsorbed on soils. There are three common adsorption mechanisms including outer-sphere surface complexation, physisorption inner-sphere complexation, and chemisorption (Welch and Stollenwerk, 2003). The complex bonds of inner-sphere are stronger than those of outer-sphere because the '*electrostatic attraction between a charged surface and an oppositely charged ion*' in solution involved in outer-sphere is weaker than the '*formation of a coordinative complex with the mineral surface*' involved in inner-sphere. Consequently, As(V) adsorption on soil via chemisorption is generally stronger than As(III) adsorption via physisorption (Ma et al., 2015). The results (**Figure 2.2(a and b**)) illustrate that As(V) had higher adsorption affinity than As(III), which agree with the results from Fendorf et al. (2010).

2.1.3.10. Bioavailability of As in soils/sediments

The bioavailability of As is dependent on several factors including soil/sediment properties, adsorption and desorption processes, plant species and microbial processes (Akter et al., 2006). The soil factors include clay content, SOM, texture, pH, Eh, cation-exchange capacity, oxides and hydroxides of Fe, Al and Mn (Akter et al., 2006). According to Yang et al. (2002), Fe oxide content and pH were the most important soil properties influencing the bioavailability of As on aging. They reported that high Fe oxide content and low pH (< 6) significantly caused the reductions of As bio-accessibility over 6 months, while As could become more bioavailable with soil pH > 6 over time. The study also found that the mean initial bio-accessibility of As(V) in 36 soils was 43.6% at the beginning of adsorption, then reduced marginally to 40.1%, 36.5%, 35.6% and 33.0% after 1, 2, 3 and 6 months, respectively. Adsorption process is also able to reduce the mobility and bioavailability of As in soils. For instance, As(III) was more bioavailable than As(V) at higher pH due to stronger adsorption affinity of As(V) on metal oxides, especially Fe oxides (Akter et al., 2006). Plant species are generally able to accumulate part of As concentrations in soils to their root and translocate to shoot and grains (Neidhardt et

al., 2015). The amount of As accumulation depends on the accumulation and translocation ability of the plants (Huang et al., 2006). As(III) and As(V) up taking mechanisms occur in different ways. For example, rice plants can accumulate As(III) in their shoots through silicon uptake pathway (Fleck et al., 2013), while plants uptake of As(V) is through phosphate transport channels (Bhattacharya et al., 2021). As(III) can be removed by microorganisms such as bacteria, fungi and algae which can reduce As(V) to As(III) (Akter et al., 2006) and release As(III) from solids to solution (Xie et al., 2018b), resulting in less bioavailability of As in soils as long as there are no limitations to soil drainage. Hence, As(V) is more bioavailable in soils due to its negative charge and stronger retention in soils, whilst more As is mobile in solution (Lombi and Holm, 2010).

Therefore, As adsorption is highly dependent on soil/sediment properties such as pH, texture, SOM, clay minerals and environmental factors namely initial As solution, sorbent dose and reaction time (Huang et al., 2013). Dias et al. (2009) suggested that iron oxide content was the most important soil parameter affecting As(III) adsorption on soils, while soil textures including sand, silt and clay fractions were the most important factors for As(V) adsorption on soils and sediments.

2.1.4. As adsorption isotherm models

The Langmuir and Freundlich isotherm models have been widely applied for As sorption as these models can provide a good fit of results under a range of different conditions. According to Ghosal and Gupta (2017), the Langmuir isotherm is most applicable for the chemisorption process since it is primarily used for unimolecular adsorption on the gas-solid interface with the assumption of monolayer surface coverage, independent and homogeneous sorption and energy, whilst Freundlich isotherm exhibits the physical adsorption which was developed for

the heterogeneous surface with the phenomena that adsorption heat distributes the non-uniform and monolayer coverage is unrestricted.

2.1.4.1. The Langmuir isotherm model

Based on the data from the previous studies, **Figures 2.6** illustrates the maximum Langmuir adsorption capacity (q_m) values of different soils for adsorbed As(III) and As(V). The selected soils were classified by USDA soil classification system (García-Gaines and Frankenstein, 2015). The average values of q_m for As(III) increased from 225.00 mg/kg (sand soil) to 2998.2 mg/kg (loam soil) (**Figure 2.6a**), while the results for As(V) varied between 114.8 mg/kg (silty clay soil) and 14950.3 mg/kg (sandy loam soil) (**Figure 2.6b**). The highest values of q_m for As(III) and As(V) were found on loam and sandy loam soils, being at 8901.0 and 42400.0 mg/kg, respectively. It can be seen that the Langmuir maximum adsorption capacities of soils for As(V) were significantly higher than those of As(III).

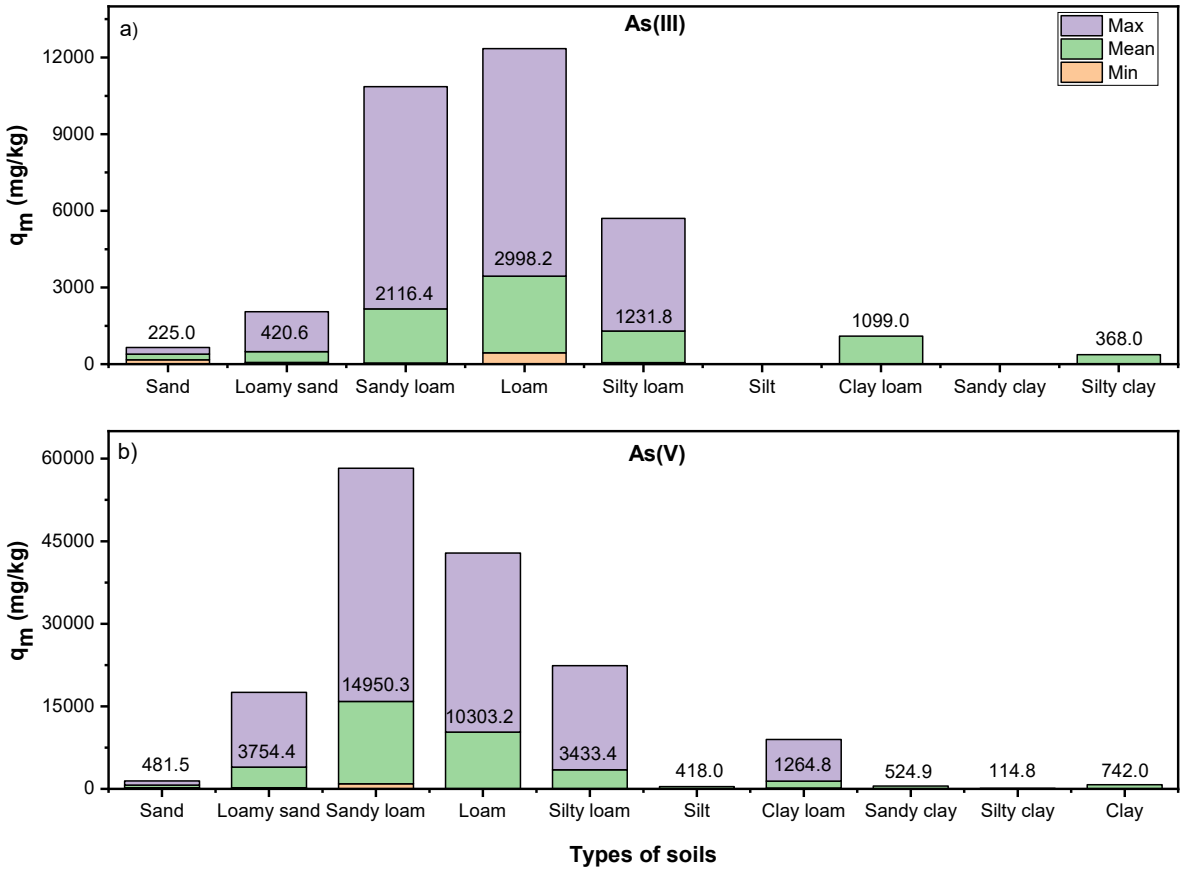

Figure 2.6. The minimum, mean and maximum values of adsorption capacity (qm) of As(III) and As(V). Data from Arco-Lázaro et al. (2016); Dias et al. (2009); Fan et al. (2020); Gedik et al. (2016); Huang et al. (2013); Jiang et al. (2005a); Luo et al. (2019); Kumar et al. (2016); Zhang and Selim (2005).

The Langmuir isotherm model exhibited better display with experimental data of metal and metalloid adsorption than Freundlich isotherm (Jiang et al., 2005a; Matouq et al., 2015). According to Gedik et al. (2016), the Langmuir isotherm model provided a better statistical correlation with various of As(V) concentrations and soils properties such as pH, Eh, OM, As concentration, Fe, Al and clay content than Freundlich model (Gedik et al., 2016; Jiang et al., 2005b; Luo et al., 2019). Both these models showed the very good fit with high r^2 values at least 0.801 for As(III) and As(V) adsorbed on soil (Dousova et al., 2012; Goldberg and Suarez, 2013; Ma et al., 2015; Wang et al., 2018). The Langmuir equation is widely known as the

Langmuir one-surface equation with hypothesis that there is the same binding energy at all adsorption sites on sorbent surfaces (Jiang et al., 2005a). However, in some cases, the plots using the Langmuir one-surface equation for adsorption data were divided into two straight line portions with different gradients, indicating that two different types of adsorption sites were available.

The Langmuir maximum sorption capacity and the isotherm constants from the experimental data vary with the controlling factors. For instance, the variation of the maximum As(V) sorption capacity of low and high energy surfaces calculated by using a two-surface Langmuir equation in 16 Chinese soils was 83% and 68%, respectively (Jiang et al., 2005b). Similarly, due to the effect of 0.5 mmol/L $Fe(OH)_3$ colloids, the maximum percentage adsorption of As(V) was 95% and 64% for As(III) on soil from Beijing and 53% and 36% on soil from Jilin, China, respectively while the percentages reached 98% and 76% for As(V) and As(III) on soil from Hainan, China when $Fe(OH)_3$ concentration was lower than 0.01 mmol/L (Feng et al., 2013). The results of Feng et al. (2013) also dictated that As adsorption on three soils in China was favoured at high temperature. The adsorption capacities (q_m) determined from the Langmuir models increased from 13.22, 9.96 and 23.27 mg/kg at the temperature of 283K to 16.37, 19.46 and 27.08 mg/kg at 323 K for soils from Beijing, Jilin and Hainan, China. Kundu and Gupta (2006) showed similar results for As(V) and As(III) adsorption capacities on iron oxide-coated cement at three investigated temperatures of 288 K, 298 K and 308 K. In addition, Zhang and Selim (2005) reported that adsorption maximum of As(V) calculated by the Langmuir equation increased with reaction time from 92.2 mg/kg, 263.0 mg/kg and 169.2 mg/kg in the first six-hour to 418.2 mg/kg, 742.0 mg/kg and 554.9 mg/kg at 504-hour for the three investigations soils (Olivier loam, Sharkey clay and Windsor sand). For As(III), the maximum adsorption on irrigated soil was 368 mg/kg (Huang et al., 2013). In addition, adsorption capacities of As(V) on MIL-101(Fe) were nearly stable at pH 3-11 (Li et al., 2019).

Generally, As(III) had higher maximum adsorption capacities than As(V), e.g. 1040 µg/g vs 520 µg/g by natural siderite (Guo et al., 2007), 180.3 mg/g vs 172.1 mg/g by iron oxide-graphene (Mishra and Ramaprabhu, 2012), and 7.7 mmol/kg vs 5.0 mmol/kg by natural soil (Dousova et al., 2012) for As(III) and As(V), respectively. However, Wang et al. (2018) reported a higher maximum adsorption capacity of As(V) at 6.949 µmol/g than for As(III) at 4.044 µmol/g by lake and river sediments in China.

2.1.4.2. The Freundlich isotherm model

The empirical equation of the Freundlich adsorption isotherm is most often used in the description of adsorption in an adsorbent (Aksentijevíc et al., 2012; Wang et al., 2018)., The Freundlich adsorption constant K_F from the study increased from 1.94 to 4.71 (mg/kg) $(L/mg)^{1/n}$, 0.58 to 0.77 (mg/kg) $(L/mg)^{1/n}$ and 3.59 to 5.38 (mg/kg) $(L/mg)^{1/n}$ for soils from Beijing, Jilin and Hainan, China when the temperature increased from 283 K to 323 K (Feng et al., 2013). The linear adsorption constant (Kd) for As(V) adsorption on saline-alkali soils varied between 86.0 mL/g and 157.1 mL/g (Luo et al., 2019). The Freundlich isotherm model exhibited better results for As(V) adsorbed on soils than As(III) due to several low r^2 values of regressions for As(III) at 0.03, 0.12 and 0.34, respectively (Kuma et al., 2016).

Furthermore, a study by Kundu and Gupta (2006) illustrated that As(V) and As(III) sorption data was better fit in linear and nonlinear systems at three temperatures (288, 298 and 308 K) by Freundlich isotherm model than Langmuir, Dubinin-Radushkevich (D-R) and Toth and Temkin isotherm equations. As(V) adsorption was highly nonlinear with the Freundlich reaction on three types of soils (Zhang and Selim, 2005) and on carbonate-rich soils (Yolcubal and Akyol, 2008). Similarly, the Freundlich isotherm equation provided a better exhibition than other isotherm models (Huang et al., 2013), for As(III) adsorption process in contaminated agricultural soil from an irrigated area, China. In another study, Guo et al. (2007) showed that

the Freundlich isotherm exhibited a better fit to the experimental data for the smaller grain size of the natural siderite (0.10-0.25 mm) in comparison to the Langmuir model, whilst the two models were comparable for the grain size range of 0.25-0.5 mm. The study of Arco-Lázaro et al. (2016) also showed the better fitting results of As(V) adsorption by soils using the Freundlich isotherm equation than the Langmuir isotherm equation. Therefore, it can be concluded that the Freundlich isotherm equation well describes the non-linear form for the adsorption of As(III) and As(V) on soils.

2.1.5. Future perspectives and implications for managing As-contaminated soil

Based on the extensive literature review, this study has identified that the maximum As-contaminated soil was found in Chihuahua region, Mexico with 116000 mg/kg of As, whilst the highest Langmuir maximum adsorption capacity of soils adsorbed As was 42400 mg/kg for Dunellen sandy loam from the State of New Jersey, United States (Dias et al., 2009). The most important controls of As adsorption on soils/sediments are pH, clay mineral and texture to enhance the efficiency of As(III)/As(V) adsorption. Therefore, there are a few lessons that we have learnt for managing soil contaminated by As. First, the sources of As contamination should be identified as soon as feasible, in order to control further contamination spreading beyond the affected areas. Secondly, the contamination hotspots should be determined through well-designed field sampling and chemical analysis with good quality control. Thirdly, the fundamental properties of soil should be determined through a range of instrumental and physicochemical analyses, in order to identify the mechanism of As-soil interactions. Finally, the decontamination of As-contaminated soils can be treated to a high standard using technologies which are effective and environmentally friendly.

2.2. Characteristics of microplastics contamination in rivers and their interactions with arsenic

2.2.1. Plastics and microplastics

Plastics provide a wide diversity of applications because they have lightweight, strong, durable characteristics (Thompson et al., 2009; Zhang et al., 2015), have thus made our life become more convenient (Fu et al., 2021; Phuong et al., 2016). The truth is that plastics have been widely used in our daily life and applied in industry, science and technologies (Wen et al., 2018). However, these materials have currently become a global and ubiquitous problem as white pollution (Fu et al., 2021) and can be detected everywhere including air, surface waters, soils, sediments, sand beaches, wastewaters, sludges, biota and marine environment (Barcelo and Pico, 2020). Virgin plastic polymers are usually mixed with various additives such as inorganic fillers (e.g. carbon or silica), stabilizers or plasticizers (Andrady, 2011), which are used in substantial quantities and productions (Meeker et al., 2009). Inorganic fillers are used to reinforce the plastic materials, while the plastics can be processed at high temperatures or prevented degradation when exposed to sunlight by adding thermal or ultraviolet stabilizers (Andrady and Neal, 2009). Plasticizers such as phthalates are used to make plastics more durable (Thompson et al., 2009).

Main plastic materials including polyethylene (PE), polypropylene (PP), polyvinyl chloride (PVC), polystyrene (PS) and polyethylene terephthalate (PET) contributed around 90% of total world plastic production (Andrady and Neal, 2009). They. These plastics have high molecular weight and are non-biodegradable resulting in extreme persistence in the environment (Lagarde et al., 2016). With the durability expected to be 70 years old (Thompson et al., 2009), plastics rise problems associated with fragmentation processes (Andrady, 2011), contributing to large amounts of plastics arriving in the environment (Lagarde et al., 2016). The production of plastic has been estimated up to 8300 million metric tonnes between 1950

and 2017, and plastic waste has been around 6300 million metric tons until 2015, 9% and 12% of waste were recycled and incinerated (Blair et al., 2019; Geyer et al., 2017). The remaining amount of this waste, 4977 million metric tons (79%) was buried in landfills or released to the natural environment. In 2017, approximately 348 million tons of plastics was produced globally, of which China was the largest producer and shared 27% of total plastic pollution (Barcelo and Pico, 2020). It is estimated that 12000 million metric tons of plastics will be produced by year 2059 (Geyer et al., 2017). Additionally, the plastic waste stored in landfills on land is often received poorly management conditions (Nizzetto et al., 2016). The major contributions of non-fibre plastics containing 93% polymer resin and 7% additives by mass are high- or low-density PE (36%), PP (21%), PVC (12%), and less than 10% each for PET, Polyurethane (PUR) and PS (Geyer et al., 2017). For the usage purposes, packing accounted for 42% of all non-fibre plastics with the predominant compose of PE, PP and PET, 19% was used in building and construction section, of which 69% from all PVC (Geyer et al., 2017). In addition, MP physical and chemical features have effects on environmental fate, for instance, PE, PP and PS may float within the water column due to their light densities, while PVC and PET with high densities can sink and settle on sediments (De Felice et al., 2019). To date, MPs are plastic polymers with diameters less than 5 mm (Dong et al., 2020; He et al., 2020b), and have received great concern worldwide (Shen et al., 2021).

2.2.2. Characteristics and sources of microplastics

2.2.2.1. Microplastic types

MPs have received an increasing attention recently due to posing a great concern to biodiversity and potentially risks for human health (Blair et al., 2019; Eerkes-Medrano et al., 2015; Zhang et al., 2015). Their naturally pervasive and persistent characteristics are the most concern related to these issues (Hu et al., 2018; Thompson et al., 2009).

MPs are defined as primary and secondary (Akdogan and Guven, 2019; Alam et al., 2019). Manufactured plastics are the primary MPs including all micro-sized particles such as microbeads from cosmetics or industrial purposes, manufactured pellets used as raw material and fibers (Andrady, 2011; Phuong et al., 2016). MP beads are often found in industrial and domestic wastewater then entering into rivers or estuaries (Blair et al., 2019). Scrubbers come from air-blasting technology during the process of blasting acrylic, melamine or polyester. This MPs are often found as contamination with heavy metals (Cole et al., 2011). The most commercially used MPs are PS, PE, PP, PVC and PET (Akdogan and Guven, 2019; Andrady, 2011; Horton et al., 2017). These MPs are expected as the major components of MP samples due to their non-biodegradable properties (Phuong et al., 2016). High proportions of PE, PP, PS in sampled MP concentrations reflect the domain of these plastics on the market (Campanale et al., 2020).

The secondary MPs including fibers and fragments often derive from the larger plastics broken down under environmental conditions such as ultraviolet rays or mechanic abrasion, sites of higher population densities (Eerkes-Medrano et al., 2015), laundry procedures (Dris et al., 2015a), paint flakes and car tires debris (Browne et al., 2011; Nizzetto et al., 2016). Fragmentation of plastic debris created by physical, chemical and biological processes, which has the smaller sizes than original plastic litter (Akdogan and Guven, 2019). Various shapes such as pellets, fibers and fragments were found in the environments due to their different sources (Akdogan and Guven, 2019; Klein et al., 2015; Nizzetto et al., 2016). The major component of MP particles distributed in river surface water and sediment is fibers (Alam et al., 2019), and can exhibit long residence times (Eerkes-Medrano et al., 2015).

2.2.2.2. Sources of MPs

There are several sources of MP entering into the fluvial systems including wastewater treatment plant (WWTP) effluents (Hoellein et al., 2017; Lebreton et al., 2017; McCormick et

al., 2014; Murphy et al., 2016), sewer overflows caused by heavy rain events, agricultural runoff, atmospheric fallout (Campanale et al., 2020; Dris et al., 2015b), urban runoff and fragmentation of plastic litter (Estahbanati and Fahrenfeld, 2016). WWTPs were the main point sources of MPs in rivers (McCormick et al., 2014). WWTPs can retain a large amount of MP particles of an effluent, from 80% (Hoellein et al., 2017) up to 98.41% (Murphy et al., 2016), which explained the function as MP sources for the rivers, depending on the MP capturing capacities of the WWTPs (Donoso and Rios-Touma, 2020). In fact, MPs can directly enter the fluvial systems throughout wastewater effluents. Urban rivers receive WWTP effluent often containing high MP concentrations, causing varies of potentially biological interactions with river biota (McCormick et al., 2014). In developing countries such as Ecuador, increasing population, poor management of urban waste, the loss of riparian plant cover, and the lack of wastewater treatment led to alarmingly high number of MPs found in rivers (Donoso and Rios-Touma, 2020). The finding data in this study surpassed those in other works with the highest value of MP found at 1,186,339 particles/m3 due to untreated wastewater discharging directly into the rivers.

Urban areas with high population density were also a major factor contributing to large amount of MP abundance. Human activities had great influence on the MPs distribution, of which MP concentrations are often higher at location with more human activities than others (Wang et al., 2017; Wen et al., 2018). An illustration is that urban river water in Ziang city was found as highest concentrations of MPs among other cities located along the Tuojiang river due to numerous factories of cars, pharmaceuticals, food, textiles and building materials (Zhou et al., 2020). Additionally, fibers were dominant particles of MPs in both river water and sediment sample sites closed to urban areas, while the number of fibers was similar to other particles (films and fragments) in remote areas (Donoso and Rios-Touma, 2020). MPs are most likely deriving from municipal sewage treatment plants and runoff from processing facilities

(Klein et al., 2015). Improper waste disposal, insufficient waste management and urban runoff are considered as the main routes of discharge MPs into the river (Alam et al., 2019; Klein et al., 2015), causing MP contamination in river water and sediment.

Agricultural and livestock uses in remote areas were considered as a source of MPs in rivers (Donoso and Rios-Touma, 2020), although the content of pollution was away from the centres (Allen et al., 2019). The pollutants from these sites are often associated with runoff. Moreover, agricultural activities led higher concentrations of MPs in the river water during the wet seasons (Campanale et al., 2020).

Spillage of preproduction pellets and powders, and bead blasting media are potential sources for primary MPs. The most recognized sources of MPs in rivers, lakes or marine systems are photodegradation and mechanical breakdown of larger plastics such as Styrofoam, plastic bags, bottles, wrappers, cigarette butts and tires (Cole et al., 2011), causing the secondary MPs. Under Ultraviolet (UV) degradation and adsorbing hydrophobic pollutants of polychlorinated biphenyls (PCBs), MPs will become smaller and more toxic over time (Fendall and Sewell, 2009).

2.2.3. Particle and mass abundance of MPs in river waters and sediments

Both primary and secondary MPs have been detected in surface water samples and the number of MP particles in river waters globally are shown in **Figure 2.7**. The lists of rivers and their authors are given in **Table 2.3**. Rivers in Asia continent (**Figure 2.7a**), particularly China and followed by Japan, were investigated for this polluted issue than other continents (**Figure 2.7(b and c)**). The average abundance of MP in Asian rivers ranged at 24.72-1780x10^3 particles/m^3. The three highest abundance numbers found in Majime River (Japan), Yellow River (China) and Arakawa River (Japan), at 1061x10^3, 1392x10^3 and 4700x10^3 particles/m^3, respectively (Han et al., 2020; Kabir et al., 2021; Sankoda and Yamada, 2021). The two former rivers

collected MPs with their sizes of 50-5000 µm compared to MP sizes 500-5000 µm from later river, indicated that Arakawa River water was extremely polluted by MPs.

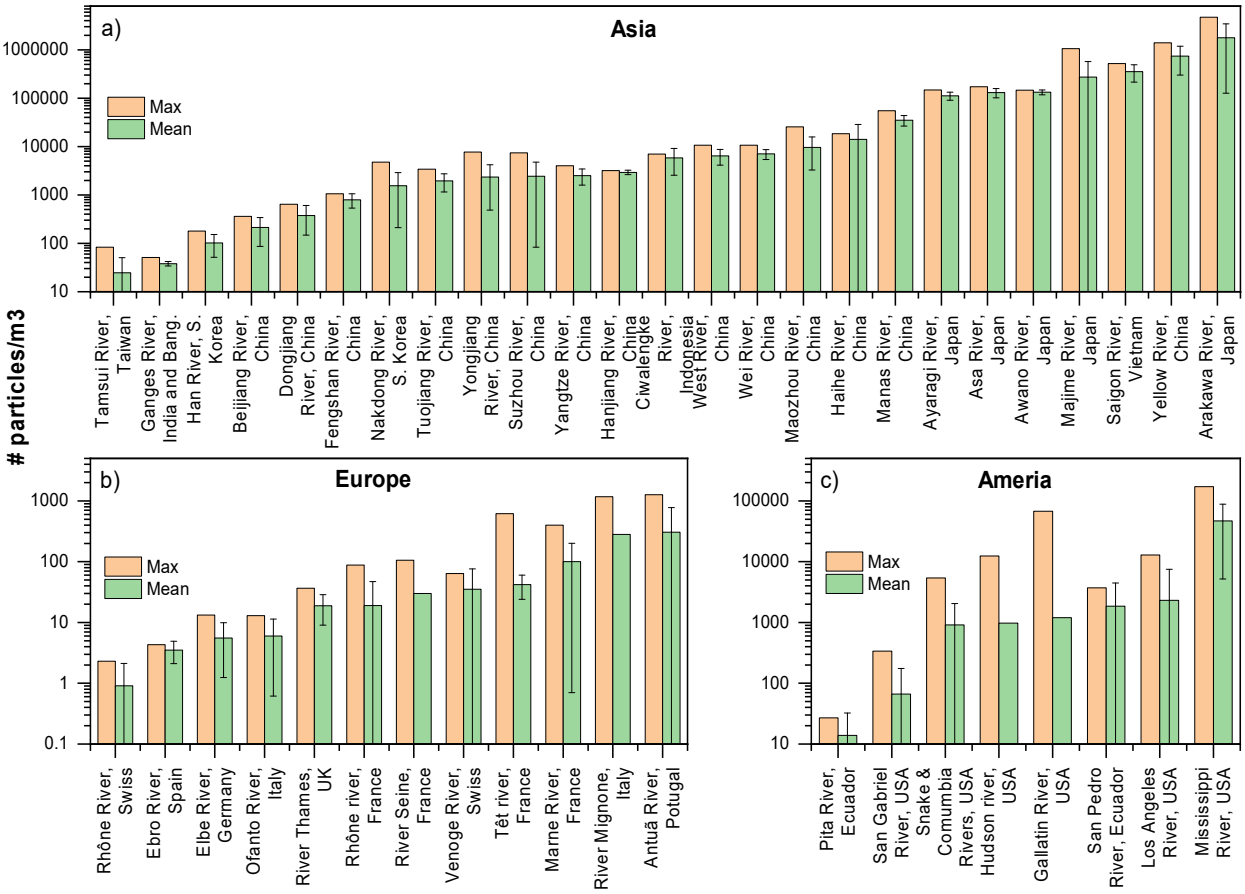

Figure 2.7. Number of MP particles in river waters globally.

The river waters in European countries were less polluted MPs than Asian and American rivers. The average abundance of MPs in this continent varied between 0.91 and 305.83 particles/m^3 and the highest value of 1265 particles/m3 was found at Antuã River, Portugal (Rodrigues et al., 2018), followed by River Mignone, Italy (Gallitelli et al., 2020). **Figure 2.7c** shows the maximum and average abundance of MPs in river waters in Ecuador and USA. Ecuadorean rivers were estimated at 13.84 particles/m^3 of average MP numbers (Pita River) and 1853.03 particles/m^3 (San Pedro River) (Donoso and Rios-Touma, 2020), while USA rivers were significantly higher with average number ranging 108.4-46711 particles/m^3

(**Figure 2.7c**). The Mississippi River was recorded with the highest amount of MP particles in America, at 172000 particles/m^3 (Scircle et al., 2020), which was equal to MPs abundance in Asa River, Japan (Kabir et al., 2021) and was lower than that in some rivers including Awano River, Majime River and Arakawa River in Japan (Kabir et al., 2021), Yellow River in China (Han et al., 2020), and Saigon River in Vietnam (Lahens et al., 2018).

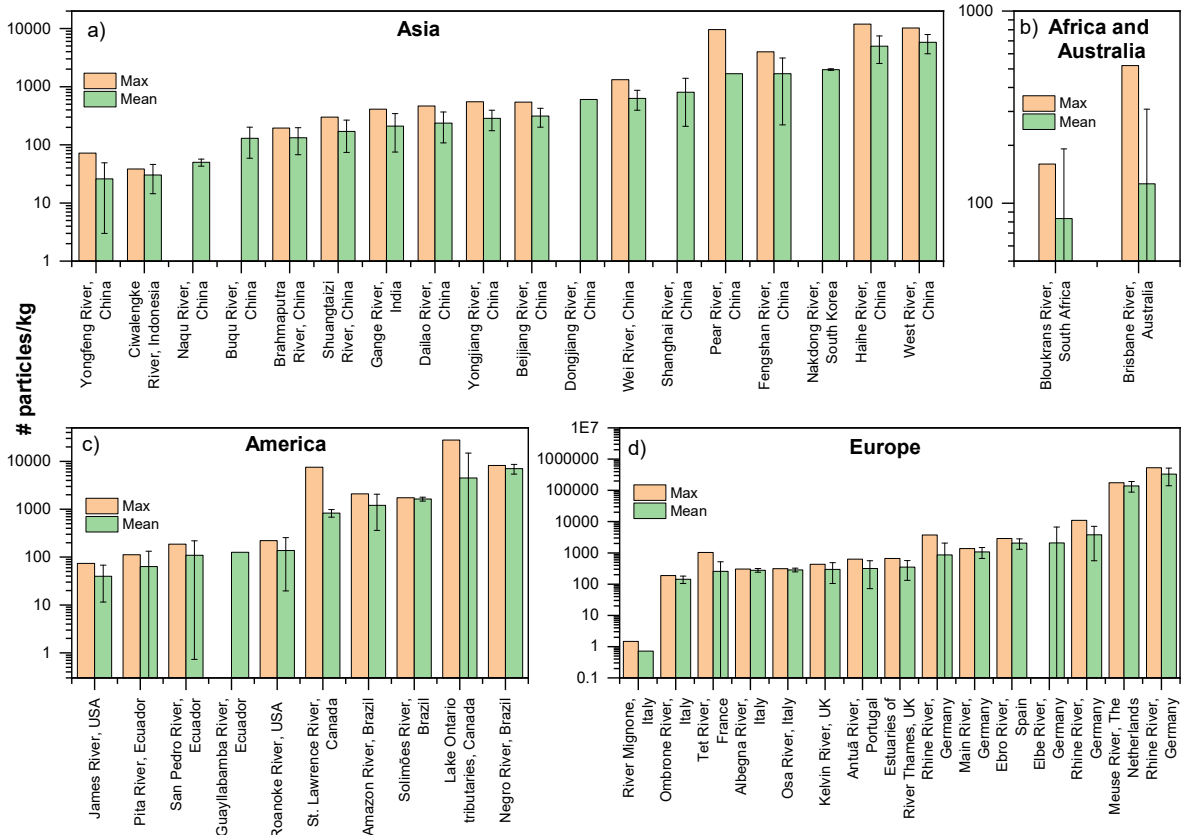

Figure 2.8. Number of MP particles in river sediments globally.

Furthermore, in the sediment environment, MPs are not easily identified by the naked eye (Barcelo and Pico, 2020) due to their sizes and colours. Nizzetto et al. (2016) found that MPs (> 0.2 mm) can be retained in the sediment in condition of their densities marginally higher than water whilst the small size (<0.2 mm) MPs do not sink and remain in the water, regardless of their density. **Figure 2.8** shows the MP abundance in river sediments throughout the world. The sources of data are shown in **Table 2.3**. The number of studies carried out in

China also dominated than other countries in comparison. Average amount of MPs in river sediments collected in Asia varied from 26 to 5795.3 particles/kg, and the highest amount was found in Haihe River, China at 11917 particles/kg (Liu et al., 2021). Bloukrans River (South Africa) and Brisbane River (Australia) were seen as slightly pollution, with their average abundance of 83.2 and 126.25 particles/kg, respectively (**Figure 2.8b**). The average MPs abundance in American countries were closed to those in Asia, ranging between 39.8 and 7023.5 particles/kg. The highest value (27830 particles/kg) was estimated in Lake Ontario tributaries, Canada (Ballent et al., 2016), which roughly doubled the highest number in Asia (**Figure 2.8c**). The most polluted MPs in river sediments were recorded in Europe, where the field MP concentrations varied greatly from 0.72 to 329750 particles/kg (**Figure 2.8d**). Rhine River in Germany was recorded as the greatest MP abundance in the world, with the maximum of 528000 particles/kg (Donoso and Rios-Touma, 2020). Consequently, river sediments are considered as the hotpots for deposition of MPs one the river sections have low stream power (Barcelo and Pico, 2020; Nizzetto et al., 2016). According to Phuong et al. (2016), MP concentrations in sediments accounted for up to 5% of sediment mass.

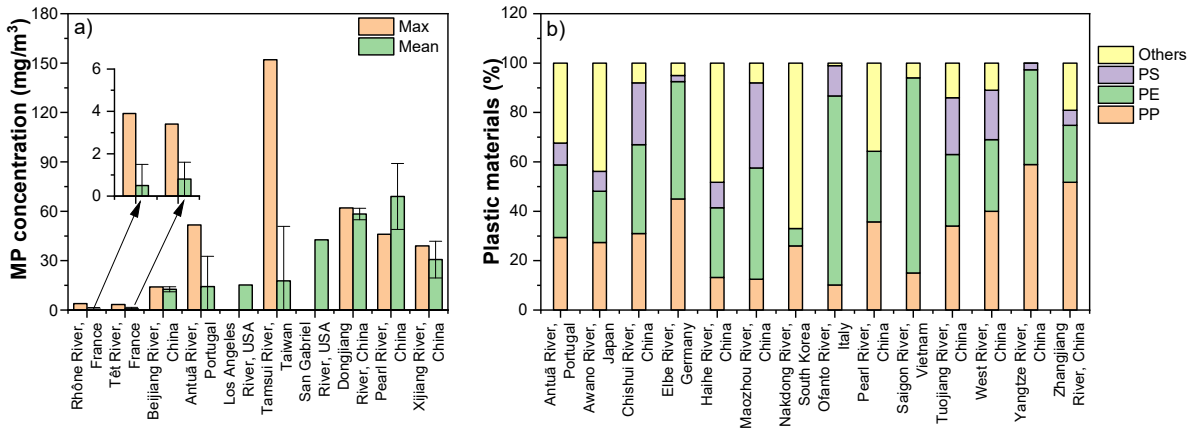

Figure 2.9. The mass fraction of MPs in river waters and their plastic materials (The sources of data are given in **Table 2.3**).

The mass fraction and plastic materials of MPs in river waters and sediments are shown in **Figures 2.9** and **2.10**. Estimation of MP weight in both river waters and sediments was far less popular as the MP particle calculation. The lowest mass fractions of MPs in rivers waters in Rhône River and Têt River, France, with the average values (0.5 and 0.8 mg/m^3) and maximum values (3.9 and 3.4 mg/m^3), respectively (Constant et al., 2020). The Dongjiang and Pearl Rivers, China were considered as highly MP contaminated with their average mass amount of 58.33 and 69 mg/m^3 (**Figure 2.9a**). However, the highest value was accounted in Tamsui River, Taiwan at 152 mg/m^3 (Wong et al., 2020). Regarding mass contamination of MPs in river sediments, the average amount increased from 5.17 mg/kg (Yongfeng River, China), 29.09 mg/kg (Brisbane River, Australia), 35.75 mg/kg (Antuã River, Portugal), 133 mg/kg (Têt River, France), 216 mg/kg (Pear River, China) and 476.9 mg/kg (Rhine River, Germany) (**Figure 2.10a**). Rhine River was also attributed to the highest content of MPs in sediments, at 932 mg/kg (Klein et al., 2015). Nizzetto et al. (2016) supported that the lack of investigation in the retention efficiency of river sediment beds resulting in river sediments may be work as permanent or important temporary sinks to store or delay discharging MPs into the sea. MP concentrations in river waters and sediments varied seasonally. For example, MPs accumulate and repose temporarily in river sediment during the dry season (Nel et al., 2018). MP abundance in sediment was 2827 times as those in surface water of Nakdong river, Korea in May before the rainy season (Eo et al., 2019).

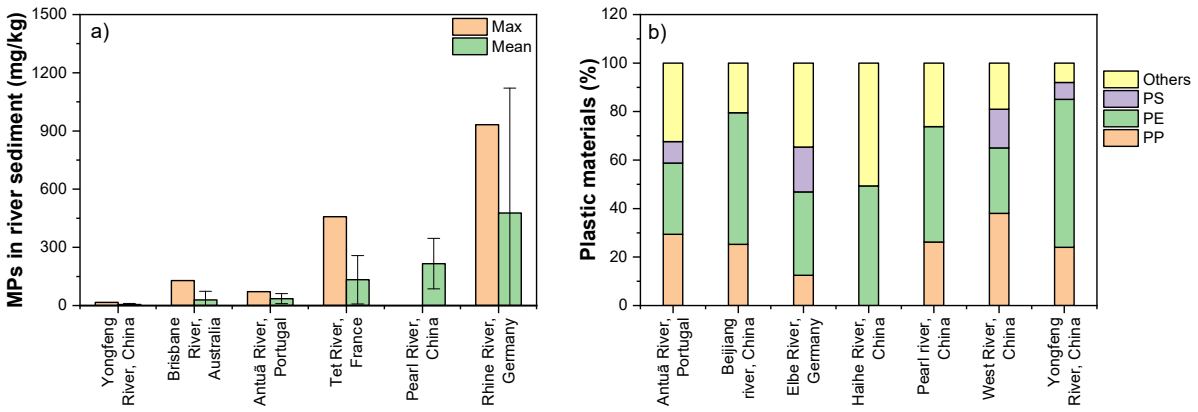

Figure 2.10. The mass fraction of MPs in river sediments and their plastic materials (The sources of data are given in **Table 2.3**).

Different polymer types such as PP, LDPE, HDPE, PVC, PUR, PET, PS and polyamide (PA) coming from a multitude of sources, and presenting in various sizes, colours, shapes and types of materials are the popular MPs (Barcelo and Pico, 2020). PP, PE and PS were dominant polymer types of MPs in river waters and sediments (**Figures 2.9b and 2.10b**). In the river waters, the percentages of PP and PE in total MPs varied at 10.2-58.9% and 7-79%, respectively. PS was generally less abundant than PP and PS, contributing to 2.5-34.5% of the total MPs in river waters. High proportion of PP and PE float in water due to their lower density (PP: 0.9-0.91g/cm^3, PE: 0.917-0.965 g/cm^3) than water, PS with a higher density (1.04-1.11 g/cm^3) than that of fresh water explained that density was one of the key factors influencing the distribution of MPs (Zhou et al., 2020). As a result, the distribution of MPs in water column depends on both environment factors and the intrinsic properties of MPs (Zhou et al., 2020). Moreover, PP in river sediments accounted for from 12.5% in Elber River, Germany (Scherer et al., 2020) to 38% in West River, China (Huang et al., 2021). PE had higher proportion than PP, ranging between 27%-61%, whilst PS contributed to less amount of the total MPs (7%-18.5%) in comparison with PP and PS (**Figure 2.10b**). Original low-density characterization is unable to explain the high content of PP and PE in the sediments. Several hypothesises were given that the density of these MPs may be increased due to interactions of aggregates,

biofouling and faecal, resulting in their settling (Cole et al., 2016; Eo et al., 2019; Long et al., 2015).

Table 2.3. Sources of MPs in river waters and sediments.

MP contaminated in river waters and location	Mean concentration (particles/m^3)	Main MP types	References
Tamsui River, Taiwan	24.7		Wong et al. (2020)
Ganges River, India and Bangladesh	38.0	PVC, PET	Napper et al. (2021)
Han River, S. Korea	102.0	PE, PS, PTFE	Park et al. (2020)
Beijiang River, China	213.3	PE, PP, PET	Fan et al. (2019)
Dongjiang River, China	376.7	PE, PP, PET	Fan et al. (2019)
Fengshan River, China	795.5	PE, PET, PA, PES	Tien et al. (2020)
Nakdong River, S. Korea	1555.0	PP, PS	Eo et al. (2019)
Tuojiang River, China	1946.8	PP, PE, PS	Zhou et al. (2020)
Yongjiang River, China	2345.0	PP, PE, PET, PS	Zhang et al. (2020)
Suzhou River, China	2437.8	PES	Luo et al. (2018)
Yangtze River, China	2516.0	PET, PP	Wang et al. (2017)
Hanjiang River, China	2933.0	PET, PP	Wang et al. (2017)
Ciwalengke River, Indonesia	5850.0		Alam et al. (2019)
West River, China	6429.5	PP, PE, PVC, PET	Huang et al. (2021)
Wei River, China	7038.0	PE, PVC, PS	Ding et al. (2019)
Maozhou River, China	9578.1	PE, PP, PS, PVC	Wu et al. (2020)
Haihe River, China	14170.0	PE, PP	Liu et al. (2020)
Manas River, China	35000.0	PP, PET, PE, PS, PVC	Wang et al. (2020)

Ayaragi River, Japan	111880.0	PE, PP, PET, PS	Kabir et al. (2021)
Asa River, Japan	130000.0	PE, PP, PET, PS	Kabir et al. (2021)
Awano River, Japan	132800.0	PE, PP, PET, PS	Kabir et al. (2021)
Majime River, Japan	272500.0	PE, PP, PET, PS	Kabir et al. (2021)
Saigon River, Vietnam	354000.0	PE, PP, PES	Lahens et al. (2018)
Yellow River, China	744250.0	PE, PP, PS	Han et al. (2020)
Arakawa River, Japan	1780000.0	PE, PP, PS	Sankoda and Yamada (2021)
Rhône River, Swiss	0.9	PE, PP, PS	Faure et al. (2015)
Ebro River, Spain	3.5	PA, PE, PES, PP	Simon-Sánchez et al. (2019)
Elbe River, Germany	5.6	PE, PP	Scherer et al. (2020)
Ofanto River, Italy	6.0	PE, PP, PS, PVC, PUR	Campanale et al. (2020)
River Thames, UK	18.8	PE, PP, PA, PCV, PS,	Rowley et al. (2020)
Rhône river, France	19.0	PET, PS, PUR	Constant et al. (2020)
River Seine, France	30.0		Dris et al. (2015)
Venoge River, Swiss	35.3	PP, PE, PS	Faure et al. (2015)
Têt river, France	42.0	PES, PP, PE, PS	Constant et al. (2020)
Marne River, France	100.6	PET, PP, PA	Dris et al. (2018)
River Mignone, Italy	280.0	PE, PP, PA	Gallitelli et al. (2020)
Antuã River, Potugal	305.8	PE, PP, PS, PET, PTFE	Rodrigues et al. (2018)
Pita River, Ecuador	13.8		Donoso and Rios-Touma (2020)
San Gabriel River, USA	66.3	PS	Moore et al. (2011)

Snake & Comumbia Rivers, USA	910.0	PP, PE, PET, PES	Kapp and Yeatman (2018)
Hudson river, USA	980.0	PET, PVC, PP	Miller et al. (2017)
Gallatin River, USA	1200.0	PET, PVC, PA, PP	Barrows et al. (2018)
San Pedro River, Ecuador	1853.0		Donoso and Rios-Touma (2020)
Los Angeles River, USA	2305.8	PS	Moore et al. (2011)
Mississippi River, USA	46710.5	PES, PP	Scircle et al. (2020)

MP contaminated in river sediments and location	**Mean concentration (particles/kg sediment)**	**Main MP types**	**References**
Yongfeng River, China	26.0	PP, PE, PET, PS	Rao et al. (2020)
Ciwalengke River, Indonesia	30.3		Alam et al. (2019)
Naqu River	50.0	PET, PE, PP, PS, PA	Jiang et al. (2019)
Buqu River, China	130.0	PET, PE, PP, PS, PA	Jiang et al. (2019)
Brahmaputra River, China	132.5	PET, PE, PP, PS, PA	Jiang et al. (2019)
Shuangtaizi River, China	170.0	PET, PE, PP, PS, PA	Xu et al. (2020)
Gange River, India	210.1	PET, PE, PP	Sarkar et al. (2019)
Dailao River, China	237.0	PE, PET, PP	Xu et al. (2020)
Yongjiang River, China	285.0	PP, PE, PS, PET	Zhang et al. (2020)
Beijiang River, China	312.5	PET, PP	Wang et al. (2017)
Dongjiang River, China	604.0	PE, PP, PET	Fan et al. (2019)
Wei River, China	630.7	PE, PVC, PS	Ding et al. (2019)
Shanghai River, China	802.0	PP, PES, PET	Peng et al. (2018)

Pear River, China	1669.0	PE, PP	Lin et al. (2018)
Fengshan River, China	1673.2	PP, PA, PE	Tien et al. (2020)
Nakdong River, South Korea	1971.0	PP, PE	Eo et al. (2019)
Haihe River, China	4980.0	PE, PP, PS	Liu et al. (2020)
West River, China	5795.3	PP, PE, PVC, PET	Huang et al. (2021)
River Mignone, Italy	0.7	PE, PP, PA	Gallitelli et al. (2020)
Ombrone River, Italy	143.3		Guerranti et al. (2017)
Tet River, France	258.0	PES, PP, PE, PS	Constant et al. (2020)
Albegna River, Italy	279.0		Guerranti et al. (2017)
Osa River, Italy	285.5		Guerranti et al. (2017)
Kelvin River, UK	296.5		Blair et al. (2019)
Antuã River, Portugal	318.2	PE, PP, PS, PET, PTFE	Rodrigues et al. (2018)
Estuaries of River Thames, UK	349.5	PP, PES	Horton et al. (2017)
Rhine River, Germany	858.8	PE, PP, PS, PA	Klein et al. (2015)
Main River, Germany	1077.0	PE, PP, PS, PA	Klein et al. (2015)
Ebro River, Spain	2052.0	PA, PE, PES, PP	Simon-Sánchez et al. (2019)
Elbe River, Germany	2080.0	PE, PP	Scherer et al. (2020)
Rhine River, Germany	3805.0	PUR, PP, PS, PES, PA	Mani et al. (2019)
Meuse River, The Netherlands	139500.0		Donoso and Rios-Touma (2020)
Rhine River, Germany	329750.0		Donoso and Rios-Touma (2020)
James River, USA	39.8	PE, PP, PS, PET	Christensen et al. (2020)

Pita River, Ecuador	63.4		Donoso and Rios-Touma (2020)
San Pedro River, Ecuador	109.6		Donoso and Rios-Touma (2020)
Guayllabamba River, Ecuador	126.0		Donoso and Rios-Touma (2020)
Roanoke River, USA	137.0	PE, PP, PS, PET	Christensen et al. (2020)
St. Lawrence River, Canada	832.0		Crew et al. (2020)
Amazon River, Brazil	1208.0		Gerolin et al. (2020)
Solimões River, Brazil	1631.0		Gerolin et al. (2020)
Lake Ontario tributaries, Canada	4500.0	PE, PS, PUR	Ballent et al. (2016)
Negro River, Brazil	7023.5		Gerolin et al. (2020)
Bloukrans River, South Africa	83.2		Nel et al. (2018)
Brisbane River, Australia	126.3	PE, PP, PA	He et al. (2020)

2.2.4. Adverse effects and risk assessment of MPs

2.2.4.1. Adverse effects of MPs on the environment

MPs have significantly affected the river ecosystems because they cause a number of potentially biological interactions with river biota (McCormick et al., 2014). Rivers are considered as a sink to receive MPs, they are also the main source and transport MPs to downstream lakes and coastal environments. Therefore, rivers play an important role in the life cycle of global MPs (Donoso and Rios-Touma, 2020; McCormick et al., 2014) or are addressed as pollutant vectors because they can adsorb and then transfer harmful organic chemicals via ingestion pathway (Cole et al., 2011; Lebreton et al., 2017).

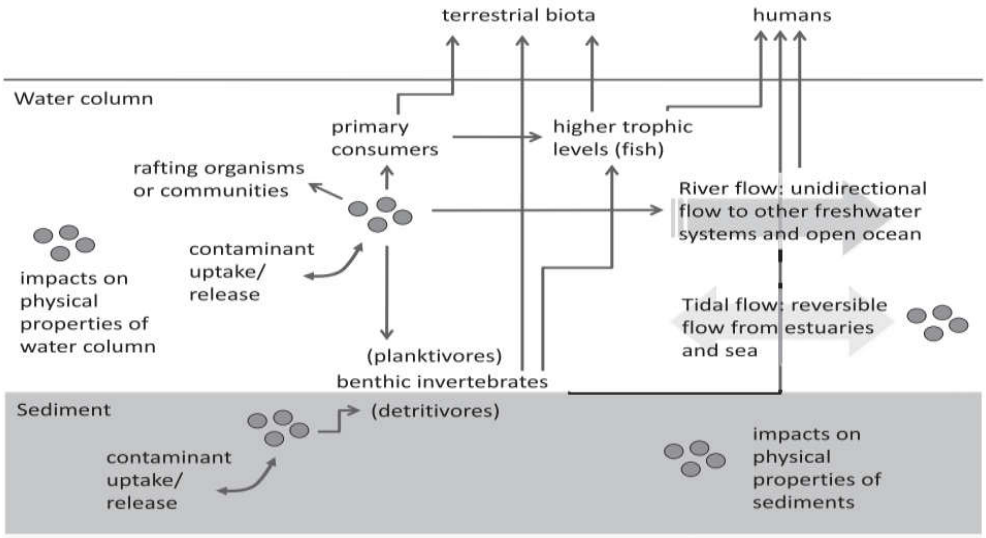

Figure 2.11. Diagram of MPs transport pathways in the environment (Eerkes-Medrano et al., 2015).

MPs become more serious and widespread ecological impacts than macro-plastics because they have small particles in size, originate from various sources (Klein et al., 2015), easily come to food-webs via ingestion pathway (Cole et al., 2011; Wagner et al., 2014). MPs containing additives such as plasticizers, flame retardants, antioxidants and stabilizers, which are easily released into environment (Liu et al., 2020). As a result, MPs can be seen as a vector

of organic contaminants and pathogens ingested by organisms and introduced into the food web (Barcelo and Pico, 2020). Plasticisers are considered toxic, resulting MPs may introduce toxins to the food chain and potential bioaccumulation for organisms via ingestion pathway (Cole et al., 2011). Pollutants, monomers and plastic additives can be transferred into organism bodies after they ingested MPs (Browne et al., 2011). Consequently, organisms could face with uncertain health effects (Browne et al., 2011). Moreover, organic airborne fibers have an aspect ratio > 3.1, and are mainly derived from surface and re-suspended (Li et al., 2020). These MPs may enter into human respiratory system (Barcelo and Pico, 2020).

Potential effects of MPs in water column, sediment, terrestrial biota and humans when they transfer in freshwater (**Figure 2.11**). Adsorbing or releasing contaminants is the main activity of MPs influencing directly other organisms such as rafting organisms, benthic invertebrates, fish in water and detritivores in sediments. In addition, Simpson et al. (2005) suggested that MPs affect the physical properties of water column e.g. altering light penetration due to accumulated in pelagic and benthic habitats, and sediments including the sizes and chemical binding capacity. In turn, these changes in water and sediment characteristics could affects back the biogeochemical cycles (Eerkes-Medrano et al., 2015). MPs also indirectly affects the terrestrial biota via food-webs, to humans via food-webs or river flows.

2.2.4.2. MP risk assessment

The index (H) of MPs for the specific polymers was firstly introduced by Lithner et al. (2011) containing 5 levels of hazards corresponding with grades, namely level I (<10), level II (10-100), level III (100-1000), level IV (1000-10000) and level V (> 10000) for each polymer. Recently, the risk categories (I, II, III and IV) to evaluate the risk level for MP pollution based on the values of the polymer index (H: <10, 10-100, 100-1000 and > 1000), and the pollution load index varies from less than 10 to over 30 (Wang et al., 2021; Zhou et al., 2020). These methodologies were similar to HI, which has been widely applied for effect of heavy metals

for human health. Wang et al. (2021) explored that Manas River, China was classified as risk levels of I-III varied from upstream to downstream and between sampling period of April and July. Additionally, Zhou et al. (2020) pointed out that among seven cities belong to Tuojiang River in China, Ziyang and Fushun were defined at great risk (category III), followed by three cites at level II, while the MP risks at Jianyang and Luzhou cities were relatively low as the category of I.

2.2.5. Interaction between MPs and arsenic

The association of MPs with metals, particularly the toxic elements like arsenic (As), has been received more attention, recently. The accumulation of metals on MPs in the environment has been widely investigated by using different types of MPs (He et al., 2020b; Vedolin et al., 2018; Wang et al., 2017). The concentrations of Al, Cr, Cu, Fe, Mn, Sn, Ti and Zn in pellets collected from São Paulo State beaches, Brazil provided high levels of Fe and Al (maximum of 227.78 and 45.27 mg/kg, respectively) (Vedolin et al., 2018). Regarding the types of MPs, the concentrations of Fe decreased as PP (7.6 mg/kg) > HDPE (4.1 mg/kg) > PE- Blue (3.3 mg/kg) > PE- Black (2.3 mg/kg), while the contents for As decreased as HDPE (16.0 mg/kg) > PE- Blue (7.4 mg/kg) > PP (5.7 mg/kg) > PE- Black (4.7 mg/kg). A study of Wang et al. (2017) showed high concentrations of Cd (2.16-17.56 mg/kg), Pb (38.24-131.11 mg/kg), Cu (80.9-500.6 mg/kg), Zn (2414.8-14815.3 mg/kg), and Ti (13617-38823.7 mg/kg) in the mixture of PE and PP films and fragments with their size < 5 mm (mainly 2-3mm) from the Beijiang River, China. To date, the interaction of MPs with arsenite [As(III)], a toxic metal classified as the first important carcinogen, was conducted in the laboratory conditions by Dong et al. (2019; 2020). The maximum adsorption amounts of As(III) on polytetrafluoroethylene (PTFE) were 1050, 980 and 910 mg/kg related to the particle's sizes of 100-1000 nm, 1000-10,000 nm and greater than 10,000 nm, respectively (Dong et al., 2019). Maximum adsorption capacity values of As(III) on PE were 920 mg/kg on the +10,000 nm particle size and up to 1120 mg/kg on the

100-1000 nm particle size (Dong et al., 2020). These findings indicated that PE has marginally higher As(III) adsorption capacity than PTFE, smaller sizes of MPs provided higher adsorbed amount of As(III). As a result, adsorption capacity of As on MPs was affected by surface area and types of MPs. These studies also pointed out that the adsorption behaviour of As(III) on these MPs were in accordance with the adsorption kinetics, adsorption isotherms of both Langmuir and Freundlich models. Moreover, these authors evaluated other parameters influencing the adsorption process of As(III) including pH, temperature, interfering nitrate and phosphate ions. The results showed that increasing in the pH, temperature and concentrations of interfering nitrate and phosphate ions led to a decrease in As(III) adsorption on PTFE and PE. Dong et al. (2020) explored the 16.3% of As(V) species after adsorption of As(III) on PE, indicating this MP had oxidation function with respect to As(III).

It is presumed that there are two proceeds of metals adsorption onto plastic resin pellets including interactions between '*bivalent cations and oxyanions with charged regions of*' plastics or via '*neutral metal-organic complexes and the hydrophobic plastic surface*' (Holmes et al., 2012; Naqash et al., 2020). Heavy metal adsorption on MPs were highly influenced by the large surface area, polarity, and organic polymer composition (Ahmed et al., 2021; Ashton et al., 2010). DOM, specific surface area, porosity and morphology are also other major factors affecting the adsorption of metals on MPs (Godoy et al., 2019). Related to As adsorption onto MP surface, Dong et al. (2020 and 2019) concluded that As(III) adsorbed on these PTFE and PE occurred on the carboxyl group through hydrogen bonding with the adsorbent surface (**Figure 2.12**), while the interactions of electrostatic forces and non-covalent were the key mechanisms of adsorption.

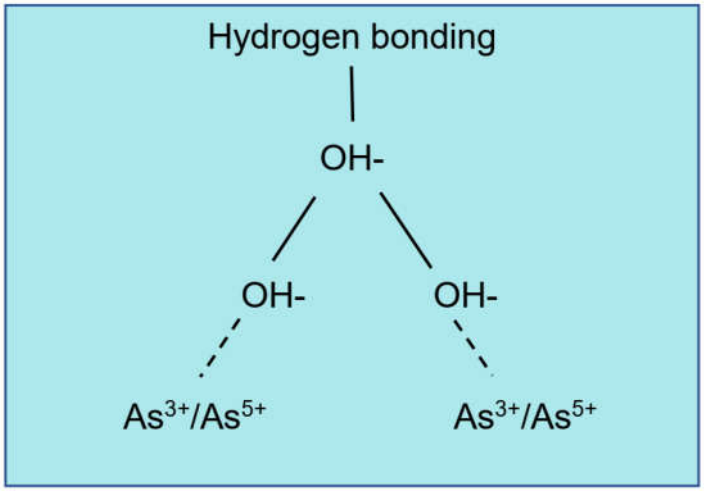

Figure 2.12. Adsorption mechanism on MP surface (Modified from Naqash et al., 2020).

2.2.6. Knowledge gap

The studies of MP abundance in the environments mentioned several limitations. They are the lack of standardised protocols and approaches for methods used in sampling and detecting MPs, investigating size classification, and units in expressing results lead to tough challenges of conducting samples and comparing data (Campanale et al., 2020; Wagner et al., 2014; Zhou et al., 2020). Moreover, models used for quantifying the risks of MPs including the quantification of human exposure to MPs, risk data and other parameters are put as another concern (Galafassi et al., 2019; Phuong et al., 2016; Zhou et al., 2020). The adsorption capacity of MPs for other contaminants is still limited related to MP behaviours and environmental fate (Wagner et al., 2014). Regarding to interactions with As, these studies above provided information of As(III) adsorption on specific MPs with various conditions. However, the adsorption mechanism of As(V) species, which is more dominant than As(III) in environments, has not been studied so far. Additionally, the impacts of some other environmental conditions such as bacteria, river water, seawater are needed to support further risk assessment.

CHAPTER THREE:

MATERIALS AND METHODS

3. CHAPTER THREE: MATERIALS AND METHODS

3.1. Sample collection and materials

River water and sediment were collected from Bargo River in May 2021 at the location of (34°14'35.1"S; 150°35'16.7"E), about 3km downstream of the Teatree Hallow creek, which receives treated wastewater for underground coal mining activity in New South Wales, Australia. Grab sampling methods of the bed material sampling was used to collect river water and sediment (Awal et al., 2019). Cleaned 5 L plastic containers were rinsed three times by river water, then filled up by river water, sealed before transporting to the laboratory and kept at room temperature for experiments. In addition, the cleaned 200 mL plastic bottles were rinsed three times before filling up by river water, then sealed by caps. The bottles were stored in a cool box at 4 °C when transferring to the laboratory for analysing the initial compounds. The sediment samples were packed in sealed polyethylene bags, then stored in a cool box at 4 °C when transferred to the laboratory. The sediment samples were dried in an oven at 105 °C for 24 hours, then passed through 2-mm sieve before further analysis.

Polystyrene (PS) and low-density polyethylene (LDPE) resin pellets (beads) purchased from Sigma-Aldrich Australia were used as the adsorbents. Multi-element standard solution 4 for ICP (As concentration of 40 mg/L) was supplied by Sigma-Aldrich Australia. The solution was diluted by Milli-Q water with a resistivity of 18 MΩ. Sodium arsenate ($HAsNa_2O_4.7H_20$) and sodium arsenite ($AsNaO_2$), purchased from Sigma-Aldrich Pty Ltd, were mixed with Milli-Q water for obtaining the stock solution of 100 mg/L of As(III) or As(V). The phosphoric acid (H_3PO_4, 85% w/w) and sodium hydroxylamine hydrochloride ($NH_2OH.HCl$, 99% purity) were also obtained from Sigma-Aldrich Pty Ltd. Then 1.0 M phosphoric acid solution was prepared by diluting the original standard solutions with Milli-Q water. 0.2 M hydroxylamine hydrochloride solution was prepared by adding 13.898 g sodium into 1 L Milli-Q water.

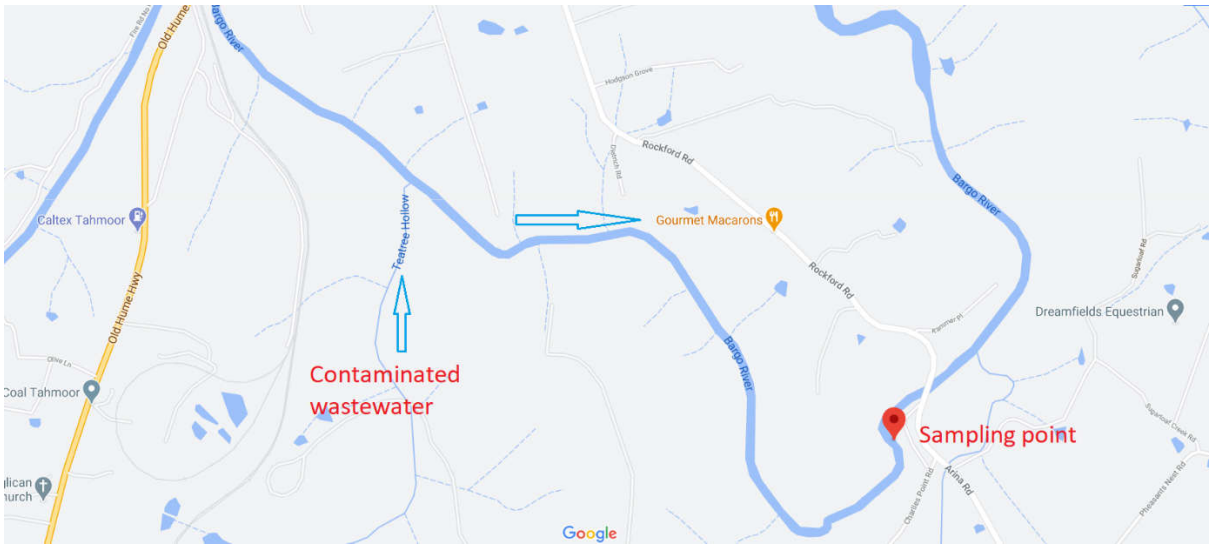

Figure 3.1. Pollution source and sediment sampling point.

3.2. Methods

3.2.1. Characterization or river sediment (RS) and river water (RW)

The content of SOM was determined by the loss-on-ignition (LOI) method, by sediment combustion at 550 ºC, according to Hoogsteen et al. (2018). The combusted sediment was named as river sediment without organic matter (RS-NOM). The sediment was fractionated by sieving through a series of sieve to obtain gravel and coarse sand (fraction S_1, 300-2000 µm), medium sand (fraction S_2, 150-300 µm), fine sand (fraction S_3, 75-150 µm), and clay-silt (fraction S4, < 75 µm). The specific surface area (SSA) of the dried sediment and different sizes were measured by a Quantachrome surface area analyser using the Brunauer–Emmett–Teller (BET) method.

The extraction of As from sediment was conducted by following a method described by Ellwood and Maher (2003). Briefly, sediment (1.0 g) was accurately weighed into each 50 mL Teflon centrifuge tube, to which 5 mL of 1.0 M of phosphoric acid and 5 mL of 0.2 M of hydroxylamine hydrochloride were added. The samples were shaken on a horizontal shaker at

120 rpm for 1 hour which were then centrifuged. Aliquots of the supernatant were removed and filtered through 0.45 µm filters, before As analysis. According to Ellwood and Maher (2003), around 90% of extractable As is obtained by using this method.

RW was analysed in triplicate to evaluate the metals concentrations (As, Fe, Al, Ni, Cu and Pb) by ICP-MS (Agilent 7900) and total organic carbon (TOC).

3.2.2. Batch adsorption and desorption experiments

The adsorption of As(III)/As(V) was assessed for various adsorbents including natural RS, sediment without organic matter (RS-NOM) content, particle sizes of 300-2000 µm (S_1), 150-300 µm (S_2), 75-150 µm (S_3) and 0-75 µm (S_4), PS, LDPE, SOM-PS and SOM-LDPE. The stock solution of 100 mg/L of As(III)/As(V) was diluted by distilled water (DI-water) or RW to obtain the solutions of 0.1-10 As mg/L. The adsorption experiments were conducted by mixing 200-mL of As(III) or As(V) (0.1-10.0 mg/L) with 2.0 g of sediment. The samples were kept at room temperature for 7 days (168h) and mixed on a shaker at 120 rpm for the first 2 days (48 h). During adsorption, 2 mL suspension samples were taken on regular intervals (3, 6, 12, 24, 72, 120 and 168 h), filtered by a 0.45 µm membrane filter, and analysed for total As by ICP-MS (Agilent 7900). The adsorption of As(III) or As(V) was evaluated by monitoring the decrease of arsenic concentration in the solution.

For the adsorption isotherm calculation, a series of As(III)/As(V) solutions with initial concentrations of 0.1, 0.25, 0.5, 1.0, 2.0, 5.0 and 8.0 mg/L were prepared by diluted stock solution from 100 mg/L by adding DI-water. Accurate 2.0 g sediment mixed with 200 mL solution was placed in 500 mL beaker for 7 days (168h) and mixed by a flatted shaker at 120 rpm for the first two days (48h). The pH of feeding solutions was adjusted to 4 ± 0.2 and 10 ± 0.2 by diluted nitric acid (0.1 M HNO_3) and sodium hydroxide (0.1 M NaOH).

Desorption experiments were immediately conducted in sequential decant-refill steps after the completion of adsorption process of As(III) and As(V) on RS, RS-PS and RS-LDPE. Supernatant was removed and replaced by 200 mL DI water or RW, the vials resealed and shaken at 120 rpm for 48 h. Aliquot (2 mL) was sampled from the supernatant at different reaction times (3, 6, 12, 24, 72, 120 and 168 h), then filtered and analysed for total As concentration using ICP-MS (Agilent 7900). The fractions of As(III) and As(V) desorbed from the adsorbents were calculated from the mass balance results based on the changes in As(III) and As(V) concentrations in solution before and after desorption.

3.2.3. Surface functional groups of sediment, PS, LDPE and minerals of sediment analysis

The FTIR-spectra (500-4000 cm^{-1}) of RS, RS-NOM, PS and LDPE before and after adsorption/desorption of As(III) and As(V) were analyzed by using IR-Spectroscopy (Shimadzu MIRacle 10, Japan) in order to investigate surface functional groups of these adsorbents involved in adsorption and desorption mechanisms. The sediment samples were ground to fine power before analyzed. Additionally, the X-ray Diffraction (XRD) method is widely used to explore the sedimentology research related to main minerals involved in sediment. The XRD analysis were conducted by Bruker D8 Discover XRD. RS surface before and after adsorption was examined by scanning electron microscopy (SEM) and energy dispersive X-ray spectroscopy (EDS) method by Oxford instrument, while X-Ray Photoelectron Spectroscopy (XPS) from Thermo Scientific was used to detect the surface of RS.

3.2.4. Sorption kinetic studies

Arsenic concentrations retained in the adsorbent phase (mg/kg) were calculated by following formula:

$$q_t = \frac{(C_o - C_t)V}{m} \quad (1)$$

$$q_e = \frac{(C_o - C_e)V}{m} \quad (2)$$

where q_t (mg/kg) and C_t (mg/L) are the concentrations of As(III) or As(V) in sediment and solution at time t; q_e (mg/kg) and C_e (mg/L) are the concentrations of As(III) or As(V) in sediment and solution at the equilibrium time; C_o (mg/L) is As(III) or As(V) concentration at the initial time; V (mL) is volume of solution; m is the weight of adsorbent (g).

The pseudo-first-order (PFO) and pseudo-second-order (PSO) equations have been widely applied to assess the adsorption of As on soils, sediments and MPs (Dong et al., 2020, 2019; Gedik et al., 2016; Guo et al., 2007; Kumar et al., 2016; Kundu and Gupta, 2006; Luo et al., 2019; Ma et al., 2015; Rawat et al., 2021). The PFO model can well describe the initial adsorption stage (Ho and McKay, 1999; Ma et al., 2015), while the PSO model was better for describing the physical or chemical adsorption at a site (Kumar et al., 2016) or the whole adsorption process (Ma et al., 2015).

The adsorption experimental data was analysed by adsorption kinetic PFO and PSO models using non-linear regression equation described by (Alkurdi et al., 2021; Ma et al., 2015). The linear forms of PFO and PSO kinetic models are straightforward for application, however, the erroneous values of calculating kinetic parameters were the drawbacks (Azizian, 2004). In contrast, the non-linear forms provided better results in comparison to linear regression analysis (Rawat et al., 2021). Thus, the non-linear forms of PFO and PSO models for the adsorption kinetics are used in this study (Ma et al., 2015):

$$q_t = q_e(1 - e^{-k_1 t}) \quad (3)$$

$$q_t = \frac{q_e^2 k_2 t}{1 + q_e k_2 t} \quad (4)$$

Another model commonly applied for simulating the kinetics of adsorption is Elovich equation, which was developed by Roginsky and Zeldovich (López-Luna et al., 2019; Plazinski et al., 2009) as below:

$$q_t = \frac{1}{\beta}\ln(1 + \alpha\beta t) \quad (5)$$

where q_t is the amount (mg/kg) of As(III) or As(V) adsorbed at time t; q_e is the amount (mg/kg) of As(III) or As(V) at the equilibrium; k_1 (1/h) is the equilibrium rate constant of the PFO model; k_2 (kg/mg-h) is the equilibrium rate constant of the PSO model; α is the Elovich initial adsorption rate (mg/kg min) and β is desorption constant (kg/mg).

For the desorption process, the PFO and PSO models are described as below (Tseng et al., 2009):

$$q_t = q_e + (q_o - q_e)\exp(-k_1 t) \quad (6)$$

$$q_t = q_e + \frac{q_e - q_o}{k_2(q_e - q_o)t - 1} \quad (7)$$

where q_o is the amount (mg/kg) of As(III) or As(V) at the initial time of desorption.

3.2.5. Sorption isotherm study

The adsorption phenomenon at the interface between solid and liquid phases is widely interpreted by the Langmuir and Freundlich adsorption isotherms (Tseng et al., 2009).

The Langmuir isotherm model is used to describe the mono-molecular layer adsorption, which is expressed as below (Rawat et al., 2021):

$$q_e = \frac{K_L q_m C_e}{1 + K_L C_e} \quad (8)$$

where K_L and q_m represent the bonding energy constant (mg/L), and the maximum adsorption capacity (mg/kg) from the Langmuir equation.

Additionally, the equilibrium parameter (R_L) was used to explain the essentiality of Langmuir adsorption isotherms by the following equation (Rawat et al., 2021):

$$R_L = \frac{1}{1+K_L C_e} \quad (9)$$

The values of $R_L > 1$, $0 < R_L < 1$, $R_L = 1$, and $R_L = 0$ indicate unfavourable, favourable, linear and irreversible of As(III) and As(V) adsorption on the surface of sediment particles, respectively (Rawat et al., 2021).

The Freundlich sorption model is an empirical adsorption equation indicating that adsorption sites on the surface of adsorbent possess different adsorption energies, which can be expressed as (Wang et al., 2018):

$$q_e = K_F \times C_e^{1/n} \quad (10)$$

where K_F is the Freundlich constant or capacity factor (mg/kg-(L/mg)^n), while $1/n$ is the Freundlich exponent. The n value < 1 indicates the ordinary adsorption while co-operative adsorption and more surface heterogeneity are referred by n > 1 and nearer to zero (Rawat et al., 2021).

A three-parameter isotherm model, Sips is formed by the combination from Langmuir and Freundlich expressions (Alkurdi et al., 2021). This model reduces to the Freundlich model at the low adsorbate concentrations or to the Langmuir model while the adsorbate concentrations are high (Foo and Hameed, 2010).

$$q_e = \frac{q_m K_s C_e n_s}{(1+K_s C_e n_s)} \quad (11)$$

Where K_s is the Sips constant related to the energy of adsorption process, and n_s is the exponential factor of the isotherm.

3.2.6. Partition coefficient

The solid-solution partition coefficient (K_p) was used to describe the interactions of heavy metals at interface of water phase and sediment (Fang et al., 2021). K_p provides the information of combined effect of desorption and adsorption processes of heavy metals (Nematollahi et al., 2021). In addition, it also was used for modelling trace metal transfer in

various catchment scales or hydraulic systems such as rivers or lakes. Garneau et al. (2015) used Kd as a sub-model of adsorption and desorption process to simulate As transport in the Garonne River, France. In this study, this relationship was described as the partition coefficients to determine the relationship the concentrations of As in sediment-water phases (Zhou and Broodbank, 2014):

$$K_p = \frac{q_e}{C_e} \text{ (kg/L)} \quad (12)$$

CHAPTER FOUR:

ADSORPTION-DESORPTION OF ARSENIC SPECIES ON RIVER SEDIMENTS ON THE ASSOCIATED MECHANISM

4. CHAPTER FOUR: ADSORPTION-DESORPTION OF ARSENIC SPECIES ON RIVER SEDIMENTS ON THE ASSOCIATED MECHANISM

This chapter covers the contents of a published review paper: **Kien Thanh Nguyen**, Amir Navidpour, Mohammad Boshir Ahmed, Amin Mojiri, Yuhan Huang, John L. Zhou (2022) Behaviour and mechanism of arsenite and arsenate adsorption and desorption at river sediment-water interface. *Journal of Environmental Management.* (Accepted 6 June 2022)

4.1. Introduction

As contamination in soils, sediments, surface water and groundwater has been long monitored due to significant threat to plants, animals and human health due to its highly toxic level (Dousova et al., 2012). Natural and anthropogenic processes cause an increasing amount of As into sediments and water environment (Goldberg and Suarez, 2013; Zhang and Selim, 2005). As contamination in soils and sediments mainly derives from anthropogenic activities (Dousova et al., 2012), among which mining is the second largest source contributing to highly contaminated As levels in environments (Akter et al., 2006). As(III) and As(V) are the soluble forms of As existing in the natural environment (Arco-Lázaro et al., 2016). As(V) is prevalent under oxidising conditions, whilst As(III) form is predominant under reducing conditions (Dousova et al., 2012). Great abundance and high toxicity of inorganic arsenics [As(III) and As(V)] have received high attention from scientists to examine As transportation behaviour (Wang et al., 2018).

Adsorption is a key process regulating As transport in the aquatic environment. Adsorption kinetics, mechanisms and controlling parameters (pH, temperature, organic carbon, texture, clay minerals, phosphorus and cations) have been studied (Arco-Lázaro et al., 2016;

Dousova et al., 2012) to have a better understanding of As sorption mechanisms. Effect of pH on As adsorbed on sediments has been investigated by Ma et al. (2015), with amount of As(III) and As(V) adsorbed on sediment increased when pH decreased from 5 to 9. Adsorption of As is highly dependent on sediment properties (Xie et al., 2018) and other parameters. Environmental parameters and sediment properties have been examined to evaluate the fate and transport characteristics of As in sediment. Sediment organic matter (SOM) has negative impacts on As adsorption, whilst smaller particle size of sediment texture enhances As adsorption on soils (Nguyen et al., 2021). It was suggested that the negative charge of humic acid (HA) and fulvic acid (FA), two types of SOM, had a high affinity for adsorption to the metal (hydro)oxide surface, resulting in competing of As(III) and As(V) with HA and FA was the adsorption mechanism on the solid surfaces (Wang and Mulligan, 2006a). However, the authors explained that As(III) and As(V) anions may be bound with the formation of SOM-metal complexes through metal-bridging mechanisms, in which these As species form aqueous complexes with HA and FA. In addition, SOM could control the release of As(V) from solid phase regardless of the adsorption mechanism (Grafe et al., 2001). Varsányi and Kovács (2006) showed a strong correlation between As and sediment organic carbon (SOC) at low SOC (0.04%) and Fe (4.91 g/kg) concentrations, but no correlation was observed at high SOC (0.775% and 0.810%) and Fe (0.09 and 0.29%) concentrations, however, it can be found how was the influence of only SOC. Therefore, As(III) and As(V) adsorption on sediment influencing by SOM was still not clear to conclude. Regarding grain size of sediment, Dias et al. (2009) considered sediment textural fractions as the most important parameter influencing As(V) adsorption on sediments. Smith et al. (2006) and Xie et al. (2018) found that decreasing particle size, with sand < silt < clay led to an increase in the adsorption of total and inorganic As species on sediments. For instance, the adsorption capacity of As(III) on sediments increased from 1.57 to 2.62 mmol/kg for sandy and clay types, and from 2.81 to 5.13 mmol/kg

for As(V) (Xie et al., 2018). The impacts of particle sizes from different sediments on As(III) and As(V) adsorption were clear when comparison among different sediment, however, the contribution of only fraction sizes is still needed to investigation.

The adsorption and desorption rates of As on sediments were observed by Xie et al. (2018). They found that As(III) and As(V) had rapid adsorption rates during the first two days, slowed down in the next 5 days, and then became relatively stable until 28 days. Similarly, the release of As from sediment into water rapidly decreased at initial stage (7-day), followed by a slow rate. Furthermore, the desorption rate of As(V) was lower than that of As(III), with a maximum of 40% compared to 60% (Xie et al., 2018). Overall, As adsorption from water and its controlling factors have been widely investigated. However, the desorption process and consequent migration to the environment are greatly important, though the study on As desorption was limited to soils (Feng et al., 2013).

In river sediments, As predominantly exists as arsenite [As(III)] in the anoxic zone, and as arsenate [As(V)] in the oxic surface layer (Akter et al., 2006; Dousova et al., 2012). The crustal earth has the average As abundance of 1.5 mg/kg, varying from <1 to 15 mg/kg in alluvial sands, glacial till, lake sediments and soils (Plant et al., 2005). According to Hettiarachchi et al. (2017), only inorganic species were present in mangrove sediments located in southeast New South Wales, Australia. Even low concentrations, contaminated As in river sediment can cause tremendous harm to living organisms (De Jonge et al., 2012; Tang et al., 2017). Adsorption and desorption studies of As on river sediment are limited. Therefore, it is necessary to explore the adsorption and desorption mechanisms of As on river sediments, which have a vital role in removing As from the water or are considered as a secondary pollution sink releasing As into the water (Chen et al., 2016).

The sorption behaviour of As on sediments were reported (Dousova et al., 2012; Goldberg and Suarez, 2013; Ma et al., 2015); however, the contribution of sediment

physicochemical characteristics to As adsorption or retention was still not entirely. Therefore, the mechanism of interaction between As species and sediment surface ligands was investigated in this study in order to have a deeper understanding and sustainable management strategies for arsenic contaminated sediments. This chapter aims to examine the adsorption kinetics, adsorption isotherms and sorption mechanisms of inorganic As species on river sediment under different conditions.

4.2. Material and Methods

4.2.1. Materials and soil preparation

The detailed descriptions about the sample collection, sediment preparation and materials are reported in **Chapter 3.1**.

4.2.2. Adsorption and desorption experiments

The adsorption of As(III)/As(V) was assessed for various characteristics of sediment including natural sediment (RS), natural sediment without organic matter (RS-NOM) content and four particle sizes including 300-2000 µm (S_1), 150-300 µm (S_2), 75-150 µm (S_3) and 0-75 µm (S_4). The stock solution of 100 mg/L of As(III)/As(V) was diluted by DI-water to obtain the solutions of 10 As mg/L. The adsorption experiments were conducted by mixing 200-mL of As(III) or As(V) (0.1-10.0 mg/L) with 2.0 g of sediment. The samples were kept at room temperature for 7 days (168h) and mixed on a shaker at 120 rpm for the first 2 days (48 h). During adsorption, 3 mL suspension samples were taken on regular intervals (3, 6, 12, 24, 72, 120 and 168 h), filtered by a 0.45 µm membrane filter, and analysed for total As by ICP-MS (Agilent 7900). The decrease of arsenic concentration in the solution was observed to evaluate the adsorption of As(III) or As(V).

For the adsorption isotherm calculation, a series of As(III)/As(V) solutions with initial concentrations of 0.1, 0.25, 0.5, 1.0, 2.0, 5.0 and 8.0 mg/L were prepared by diluted stock solution from 100 mg/L with DI-water. Accurate 2.0 g sediment mixed with 200 mL solution was placed in 500 mL beaker for 7 days and mixed by a flatted shaker at 120 rpm for the first two days.

The desorption experiments were immediately conducted in sequential decant-refill steps after the completion of adsorption process of As(III) and As(V) on SOM. Supernatant was removed and replaced by 200 mL Milli-Q water, the vials resealed and shaken at 120 rpm for 48 h. Aliquot (3 mL) was sampled from the supernatant at different reaction times (3, 6, 12, 24, 72, 120 and 168 h), then filtered and analysed for total As concentration using ICP-MS (Agilent 7900). The mass balance results based on the changes in As(III) and As(V) concentrations in solution before and after desorption were used to calculate the fractions of As(III) and As(V) desorbed from the RS.

4.2.3. Experimental analysis

The RS characteristics, adsorption and desorption kinetics, adsorption isotherms and partition coefficient are described in **Chapter 3 (3.2.3-3.2.6**).

4.3. Results and discussion

4.3.1. Characteristics of river sediment

Total As content and other physicochemical characteristics of the river sediment compared to other sediments collected in New South Wales, Australia are given in **Table 4.1**. In this study, the concentrations of metals were lower than those from Fleming et al. (2021), who collected the samples closer to coal mining. **Table 4.1** indicated that water quality in sediments in New South Wales related to heavy metals are influencing by coal mining activities, although the

concentrations of heavy metals are below the guideline values for sediment in Australia. Thus, the selected sediment in this study is not contaminated above background value. In addition, these heavy metal concentrations were less than those of other sediments collected from several ports in New South Wales (Jahan and Strezov, 2018). It is suggested that the treated wastewater from mining activities in the upstream area causes marginal effect on polluted sediment in the downstream. As concentration (0.16 mg/kg) in this sediment was remarkably lower than average concentrations of As (32.0 mg/kg) in three mangrove surface sediments collected at Candalagen creek, Batemans bay and Sussex inlet in southeast New South Wales, Australia (Hettiarachchi et al., 2017). The SSA of the river sediment was 4.60 m^2/g, which was between those of two sediments collected from the Elbe River basin in Czech Republic (7.30 m^2/g and 3.50 m^2/g) (Dousova et al., 2012). This value was also smaller than that for goethite, kaolinite and oak bark char, but higher than pine wood char, oak wood char and pine bark char investigated by Mohan and Pittman (2007). The SOC content of the Bargo river sediment was lower than any sediments investigated by Dousova et al. (2012).

Table 4.1. The composition of the Bargo River sediment (in triplicate), in comparison to other sediments in New South Wales, Australia.

	SSA (m^2/g)	SOM (%)	SOC (%)	Al (mg/kg)	Fe (mg/kg)	As (mg/kg)	Cr (mg/kg)	Ni (mg/kg)	Zn (mg/kg)	Cd (mg/kg)	Pb (mg/kg)	Reference
Bargo River	4.60	0.40	0.046	33.7±7.9	36.7±9.9	0.2±0.05	).08± 0.008	0.1±0.02	1.8±0.02	0.06±0.001	0.2±0.08	This work
Bargo River				3000	5800	< 4	4	3	20		5	Fleming et al. (2021)
Coxs River				5800	30000	16	8	13	43		6	Fleming et al. (2021)
Wollangambe River				270	900	< 4	< 1	< 1	1		< 1	Fleming et al. (2021)
Georges River				1100	4000	< 4	2	1	5		2	Fleming et al. (2021)
Redbank Creek				4000	33000	8	16	6	33		11	Fleming et al. (2021)
Nepan River				990	2400	< 4	2	1	4		2	Fleming et al. (2021)
Port Jackson				895±7	7300±142	6	4	3±1	85±7		18	Jahan and Strezov (2018)
Port Botany				930±28	765±248	-	2±1	-	7±3.6		2	Jahan and Strezov (2018)
Port Kembla				1250±212	8000 ± 778	18.5±20	11±3	20±20	235±78		74±66	Jahan and Strezov (2018)
Port Newcastle				1550±778	5300±566	4	4	3	78 ± 3		24	Jahan and Strezov (2018)
Port Yamba				383±78	760± 198	0	1	-	3		1	Jahan and Strezov (2018)
Port Eden				2250±354	46000 ± 46669	29±30	31±17	12±4	2345 ± 2057	0.6	165±205	Jahan and Strezov (2018)
DGV						20	80	21	200	1.5	50	AGI (2019)

DGV: Australian default guideline values for sediment quality.

4.3.2. Effects of pH, sediment properties and initial As solution on adsorption kinetics

Figures 4.1a and **b** depict the time variation of As(III) and As(V) concentrations in RS with the different pH levels (4, 10 and uncontrolled conditions) in aqueous media. By doing this, the experiments examined the statement that "the adsorption of As(V) in sediments is stronger under acidic condition (pH varies 3.7-7.0) and weaker under alkaline conditions (pH 8-10), while the effect h pH on As(III) is weakened" (Chen et al., 2016; Maji et al., 2007; Mamindy-Pajany et al., 2011). Therefore, selecting the low acidic and high alkaline pH levels would provide the better results. The PFO and PSO models were well fitted experimental data in accordance with the correlation coefficient (R^2), varied 0.980 and 0.999 for As(V) and slightly higher for As(III), at 0.995-0.998 (**Table 4.2**). The amounts of As(III) adsorbed on RS estimated were 109.92 mg/kg (pH 4) and 89.39 mg (pH 10) by PSO, which were better than those by PFO, at 104.03 mg/kg (pH 4) and 84.41 mg/kg (pH 10). The results for As(V) were less accurate in comparison to As(III), at 168.13 mg/kg (pH 4, PFO), 88.18 mg/kg (pH10, PFO), 203.28 mg/kg (pH 4, PSO), and 97.73 mg/kg (pH 10, PSO), respectively. The results from PSO for As(V) were a bit far away from experimental data. It can be found that As(III) was favourable in alkali condition because its concentrations in sediment at the equilibrium time of pH 4 (112.35 mg/kg) were higher than those of pH 10 (89.03 mg/kg) or without controlling pH (RS) (105.64 mg/kg, respectively). However, at neutral pH (RS), As(V) concentration in sediment was highest at 168.63 mg/kg, which was slightly higher than its concentration at pH 4 (167.11 mg/kg) and pH 10 (91.29 mg/kg) (**Table 4.2**). The results for As(V) agreed with the statement that As(V) adsorbed on sediment, which was generally stronger under acidic conditions and weaker under alkaline conditions (Chen et al., 2016; Mamindy-Pajany et al., 2011), while pH had less effect on As(III) than As(V) due to its incomplete ionized state (Chen et al., 2016). Adsorption of As(III) and As(V) on sediment decreased when pH degrees increased and higher adsorption capacity for As(V) than As(III) in all pH conditions (5, 7, 9) (Ma et al., 2015). This study agreed with those findings, except for the highest adsorption capacity for As(V).

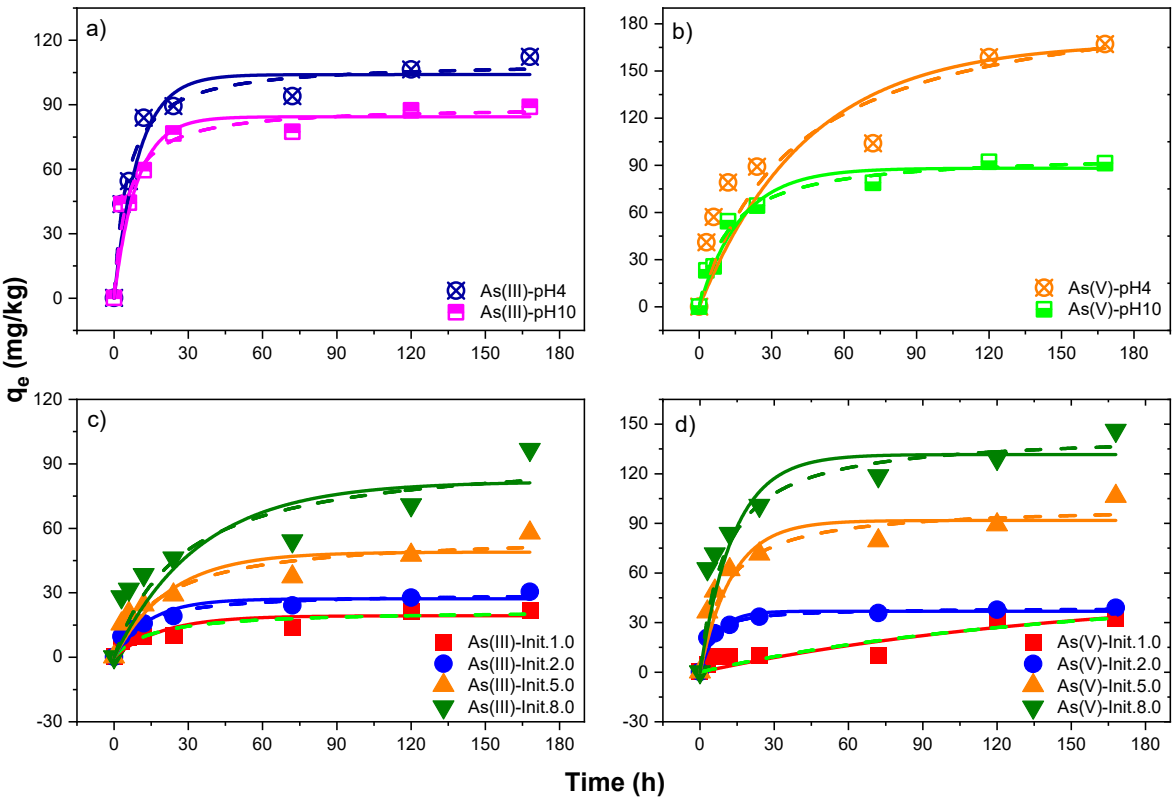

Figure 4.1. Effect of pH (a, b) and initial As concentrations in solution (c, d) on the adsorption of As(III) and As(V) on the RS. Symbols are experimental data; the straight and dash lines represent the PFO and PSO kinetic models.

Adsorption of As(III) and As(V) on sediment at varying As concentrations (1 – 8 mg/L) is shown in **Figure 4.1(c** and **d)**. As(III) and As(V) adsorption rates showed initial rapid stage up to 24h, followed by a slow stage at the end of observation time. It was suggested that a rapid increase in As adsorption caused by the enhancement in the specific surface area and presence of more active surface groups of solid particles (Rawat et al., 2021). The PFO and PSO exhibited well with experimental data, with the R^2 values ranged 0.953-0.999 and 0.989-1.000 for As(III) and As(V), respectively, except the data for As(V) at initial concentrations of 1.0 mg/L. The q_e values were 50.02 and 71.07 mg/kg estimated from PFO and PSO, in comparison with experimental data (32.61 mg/kg). Other results were closed to the experimental data (**Table 4.2**).

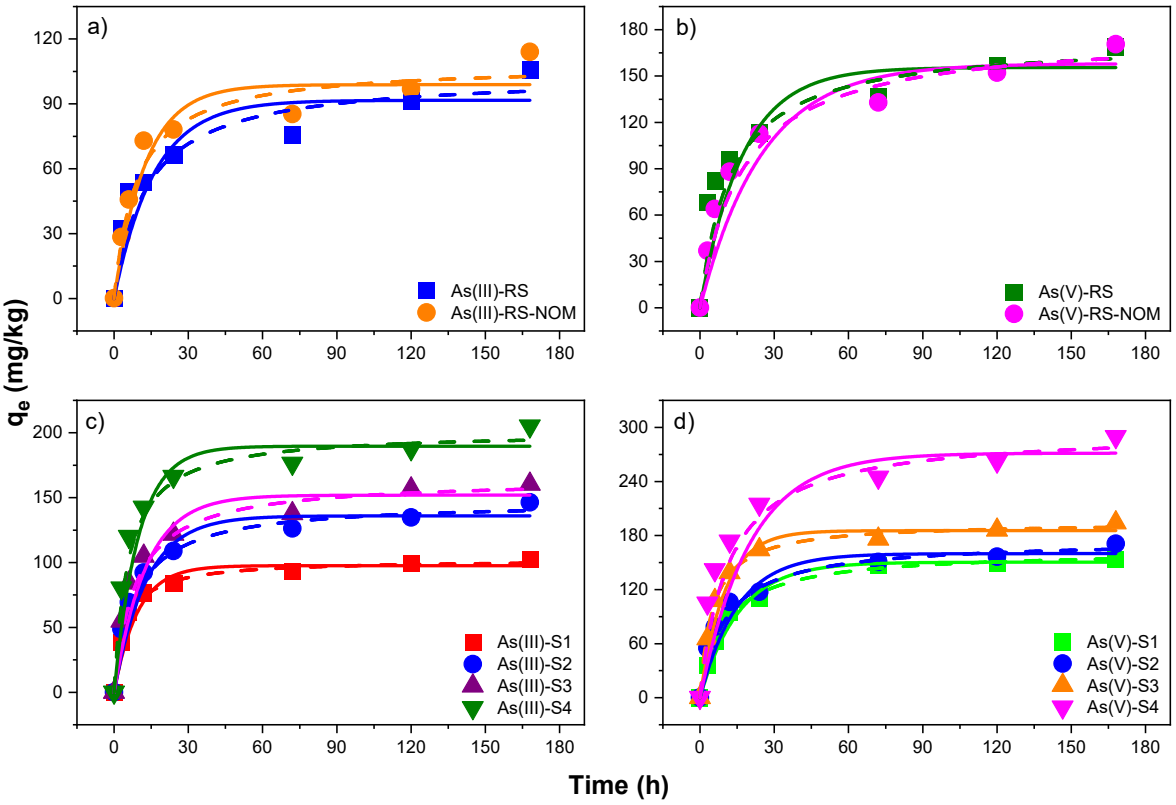

Figure 4.2. Effect of RS and RS-NOM (a, b) and sediment fraction sizes (c, d) on the adsorption of As(III) and As(V) on the river sediment. Symbols are experimental data, and the straight and dash lines represent the PFO and PSO kinetic models.

Effects of RS and RS-NOM on As(III) and As(V) adsorption on sediment are shown in **Figure 4.2(a** and **b)**. The experimental data of As(III) and As(V) adsorption were in good exhibition of the PFO and PSO models. The R^2 values were at 0.987-1.000 for As(III) and 0.989-0.995 for As(V). The q_e estimated by PSO for As(III) and were better than by PFO, at 103.52 mg/kg (RS) and 108.39 mg/kg (RS-NOM) compared to 91.65 mg/kg (RS) and 98.87 mg/kg (RS-NOM), however these values were lower than experimental data. The degrees of q_e for As(V) from PFO showed the similar trend, at 155.58 mg/kg and 158.06 mg/kg for RS and RS-NOM, whilst the PSO provided higher q_e values for both RS (173.49 mg/kg) and RS-NOM (178.00 mg/kg). The amount of As(III) on RS-NOM from the experiment was 114.03 mg/kg at the equilibrium, which was 8% higher than that of RS (105.64 mg/kg), whilst the values for As(V) was slightly higher (170.64 mg/kg compared to 168.63 m/kg, respectively). Dousova et al. (2012) found that an

increasing of organic matter and Fe contents led to an increase in adsorption capacities of As(V) on three sediments. However, the adsorption capacity of As(III) only increased with the increase of Fe contents. Xie et al. (2018) pointed out that adsorption of As(III) and As(V) on three sediments increased with increasing the organic matter and clay contents. It is hard to conclude that this study revealed the contradictory results to these outcomes. This comparison may not be completely accurate because the two investigations above used different types of sediment with different characteristics, while only one type of sediment was used in this study and other characteristics of the selected adsorbent are assumed as unchangeable. An illustration is that humic acid can bind a portion of As through positively charged amine groups (Varsányi and Kovács, 2006). It is suggested that As adsorption on RS is partly prevented because organic matter may inhibit the binding of As(III) and As(V) with functional groups of sediment surface.

Table 4.2. Kinetic parameters and equilibrium adsorption capacity of Bargo River sediment from the PFO and PSO models.

As	Exp. conditions	PFO			PSO			q_e[c] (mg/kg)
		R^2	K_1 (1/h)	q_e[a] (mg/kg)	R^2	K_2 (kg/mg-h)	q_e[b] (mg/kg)	
Adsorption								
As(III)	pH 4	0.995	0.103	104.03	0.9968	0.0017	109.92	112.35
	pH 10	0.997	0.109	84.41	0.9983	0.0022	89.39	89.03
	Conc. 1.0	0.998	0.052	19.33	0.9530	0.0030	21.89	21.95
	Conc. 2.0	0.999	0.071	27.23	0.9616	0.0032	30.04	30.50
	Conc. 5.0	0.992	0.045	48.95	0.9600	0.0009	57.09	57.90
	Conc. 8.0	0.975	0.029	81.76	0.9826	0.0004	95.61	96.65
	RS	0.987	0.062	91.65	0.9996	0.0007	103.52	105.64
	RS	0.988	0.078	98.87	0.9893	0.0010	108.39	114.03
	S_1	0.998	0.106	97.64	0.9994	0.0021	102.33	102.20
	S_2	0.995	0. 077	135.99	0.9982	0.0008	147.19	146.37
	S_3	0.993	0.078	151.94	0.9974	0.0007	164.60	160.46
	S_4	0.993	0.106	189.68	0.9960	0.0009	200.93	205.20
As(V)	pH 4	0.980	0.023	168.13	0.984	0.0001	203.28	167.11
	pH 10	0.997	0.058	88.18	0.999	0.0008	97.73	91.29
	Conc. 1.0	0.993	0.065	50.02	0.994	0.0001	71.07	32.61
	Conc. 2.0	0.999	0.143	36.90	1.000	0.0067	38.86	39.00
	Conc. 5.0	0.989	0.077	91.77	0.993	0.0010	100.81	106.38
	Conc. 8.0	0.990	0.074	131.68	0.995	0.0007	144.66	146.22
	SOM	0.989	0.059	155.58	0.995	0.0005	173.49	168.63
	NOM	0.989	0.040	158.06	0.995	0.0003	178.00	170.64
	S_1	0.999	0.064	105.42	1.000	0.0006	163.37	153.22
	S_2	0.995	0.067	159.93	0.998	0.0005	175.09	170.88
	S_3	0.997	0.101	185.41	0.999	0.0010	194.90	194.22
	S_4	0.990	0.049	271.42	0.996	0.0003	296.27	289.75
Desorption								
As(III)	RS	1.000	0.142	98.56	1.000	0.028	98.07	98.49
As(V)	RS	1.000	0.188	162.42	1.000	0.043	162.00	162.01

a. estimated equilibrium adsorption capacity from the PFO model.

b. estimated equilibrium adsorption capacity from the PSO model.

c. estimated equilibrium adsorption capacity in the experiments.

Figure 4.2(c and **d)** exhibit the PFO and PSO models for As(III) and As(V) adsorption on the sediment fraction sizes. The results indicated that a fast stage of adsorption occurred in first 24h, then the adsorption rate decreased for rest of experimental observation. Similarly, other conditions, PFO and PSO models provided high R^2 values (at least 0.990) for all As(III) and As(V) adsorption (**Table 4.2**). It can be seen that there was a marginal difference on As(III) adsorption between S_2 and S_3, while As(V) adsorption on S_1 was closed to S_2. As(III) and As(V) adsorption was also affected by the initial As concentrations and sediment fraction sizes. **Table 4.2** shows that at the equilibrium, the adsorption capacity for As(III) increased from 102.20 mg/kg for the largest size (S_1) to 146.37 mg/kg for S_2, 160.46 mg/kg for S_3 and 205.20 mg/kg for the smallest size (S_4). This value for S_4 was nearly double those of RS at the same time. Regarding As(V) adsorption, the q_e values were 153.22, 170.88, 194.22 and 289.75 mg/kg for S_1, S_2, S_3 and S_4, respectively (**Table 4.2**). As(V) adsorption capacities on different sizes of sediment were higher than those of As(III). Xie et al. (2018b) showed similar results in higher adsorption affinity for A(V) than As(III) related to the smaller fraction sizes regardless of sediment sizes. Based on the surface area analysis including SOM (4.6 m^2/g), S_1 (3.1 m^2/g), S_2 (6.0 m^2/g), S_3 (6.5 m^2/g) and S_4 34.2 m^2/g), S_1 had smaller surface area than RS, resulting in less adsorption capacity, while S_2, S_3 and S_4 showed higher adsorption than RS due to larger surface areas. It is clear that the smaller sediment fraction sizes than natural size had a positive impact on As(III) and As(V) adsorption, whilst larger size showed a negative effect.

According to López-Luna et al. (2019), the nonlinear form of PFO needs to be carefully applied due to linear adjustment failure, while PSO model provided better results for low initial solute concentrations (Azizian, 2004). PSO generally provided better results in kinetic adsorption of both As(III) and As(V) than PFO based on the R^2 and the q_e values. The results revealed the statement of López-Luna et al. (2019) that it is highly recommended to apply PSO nonlinear model due to advantages in calculating the adsorption values at equilibrium and initial

adsorption rate. However, Ma et al. (2015) reported that better results evaluated by PFO than PSO while the R^2 were not significant different between two models.

4.3.3. Kinetic models for desorption process of As(III) and As(V)

The desorption kinetics of As(III) and As(V) adsorption on RS were displayed by PFO and PSO models (**Figure. 4.3**). It can be seen that the high rate desorption at initial stage (0-12h), followed by stable rate for the remaining time. The amount of As(III) in sediment reduced from 105.638 mg/kg at the beginning to 100.16 mg/kg at 12h, then finished at 98.49 mg/kg at the equilibrium time. For the As(V), the concentrations in sediment were 168.63, 163.02 and 162.01 mg/kg at these observation time, respectively. The results supported for the statement of Ho and McKay (1999) and Ma et al. (2015) that PFO model can well described at the first step of kinetic sorption rather than the late time. The concentrations of As adsorbed on RS at the equilibrium time calculated PFO and PSO models were closed to the experimental data. Amounts of As(III) were 98.56 mg/kg and 98.07 mg/kg from PFO and PSO, whilst the results for As(V) were 162.42 mg/kg and 162.00 mg/kg, respectively (**Table 4.2**). Moreover, the PSO model well fitted with all experimental data, indicated that the physicochemical sorption including surface complexation and the sorption sites' diffusion was associated with the desorption processes of both As(III) and As(V). Consequently, the desorption of As(III) and As(V) on RS was similar behaviour in terms of adsorption kinetics.

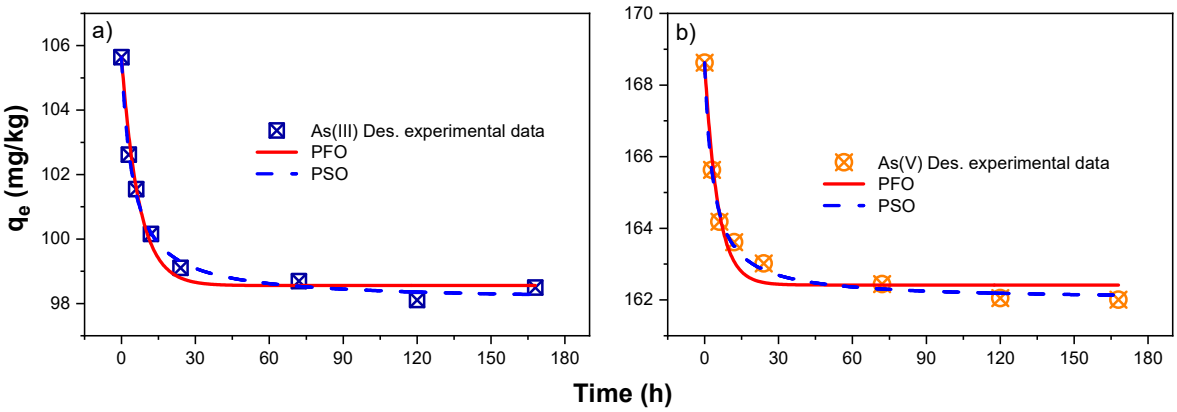

Figure 4.3. The nonlinear regression in the PSO and PSO kinetic models of As(III) and As(V) desorption on the RS.

4.3.4. Equilibrium adsorption studies

The Langmuir and Freundlich adsorption equations were used to model the adsorption isotherms of As(III) and As(V) for RS (**Figure 4.4(a** and **b**)). It can be seen that both Langmuir and Freundlich models fitted well to As(III) and As(V) adsorption isotherms at the equilibrium time and exhibited nonlinear behaviour. In addition, the best-fit parameter values (q_m, K_L, K_F, n) and R^2 for As(V) and As(III) at the equilibrium time and from the previous studies for sediments are presented in **Table 4.3**. The experimental data was fitted significantly better by the Freundlich model for As(III) and by than the Langmuir model for As(V) due to lower values of Reduced Chi-Sqr.

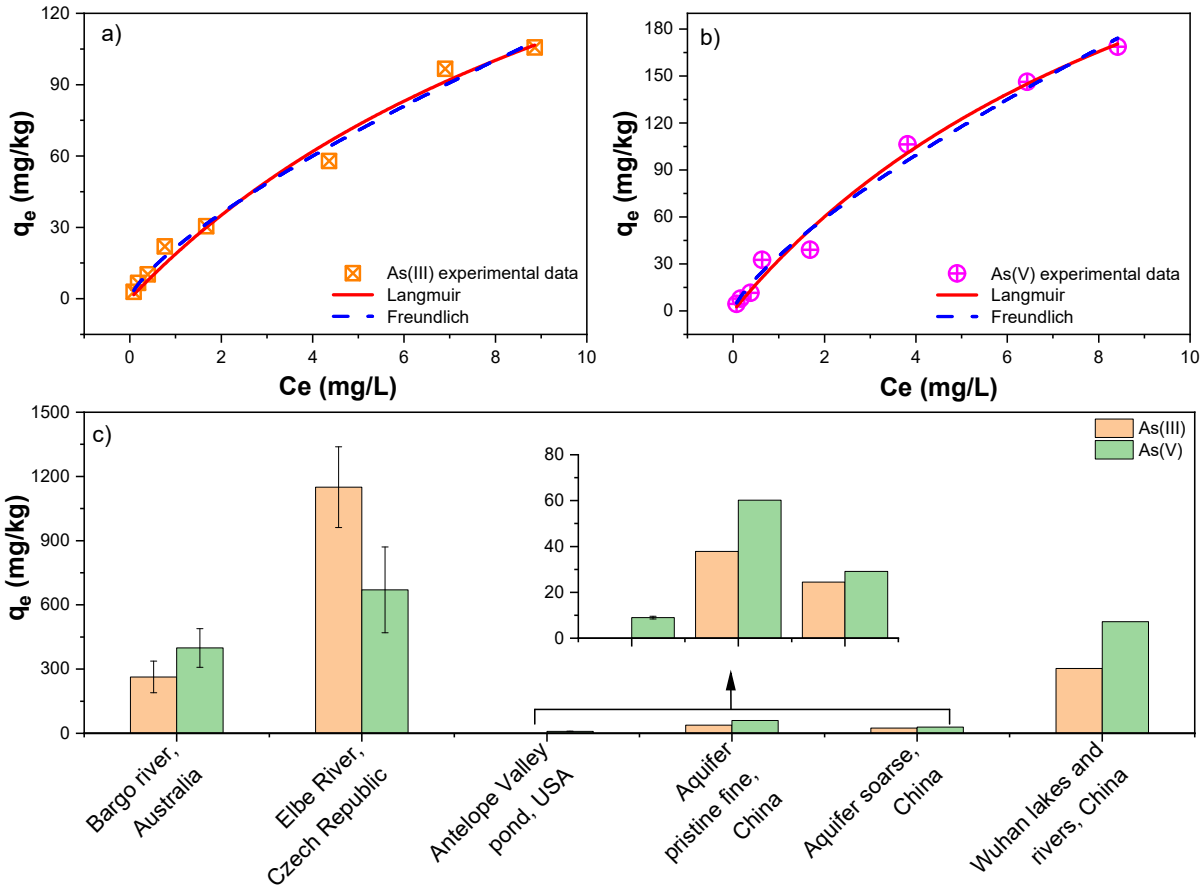

Figure 4.4. a) and b) adsorption isotherms of As(III) and As(V) on RS at the equilibrium time; c) maximum adsorption amount of As(III) and As(V) on RS estimated by Langmuir isotherm model in this study and from previous studies (Dousova et al., 2012; Goldberg and Suarez, 2013; Ma et al., 2015; Wang et al., 2018).

According to Zhang and Selim (2005), low 1/n values (< 0.4) indicated extensive heterogeneity of sorption sites. However, the 1/n values for As(III) was 0.741 0.752 for As(V) at the equilibrium time, suggesting the extensive homogeneity of the adsorption sites in the selected sediment. It is suggested that 1/n values between 0 and 1 are favourable for both As(III) and As(V) adsorption on the river sediment. Furthermore, the R_L values for As(III) and As(V) varied 0.115-0.920 and 0.098-0.902 at initial As concentrations of 0.11 - 10.30 mg/L. High surface activity of sediment associated with high mobility of As mobility in the sediment-water interface led to the favourable adsorption of both As(III) and As(V) on river sediment (Dousova et al., 2012). The adsorption maxima (q_m) estimated by Langmuir equation were 263.31 and 398.70

mg/kg for As(III) and As(V), respectively, lower than those of sediments investigated by Dousova et al. (2012) and Wang et al. (2018), and significantly higher than q_m values for As(III) and As(V) adsorbed on sediments from other studies (Goldberg and Suarez, 2013; Ma et al., 2015) (**Figure. 4.4c**).

Table 4.3. Calculated Langmuir and Freundlich equation parameters for As(III) and As(V) adsorption at the equilibrium time in this study and data from the previous studies.

Langmuir	As(III)			As(V)			Reference
	q_m (mg/kg)	K_L (L/mg)	R^2	q_m (mg/kg)	K_L (L/mg)	R^2	
Bargo RS	263.31 ±73.81	0.077 ±0.03	0.986	398.70 ±90.0	0.089 ±0.03	0.989	This study
SD1, Elbe River	1350	0.0133	0.969	900	0.0133	0.997	Dousova et al. (2012)
SD2, Elbe River	975	0.020	0.972	577.5	0.0124	0.931	Dousova et al. (2012)
SD3, Elbe River	1125	0.0537	0.991	532.5	0.0129	0.964	Dousova et al. (2012)
Surface sediment, Antelope Valley pond				8.96 ± 0.62	0.00082	0.975	Goldberg and Suarez (2013)
Aquifer pristine fine	37.8	0.33	0.990	60.2	0.46	0.974	Ma et al. (2015)
Aquifer coarse[a]	24.5	0.30	0.967	29.1	0.27	0.997	Ma et al. (2015)
Wuhan rivers and lakes[a]	303.3	0.0048	0.936	521.175	0.00268	0.944	Wang et al. (2018)
Freundlich	K_F	n	R^2	K_F	n	R^2	
Bargo RS	21.50 ±2.18	1.35 ±0.10	0.991	35.10 ±4.24	1.33 ±0.11	0.987	This study

[a.] the data at pH 7 were used.

In summary, the isotherm adsorption results in this study showed no significant difference in exhibiting the adsorption mechanism between As(III) and As(V). Ma et al. (2015) reported that Langmuir model can describe homogeneous adsorbent surface while Freundlich model displayed multi-layers of adsorption. Thus, both types of adsorption processes can be fitted well by the data from this study. As a result, As(III) and As(V) adsorbed on this RS occurs in both chemisorption and physisorption with higher adsorption capacity of As(V) than As(III). The results were

agreement with the findings from Ma et al. (2015) and Wang et al. (2018) but opposite to values from Dousova et al. (2012).

4.3.5. Sediment-water distribution of As(III) and As(V)

Partition coefficients (K_p) for both adsorption and desorption processes of As(III) and As(V) are shown in **Figure. 4.5**. The results were used to provide further understanding the migration and transformation of As(III)/As(V) between RS and overlying water. According to Nematollahi et al. (2021), log Kp values > 1 reflected a stronger affinity of adsorption and the element strongly remained in the sediment phase compared to lower values. The log K_p of pH4 was higher than that of pH10, indicating higher adsorption affinity in acidic condition than alkaline solution. **Figure 4.5** illustrates the less adsorption affinity of pH10 compared to other conditions. Regarding sediment properties, RS-NOM had marginally higher adsorption affinity than RS for As(III) and the opposite trend was for As(V). The effect of sediment sizes was similar for both As species, which highest adsorption affinity for the smallest size (S_4), then reduced followed by $S_3 > S_2 > S_1$. The log K_p values in this study were significantly higher than those investigated from the southern Caspian Sea (mean: 0.35, range: -0.21-0.75) reported by Nematollahi et al. (2021). Moreover, log K_p values for As(V) were higher than those of As(III), reflected that higher adsorption affinity of As(V) on sediment than As(III) regardless of controlling factors. The results were supported for the findings from the adsorption kinetic and isotherm sections above.

The statement of Nematollahi et al. (2021) was also revealed from the log K_p values for the desorption process. It can be seen that lower log K_p for As(III) than As(V), in which As(III) easily released from sediment to water phase in comparison to As(V). The amount of As(III) released from sediment at the equilibrium of desorption was 7.146 mg/kg compared to 6.621 mg/kg for As(V) evidenced for this hypothesis.

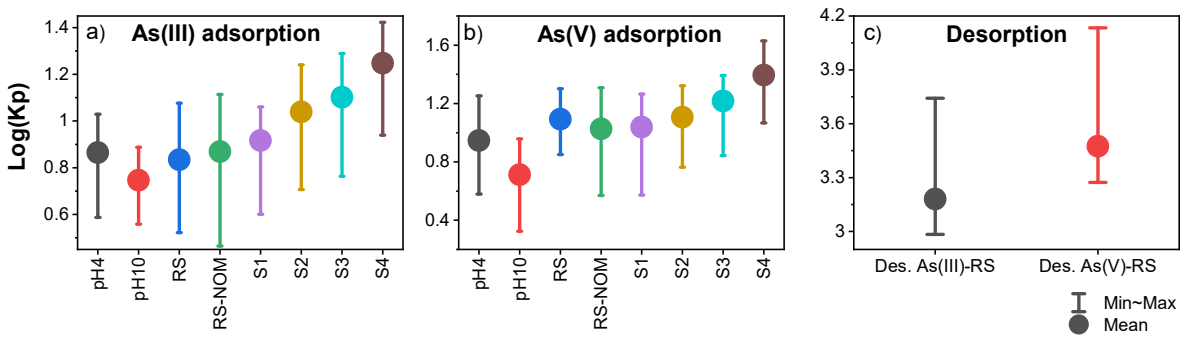

Figure 4.5. Distribution coefficient of As(III) and As(V) with different conditions.

4.3.6. As-sediment surface adsorption mechanisms

As(III) and As(V) are triprotic acids, which dissociate and present in aqueous media in the forms of H_3AsO_3 (pH=0-9), $H_2AsO_3^-$ (pH 10-12), $HAsO_3^{2-}$ (pH 13) and AsO_3^{3-} (pH 14) for As(III), and H_3AsO_4 (pH 0-2), $H_2AsO_4^-$ (pH 3-6), $HAsO_4^{2-}$ (pH 7-11) and AsO_4^{3-} (pH 12-14) for As(V) (Mondal et al., 2007; Yin et al., 2019; Yohai et al., 2019).

The interaction between As(III) and As(V) and with sediment particles in the adsorption process was investigated by performing FTIR of different sediment types including RS and RS-NOM before and after As(III) and As(V) adsorption. The FTIR spectra for RS is shown in **Figure 4.6a**. A new IR adsorption peak appeared at 1516 cm^{-1} attributed to carboxyl group (Kaufhold et al., 2012; Li et al., 2018) or amine C=O stretching (Yu et al., 2015) after As(III) and As(V) adsorption on RS. The band at 3742 cm^{-1} corresponds to O–H stretching vibrations of phenolic hydroxyl groups or adsorbed water (Luo et al., 2012a; Yu et al., 2015). The IR peaks shifted from 1057 cm^{-1} to 1088 cm^{-1} and 1080 cm^{-1} after As(III) and As(V) adsorption, which can be associated with Si(Al)–O vibration or antisymmetric stretching vibrations of Si–O tetrahedron (Hahn et al., 2018). The IR adsorption bands of all samples recorded at 779 cm^{-1} before adsorption and 787 cm^{-1} as well as 694 cm^{-1} are assigned to Si–O symmetrical stretching vibrations of quartz, exhibiting the roles of these surface functional moieties in As(III) and As(V) binding with sediment particles (Hahn et al., 2018; Rawat et al., 2021). Furthermore, the small shift in the IR peaks from 563 cm^{-1} to 553 cm^{-1} and 559 cm^{-1} after As(III)

and As(V) adsorption, respectively can be contributed to the involvement of Fe–O/Fe–OH vibration of the magnetite phase in the As(III) and As(V) adsorption (Luo et al., 2012; Rawat et al., 2021). Finally, the IR bans at around 420-428 cm^{-1} before and after As(V) adsorption can be related to the formation of Si–O–Mn bonds (Hahn et al., 2018; Kaufhold et al., 2012), while its disappearance after As(III) adsorption indicated the involvement of these functional groups in As(III) binding with sediment particles.

Regarding RS-NOM, no new groups appeared in the FTIR diagram (**Figure 4.6b**), indicating that the interaction between As(III) and As(V) and sediment particles only occurred in the available functional groups of sediments. Moreover, the IR bands under 500 cm^{-1} can be assigned to Si–O–Mn bonds (Hahn et al., 2018; Kaufhold et al., 2012), which disappeared after adsorption of As(III) on RS and indicated the involvement of these functional groups in As(III) binding with sediment particles. XRD analysis for RS and RS-NOM before and after As(III) and As(V) adsorption (**Figure 4.6(c** and **d**)) indicated that quartz was dominant and had the strongest peak in all samples. The results revealed to findings from previous studies of XRD for river sediments (Maity and Maiti, 2016; Xie et al., 2018a). Hahn et al. (2018) indicated that quartz peaks attributed to the Si-O-Si symmetric stretching of antisymmetric stretching vibrations. Additionally, the changes of quartz peaks may be due to either reaction of anionic As species with organic-Si or with SiO_2 in the presence of OM (Rawat et al., 2021).

Furthermore, the SEM-EDS images of RS before and after adsorption of As(III) and As(V) was given in **Figure 4.7**. It can be seen that **Figure 4.7 (a** and **b)** showed high Al contents was detected on RS before adsorption and after adsorption of As(III), while low Al contents was found on RS after adsorption of As(V) from Figure 4.7c revealed the results higher enrichment of As(V) on RS than As(III) (Matera et al., 2003). Highly rich contents of Al and Si in RS particles may affect the Al signal after adsorption of both As(III) (Matera et al., 2003). Moreover, XPS results showed no detection of As for RS before and after adsorption of As(III), whilst both As2p3A and As2p3B corresponding to As(III) and As(V) were detected on RS after

adsorption of As(V) (**Figure 4.8**). The results indicate that there was reduction from As(V) to As(III) on RS after adsorption (Guo et al., 2022). Additionally, the % atomic of As(V) and As(III) on RS particles after adsorption of As(V) were 0.08% and 0.04%, respectively, revealing for this finding.

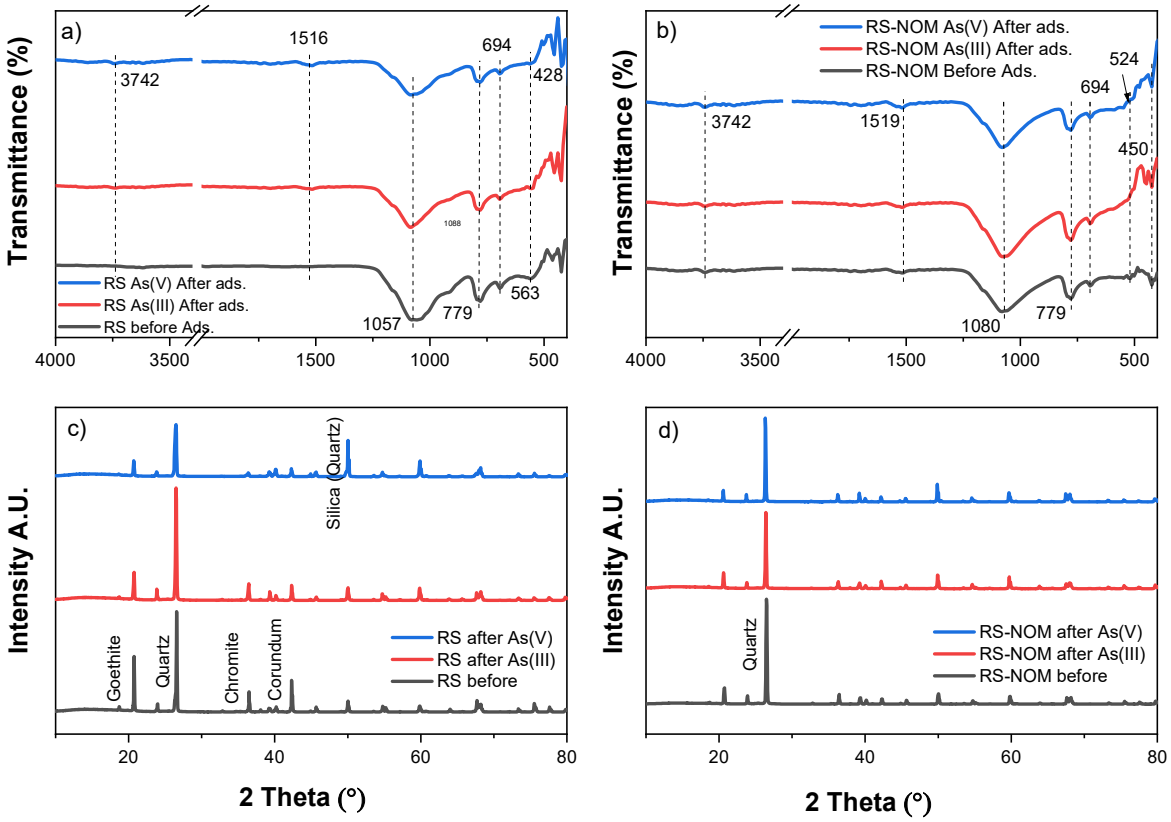

Figure 4.6. FTIR spectra (400-4000 cm^{-1}) of RS (a), RS-NOM (b); XRD patterns of RS (c) and RS-NOM (d) before and after As(III) and As(V) adsorption.

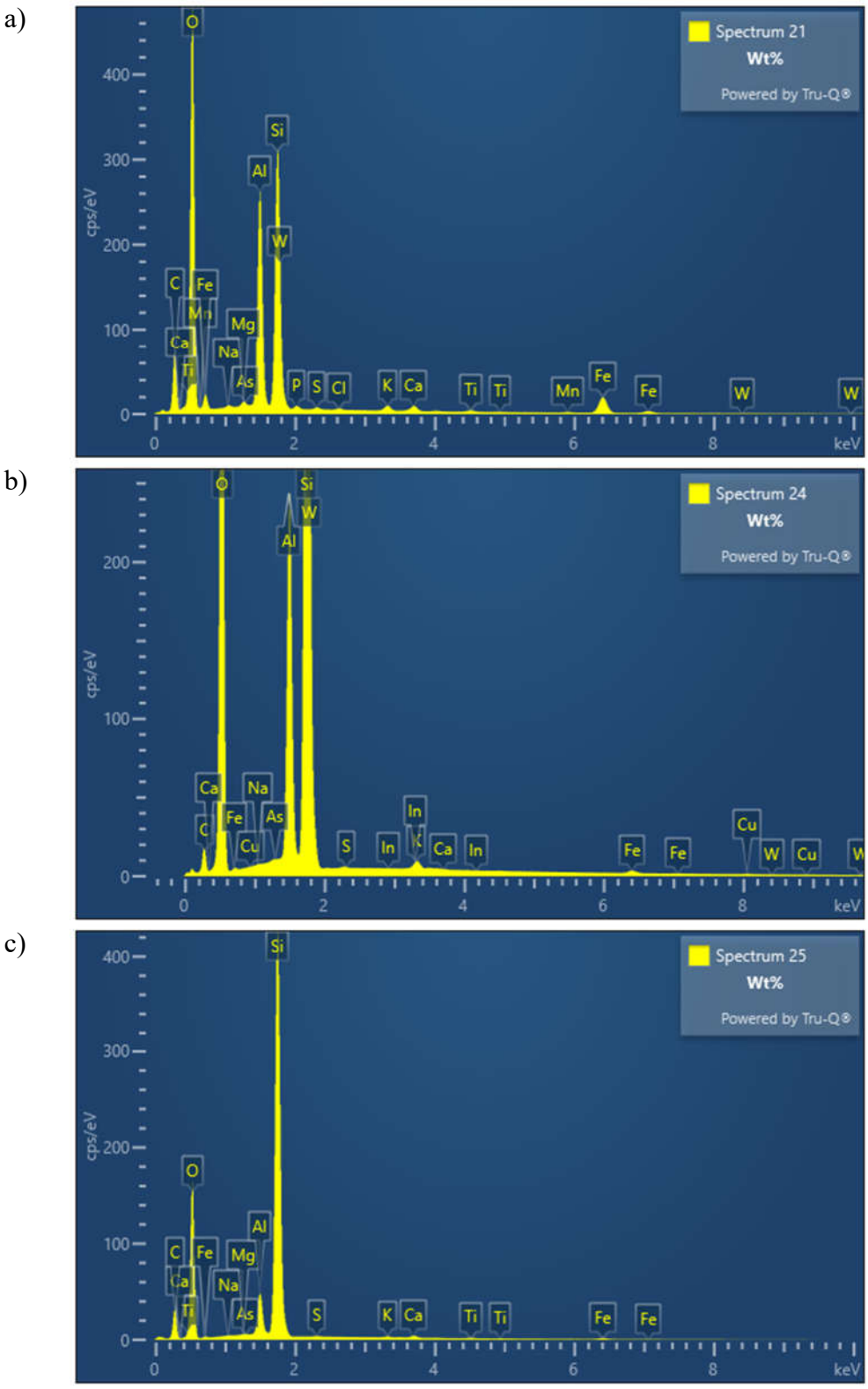

Figure 4.7. SEM-EDS analysis of RS (a) before adsorption, (b) after adsorption of As(III), and (c) after adsorption of As(V).

a)

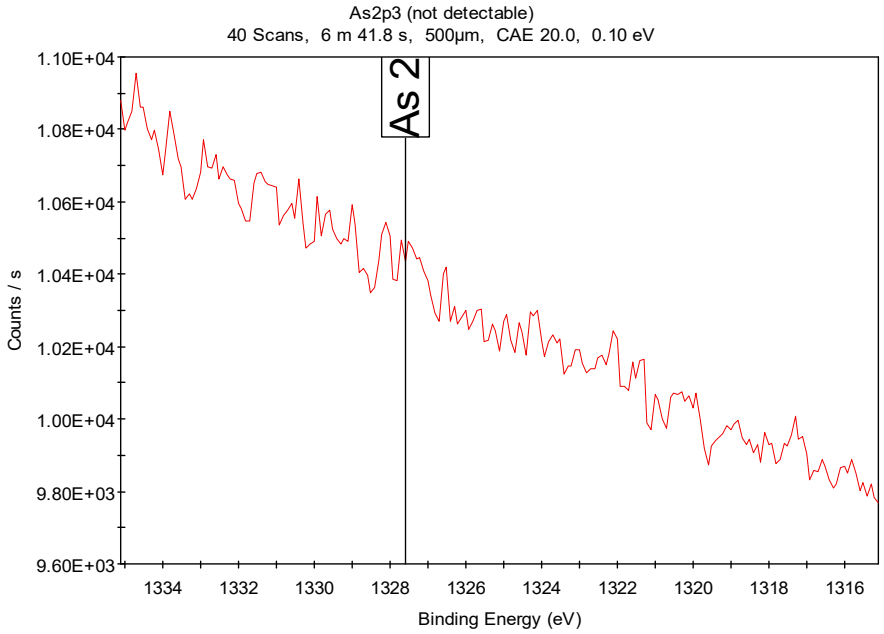
As2p3 (not detectable)
40 Scans, 6 m 41.8 s, 500µm, CAE 20.0, 0.10 eV
As 2
Counts / s
1.10E+04
1.08E+04
1.06E+04
1.04E+04
1.02E+04
1.00E+04
9.80E+03
9.60E+03
1334
1332
1330
1328
1326
1324
1322
1320
1318
1316
Binding Energy (eV)

b)

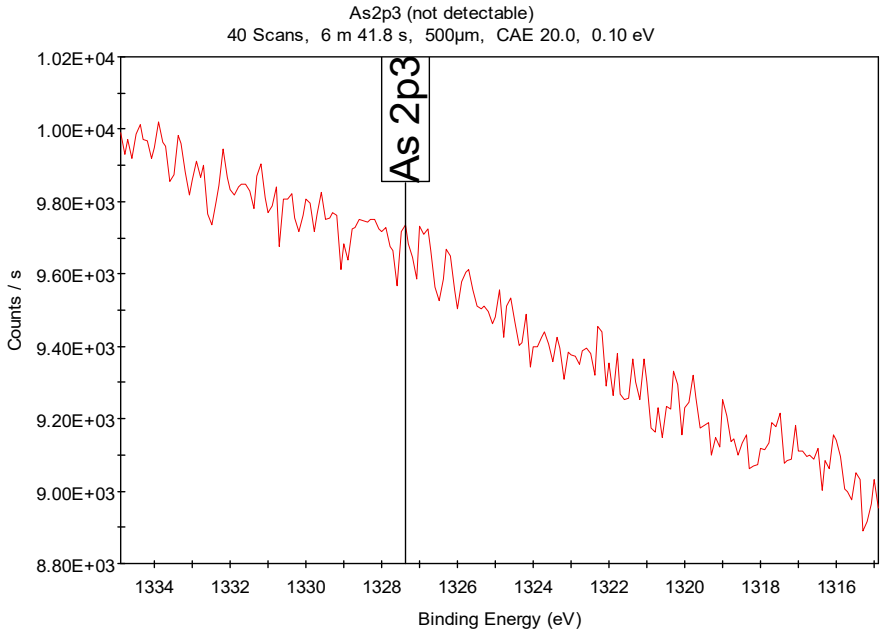
As2p3 (not detectable)
40 Scans, 6 m 41.8 s, 500µm, CAE 20.0, 0.10 eV
As 2p3
Counts / s
1.02E+04
1.00E+04
9.80E+03
9.60E+03
9.40E+03
9.20E+03
9.00E+03
8.80E+03
1334
1332
1330
1328
1326
1324
1322
1320
1318
1316
Binding Energy (eV)

c)

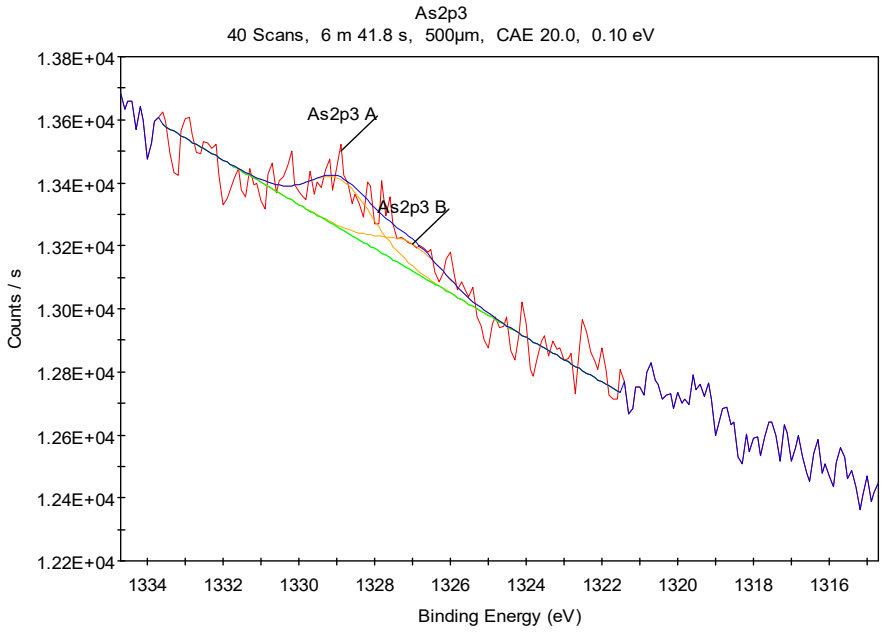

Figure 4.8. XPS analysis of RS (a) before adsorption, (b) after adsorption of As(III), and (c) after adsorption of As(V).

4.4. Conclusions

The adsorption and desorption of As(III) and As(V) at sediment-water interface were studied. Adsorption kinetics were well modelled by PFO and PSO, with better results by PSO based on the R^2 values. The Langmuir and Freundlich isotherms well modelled and As(III) and As(V) adsorption equilibrium on sediment. As(V) had higher monolayer surface adsorption (398.70 mg/kg) than that of As (III) (263.31 mg/kg), indicating stronger surface affinity of RS toward As(V) than As(III). As a result, As(III) and As(V) adsorption on river sediment was favour from acidic to neutral conditions. SOM caused a reduction of As(III) and As(V) adsorption on RS, by inhibiting As complexation with sediment functional groups. As adsorption decreased with increasing sediment fraction size, and increased with sediment surface area. The physicochemical characteristics, FTIR and XRD analysis of sediment showed that As(III) and As(V) adsorption on the surface of sediment occurred by interactions with Fe–O/Fe–OH, Si(Al)–O, hydroxyl (O─H) and carboxyl (─COOH) functional groups. The SEM-EDS evidenced higher adsorption of As(V) than As(III) and there was reduction from As(V) to

As(III) on the RS surface under XPS analysis. The results are valuable for assessing the long-term fate and management of As contaminated river sediment.

CHAPTER FIVE:

ADSORPTION OF ARSENIC SPECIES ON DISTILLED AND RIVER WATER

5. CHAPTER FIVE: ADSORPTION OF ARSENIC SPCIES ON DISTILLED AND RIVER WATER

Section 5.3.1.1 covers the contents of a published review paper: **Kien Thanh Nguyen**, Amir Navidpour, Mohammad Boshir Ahmed, Amin Mojiri, Yuhan Huang, John L. Zhou (2022) Behaviour and mechanism of arsenite and arsenate adsorption and desorption at river sediment-water interface. *Journal of Environmental Management.* (Accepted 6 June 2022).

5.1. Introduction

Plastics, which are composed of synthetic polymers, play an indispensable role in people's lives in this era. Increasing amounts of plastics enter the natural environment due to their large-scale production and widespread applications (Zong et al., 2021). In 2019, the plastic was globally produced by 368 million tonnes, of which China was the largest producer by sharing 31% of world's plastic production (Plastics Europe, 2020). It cannot deny that the proportion of recycled plastic waste was still small. For example, the high rate of recycling in Europe was 15% of total plastic waste compared to 25% that was sent to landfill in 2018 (Plastics Europe, 2019). In Australia, roughly 3.5 million tonnes of plastic were consumed in 2018-2019, of which only 13% of used plastic was recycled and 84% was sent straight to landfill (Australian Bureau of Statistics, 2020). Plastic materials have become an increasing environmental problem of plastic contamination in both anthropic and natural ecosystems due to the persistence and the inappropriate disposal (De Felice et al., 2019).

MPs are plastic polymers with diameters smaller than 5 mm (Dong et al., 2020; He et al., 2020b), and have received a great concern worldwide due to their pollution in environments and ecological effects (Shen et al., 2021). There are five types of MPs including hard and jagged-edged fragments, hard and rounded micro-pellets, fibrous or thin uniform fibers, thin and 2-dimensional plastic films, and foam. In terms of sources, MPs are grouped into primary

and secondary categories (Akdogan and Guven, 2019; Alam et al., 2019. Primary MPs are generally manufactured plastics while secondary MPs often derive from the breakdown of larger plastic items (Akdogan and Guven, 2019; Dris et al., 2015b; O'Brine and Thompson, 2010). Another concern about the MPs is that they can carry other pollutants such as hydrophobic organic, heavy metals and microorganisms (Shen et al., 2021). Regarding adsorption behaviours of heavy metals onto MPs, the properties of MPs, adsorbates and environmental conditions were the main factors influencing the adsorption capacities of MPs (Wang et al., 2020).

Polyethylene (PE) and polystyrene (PS) are the most popular MP products and contaminants in fluvial environment. The PE density varies from 0.917 to 0.965 g/cm^3, while the density of PS (1.04-1.11 g/cm^3) is slightly higher than that of fresh water (Zhou et al., 2020). Studies found that PE shared high proportion of total MPs concentrations in river water and sediments. For example, it is estimated that PE accounts for 38% of total MPs in the Yangtze River, China (Zhang et al., 2015), 47.5% of total MPs in Elbe River, Germany (Scherer et al., 2020), or even up to nearly 80% in Ofanto River, Italy and Saigon River, Vietnam (Campanale et al., 2020; Lahens et al., 2018). PE had less proportion in river sediments than in river waters, varying from 27-61% in Portugal, Germany and China (Huang et al., 2021; Lin et al., 2018; Liu et al., 2021; Rao et al., 2020; Rodrigues et al., 2018; Scherer et al., 2020; Wang et al., 2017). Moreover, high PS abundance in water was explored in some Chinese rivers such as West Rivers (20%), Tuojiang River (23%), Chishui River (25%) and Maozhou River (34.5%) (Huang et al., 2021; Li et al., 2021; Wu et al., 2020; Zhou et al., 2020). High concentration of PS was detected in river sediments. For example, the concentrations of PS in Elbe River, Germany and West River, China accounted for 18.5% and 16% of total MPs in sediments, respectively (Huang et al., 2021; Scherer et al., 2020). Studies revealed that PS can adsorb pollutants such as antibiotics (Li et al., 2018), perfluorooctanoic sulphonamide (Wang et al., 2015) and heavy metal (Holmes et al., 2012). The adsorption of heavy metals such as Cu, Cd, Cr, Pb, As, Zn, Ni

and Co on MPS has been investigated to understand potential capturing of metals, adsorption behaviours and mechanisms by MPs, specifically PE and PS (Dong et al., 2020; Godoy et al., 2019; Wang et al., 2020; Zhang et al., 2020; Zong et al., 2021). These investigations indicated that MPs could adsorb metals, and the adsorption kinetics could be described by PFO and PSO, and the Langmuir and Freundlich isotherms models for adsorption equilibrium. Godoy et al. (2019) suggested that chemical adsorption was a main adsorption mechanism due to better description of experimental data by the Langmuir model than by the Freundlich model for several types of MPs including PE, PET, PP, PS and PVC.

As is a ubiquitous toxic metalloid, and elevated levels of this element in the biota are mainly derived from natural processes and anthropogenic sources (Dousova et al., 2012; Osuna-Martínez et al., 2021). In natural waters, As exists in many different physicochemical forms, but As(III) and As(V) are dominant (Xie et al., 2018b) forms in various As compounds (Dong et al., 2020). As concentration in natural water was high as 5000 µg/L (Tahira et al., 2019). To date, As has not been recognized as a single pollution in aqueous environment, but higher attention has been considered when it interacts with MPs. Dong et al. (2020; 2019) investigated the adsorption of As(III) onto different MPs and reported that higher adsorbed amount of As(III) onto polytetrafluoroethylene (PTFE) and polystyrene (PE) MP particles was accordance with larger SSA of the particles, low pH solution values, low concentration of interfering nitrate and phosphate ions in the solution. For instance, amount of As(III) maximum adsorption on PTFE decreased from 1.05 to 0.98 and then to 0.91 mg/g when the particle sizes increased from 0.1-1 µm (PTFE 0.95 m^2/g) to 1-10 µm (PTFE 0.40 m^2/g) and 10-100 µm (PTFE 0.32 m^2/g), respectively. In contrast, the maximum adsorption capacity of As(III) on PE was 1.12 mg/g for particle size 10-100 µm (9.8 m^2/g) and decreased to 0.92 mg/g for particle size 0.1-1 µm (9.8 m^2/g) (Dong et al., 2020). Moreover, As(III) adsorption on PTFE and PS was not significant at pH of 3 and 4, then decreased gradually when pH was increased from 4 to 7. This process was explained by the change of OH^- content related to pH in the solution. Low OH^- content at low

solution pH (3-4), covering the levels of the point zero charged (PZC) of PTFE and PS, does not compete with arsenic anion during the adsorption process. When the solution pH exceeded 4, these adsorbents became negatively charged and repulsed arsenate ions led to the reduction of As(III) adsorption. These studies also found that the presence of NO_3^- and PO_4^{3-} in the solution inhibited the adsorption of As(III) onto PTFE and PS, in which higher concentrations of these anions caused a decrease in As(III) adsorption.

The hypothesis for the metals adsorbed onto plastic resin pellets is that cations and oxyanions interact with plastics' charged regions or complexes or the hydrophobic surface (Holmes et al., 2012; Naqash et al., 2020). Heavy metal adsorption on MPs was highly influenced by the large SSA, polarity, and organic polymer composition (Ahmed et al., 2021; Ashton et al., 2010). DOM, SSA, porosity and morphology were other major factors affecting the adsorption of metals on MPs (Godoy et al., 2019). Regarding As adsorption mechanisms onto MP surface, Dong et al. (2020 and 2019) concluded that As(III) adsorbed on PTFE and PE occurred on the carboxyl group throughout hydrogen bonding of the adsorbent surface.

Studies on the roles of environmental factors such as urban wastewater, irrigation water and sea water were conducted for Cd, Co, Cr, Cu, Ni, Pb and Zn metals (Godoy et al., 2019). Adsorption capacities of Cr onto PE by using these solutions with initial concentration of 8 mg/L followed a decreasing order as: urban wastewater (7.90 mg/g), irrigation water (6.67 mg/g), distilled water (3.34 mg/g) and seawater (2.56 mg/g). The results for Pb adsorption on PE were urban wastewater (7.63 mg/g), irrigation water (5.69 mg/g), seawater (3.28 mg/g) and distilled water (1.77 mg/g). The adsorption capacities of Pb on PS with the same above conditions were urban wastewater (7.40 mg/g), irrigation water (5.64 mg/g), seawater (3.29 mg/g) and distilled water (2.39 mg/g). The outcomes revealed that the adsorption capacities of metals on MPs depended on not only the specific MP properties and types of metals, but also environment conditions (Li et al., 2018; Wang et al., 2020). Regarding the adsorption of As on MPs, so far studies are limited in using distilled water as the background matrix.

Therefore, this study aims to(1) explore the structure and properties of virgin bead PS and LDPE by Fourier transform infrared (FTIR) spectroscopy and scanning electron microscopy (SEM) before and after adsorption of As(III) and As(V); (2) investigate the adsorption kinetics and isotherms of these As species onto MPs by using distilled water and river water; and (3) study the adsorption mechanism of As(III) and As(V) related to MPs surface functional groups.

5.2. Material and Methods

5.2.1. Materials and analysis

The detailed descriptions about the sample collection, sediment preparation and materials are described in **Chapter 3.1**.

In this chapter, two types of MPs including PS and LDPE were selected to investigate the adsorption behaviours of inorganic As species on MPs. The previous experimental results have provided the details related to sorption behaviours, adsorption mechanism and the effects of controlling factors such as pH, initial As concentrations in solution and sediment properties on adsorption of As(III) and As(V) on river sediment. Currently, the adsorption behaviour of MPs for heavy metals receives higher attention. Thus, this chapter investigated the batch experiments related to adsorption of As(III) and As(V) on PS and LDPE under DI water and RW solutions. The PS and LDPE surface functional groups were characterized by using FTIR analysis. In addition, adsorption kinetics and adsorption isotherms were carried out as described in **Chapter 3** (**3.2.4-3.2.5**).

5.2.2. Adsorption experiments

The adsorption kinetics experiments of As(III)/As(V) adsorption onto PS and LDPE were performed in triplicate. The stock solution of 100 mg/L of As(III)/As(V) was diluted by DI water or river water (RW) to obtain the solutions of 10 As mg/L. A mixture of approximately 2.0 g PS or LDPE and 200 mL diluted solution was placed in 500 mL beaker for 7 days and

mixed by a flatted shaker at 120 rpm for the first two days. During adsorption process, 3 mL suspension samples were taken on regular intervals (3, 6, 12, 24, 72, 120 and 168 h), filtered by a 0.45 μm membrane filter, and analysed for total As by ICP-MS (Agilent 7900). The adsorption of As(III) or As(V) was evaluated by monitoring the decrease of arsenic concentration in the solution.

For the adsorption isotherm calculation, a series of As(III)/As(V) solutions with initial concentrations of 1.0, 2.0, 5.0 and 8.0 mg/L were prepared by diluted stock solution from 100 mg/L by adding DI-water or RW. Approximately 2.0 g PS or LDPE mixed with 200 mL solution was placed in 500 mL beaker for 7 days and mixed by a flatted shaker at 120 rpm for the first two days.

5.3. Results and discussion

5.3.1. River water and selected MPs characterisation

5.3.1.1. River water characteristics

The total As content and other physicochemical characteristics of the Bargo river water were analysed, in comparison with results reported for Teatree Hallow in September 2021 receiving treated wastewater due to coal mining activities by SIMEC group in New South Wales, Australia (**Table 5.1**). The metals concentrations in Bargo River water were lower than its upstream, Teatree Hallow, except the Al concentration, due to the dilution and sedimentation or sorption processes. All water quality values in Bargo River and Teatree Hallow were below the standard of Australia freshwater (AWQG, 1992), except concentrations of Ba and Zn in Teatree Hallow. Hence, water quality in Bargo River and its tributary was slightly polluted in some cases.

Table 5.1. River water characteristics from Bargo River, NSW, Australia and its tributary.

	Bargo river (this study)	Teatree Hallow	AWQG[a]	Unit
Al	35.69 ± 4.95	30	100	µg/L
As	12.93 ± 0.29	56	50	µg/L
Ba	307.72 ± 21.66	1590	1000	µg/L
Cr (total)	8.32 ± 0.01		10	µg/L
Cu	2.02 ± 0.56	1	2-5	µg/L
Fe (total)	110.77 ± 13.71		1000	µg/L
Mn	2.93 ± 0.25		100	µg/L
Ni	11.09 ± 0.22	30	15-150	µg/L
Pb	17.24 ± 0		1-5	µg/L
Zn	48.99 ± 0.53	71	5-50	µg/L
Electrical Conductivity	473 ± 10	1930		µg/L
Turbidity	223 ± 5			
TOC	30.20 ± 0.26			mg/L
References	This study	SIMEC (2021)	SIMEC (2021)	

a. Australian Water Quality Guidelines for Freshwater.

5.3.1.2. PS and LDPE characteristics

The FTIR of PS before and after adsorption of As(III) and As(V) is shown in **Figure 5.1a** to evaluate the changes of surface functional groups related to interactions between As species and PS pellets. As can be seen from IR spectra of PS (**Figure 5.1a**), the IR adsorption peak at 3024 cm^{-1} disappeared after As(III) adsorption under DI water conditions, however, two new peaks of 3742 cm^{-1}, and 3842-3858 cm^{-1} appeared after adsorption of both As(III) and As(V). The peaks of over 3000 cm^{-1} were attributed to O–H stretching vibrations (Dong et al., 2020). The IR peaks at 14423-1697 cm^{-1} characterised the amide C=O stretching (Dong et al., 2020; Rawat et al., 2021). In this functional group, the peak of 1597 cm^{-1} before the adsorption on PS

was disappeared after adsorption of As(III) under DI water condition, while it shifted to 1690 cm^{-1} after adsorption of As(V) by DI water, and to 1697 cm^{-1} after adsorption of As(III) and As(V) by RW. The IR bands at 1497 cm^{-1} and 1443 cm^{-1} were stable in RW conditions, but shifted to 1512 cm^{-1} and 1450 cm^{-1} under ID water environment for both As(III) and As(V). Moreover, the IR band at 1018 cm^{-1} before adsorption, which slightly shifted to 1080 cm^{-1} after adsorption of As(III) under DI water, was disappeared after adsorption of As(V) under DI water, and divided into two peaks 1022 and 1026 cm^{-1} after adsorption of As(V) under RW, contributed to O–H bend of PS (LibreTexts, 2021). According to Dong et al. (2020), the peak at 748 cm^{-1}, which shifted to 756 cm^{-1} after As(III) and As(V) adsorption attributed to the long chain CH_2. Generally, two disappear peaks were involved in As(III) binding with PS pellets, while the new peaks indicated strong surface interaction and formation of new bonds between As(III) or As(V) and surface functional groups of hydroxyl and carboxyl. In contrast, no new peak was formed as well as no peak was also disappeared.

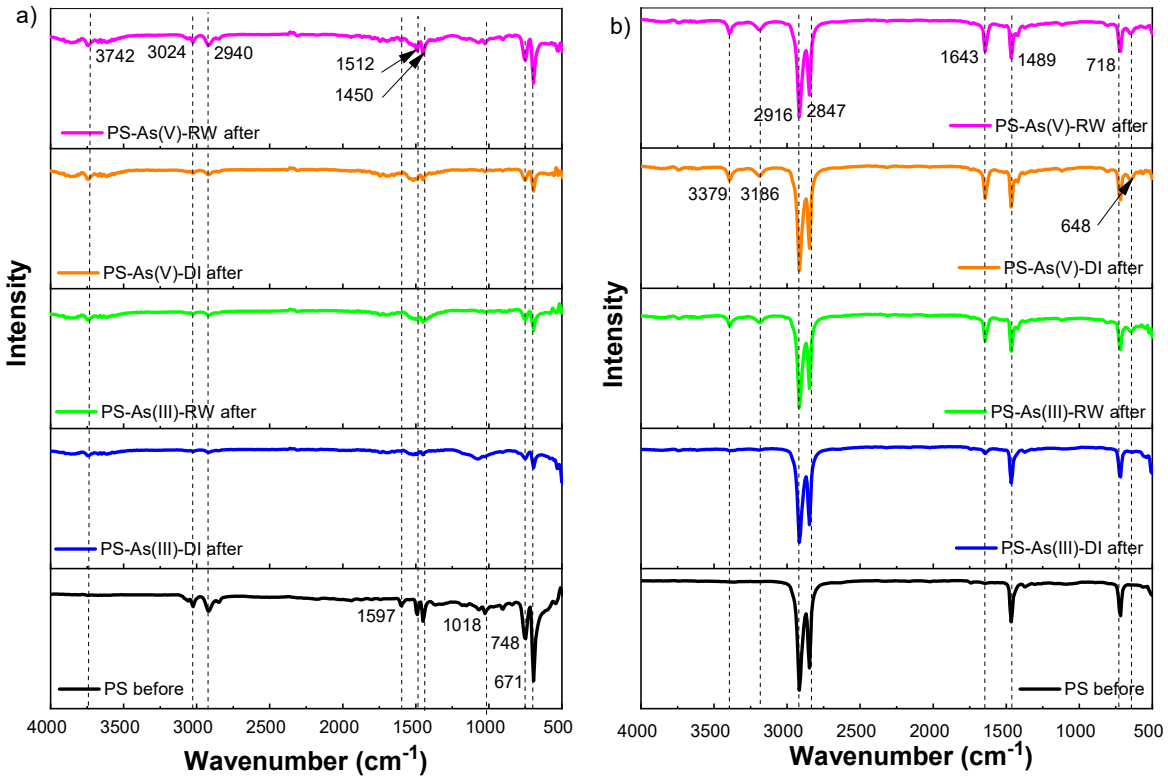

Figure 5.1. FTIR spectra before and after As(III)/As(V) adsorption on PS (a) and LDPE (b).

The FTIR spectra results for surface functional groups of LDPE related to adsorption of As(III) and As(V) are shown in **Figure 5.1b**. According to Chen et al. (2001), the peaks of 2909 cm^{-1} and 2847 cm^{-1} correspond strong C–H asymmetric stretching and medium strong C–H symmetric stretching, of which the band 2909 cm^{-1} slightly shifted to 2916 cm^{-1} after adsorption of As(V) in both DI water and RW, whilst the later peak was stable after adsorption regardless of conditions. Two new bands of 3379-3395 cm^{-1} and 3186-3194 cm^{-1} were appeared after As(III) and As(V) adsorption indicated there was forming new bonds between As(III) or As(V) and surface hydroxyl functional group. Additionally, two other new bands at 1643 cm^{-1} and 648 cm^{-1} assigned to the amide C=O stretching and O–H bend functional groups (Dong et al., 2020; LibreTexts, 2021). As a result, although there were difference among the values of IR peaks of LDPS and PS, they shared the similar surface functional groups for interactions with As(III) and As(V).

5.3.2. Sorption kinetics

Figure 5.2 shows the fitting results of PFO and PSO models for As(III) and As(V) adsorption. The results on time dependent of As(III) and As(V) adsorption by DI water and RW on PS and LDPE adsorbents showed initial fast stage of adsorption up to 24h, followed by a slower stage. Studies by Dong et al. (2020 and 2019) pointed out that the adsorption rate of As(III) on PTFE and PS slowly increased during the 120 minutes, followed by rapidly increasing up to 1440 minutes for PTFE and 960 minutes for PS, respectively. Thus, this study did not observe the adsorption before the first 3h, but revealed the results for As(III) adsorption of PS at later stages. The rapid adsorption phase was explained the rapid invading by As(III) (Dong et al., 2020) or As(V) on external surface adsorption sites of these MPs, then As species entered the adsorption sites in the inner surface. Generally, PS has higher adsorption capacities for As(III) in both DI water and RW conditions (**Figures 5.2a** and **b**) and for As(V) in DI water (**Figure 5.2c**),

particularly in the slower stage for As(III) adsorption in both DI water and RW environments. More specific, the adsorption capacities of PS calculated from the experimental data at the equilibrium time in DI water were higher in RW for both As(III) and As(V) (**Table 5.2**), at 93.77 and 90.36 mg/kg for As(III), and 82.67 and 78.48 mg/kg for As(V), respectively. Similar trend was found for adsorption of As(III) on LDPE, at 74.45 mg/kg in DI water compared to 49.34 mg/kg in RW. However, the adsorption of As(V) on LDPE was higher in RW (93.05 mg/kg) than in DI water (78.03 mg/kg). These opposite outcomes could be explained that environmental factor has a significant influence on the amount of As adsorbed on these selected MPs. Amount of As(III) adsorbed on PS in this study was significantly lower than those from the study of Dong et al. (2020), varied between 1035 and 1165 mg/kg for different sizes of PS particles. The correlation coefficient (R^2) for adsorption of As(III) and As(V) on PS and LDPE were high, varying between 0.988 and 0.997 indicated that PFO exhibited well with the experimental data. These R^2 values from the non-linear PFO model were higher than those calculated from the linear regression for As(III) adsorption on PS (Dong et al., 2020), supporting the state that the non-linear form would be better for description of kinetic adsorption (Rawat et al., 2021). In addition, the estimated adsorption capacities of these MP beads at the equilibrium from PFO model were lower than those calculated from the experimental data (**Table 5.2**). The PFO q_e values (mg/kg) for As(III) were 80.42 (PS-DI), 67.22 (LDPE-DI), 82.741 (PS-RW) and 42.703 (LDPE-RW), whilst the degrees for As(V) were 76.23 (PS-DI), 70.53 (LDPE-DI), 70.76 (PS-RW) and 84.02 (LDPE-RW).

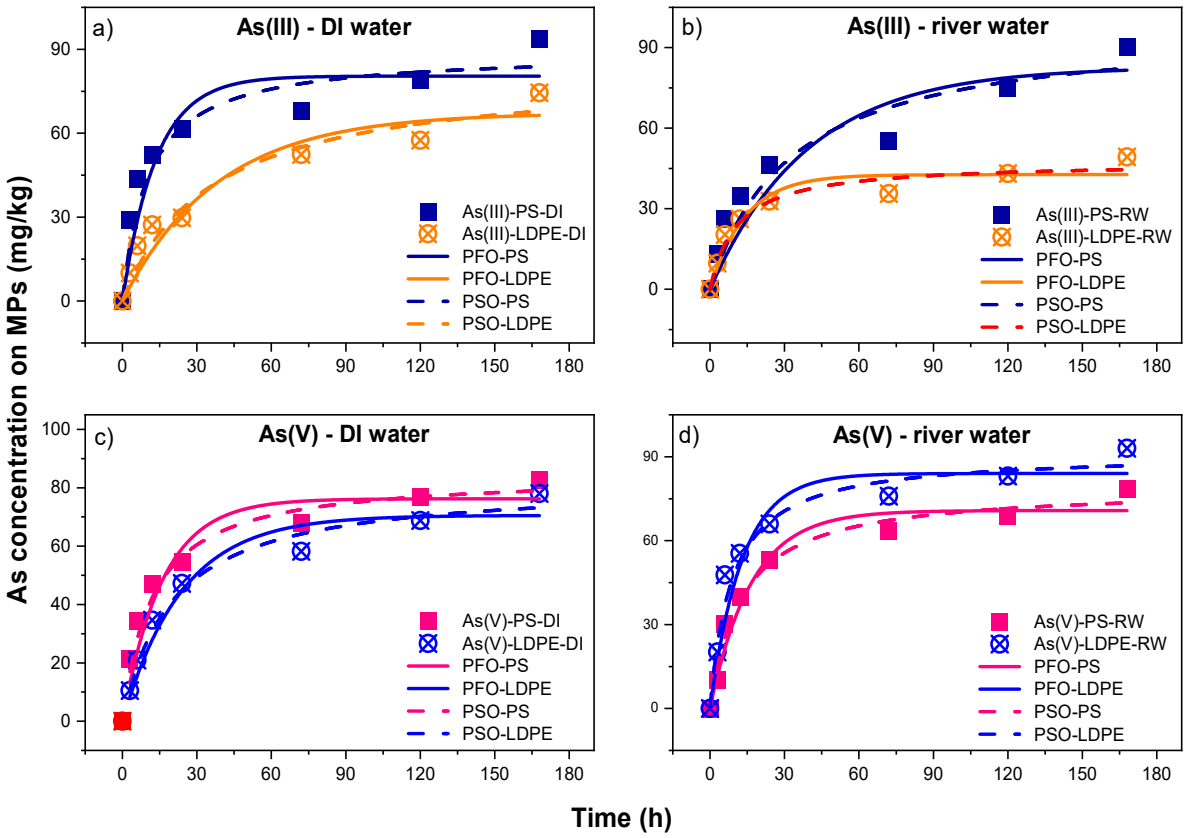

Figure 5.2. The PFO and PSO kinetic models of As(III) and As(V) adsorption. Symbols are experimental data, the solid and dash lines represent the non-linear fitting by PFO and PSO, respectively.

The contents of As(III) and As(V) adsorption on PS and LDPE estimated by PSO model were closed to the experimental values than those from PFO (**Table 5.2)**, which was opposite to the results estimated by linear regression (Dong et al., 2020). Azizian (2004) and Rawat et al. (2021) stated that non-linear forms of kinetic adsorption (PFO and PSO) describe better results than linear forms. The R^2 results for As(III) ranged at 0.992 – 0.998 and 0.998 – 0.999 for As(V), which were slightly higher than those from PFO model. As a result, PSO model was more accurate than PFO for describing As(III) and As(V) adsorption. Thus, our results revealed role of PSO model in describing physicochemical adsorption at a particular site or the whole adsorption process (Kumar et al., 2016; Ma et al., 2015).

Table 5.2. PFO and PSO kinetic parameters and equilibrium adsorption capacity.

As	Exp. conditions	PFO			PSO			q_e^c (mg/kg)
		R^2	K_1 (1/h)	q_e^a (mg/kg)	R^2	K_2 (kg/mg-h)	q_e^b (mg/kg)	
As(III)	PS-DI[d]	0.989	0.0738	80.42	0.994	0.0011	88.96	93.77
	LDPE-DI[d]	0.994	0.0261	67.22	0.996	0.0003	82.45	74.45
	PS-RW[e]	0.988	0.0254	82.74	0.992	0.0003	98.35	90.36
	LDPE-RW[e]	0.997	0.0712	42.70	0.998	0.0020	47.46	49.34
	PS (0.1-1µm)	0.908		1154	0.987		2094	1165
	PS (1-10µm)	0.602		1110	0.899		2013	1115
	PS (>10µm)	0.771		1033	0.957		2043	1035
As(V)	PS-DI[d]	0.995	0.0623	76.23	0.998	0.0010	84.60	82.67
	LDPE-DI[d]	0.994	0.0419	70.53	0.998	0.0006	81.78	78.03
	PS-RW[e]	0.997	0.0604	70.76	0.999	0.0010	79.01	78.48
	LDPE-RW[e]	0.995	0.0773	84.02	0.998	0.0013	91.28	93.05

a and b. Estimated equilibrium adsorption capacity from the PFO and PSO models; c. estimated equilibrium adsorption capacity from the experiments; d and e. Using DI water and river water for experiments; f, g and h. PS particle sizes of 0.1-1, 1-10 and greater 10 µm.

5.3.3. Sorption isotherms

The adsorption isotherms of As(III) for PS and LDPE by using DI water and RS were modelled by the Langmuir and Freundlich adsorption equations (**Figure 5.3**), while **Figure 5.4** shows the isotherms of As(V). It can be seen that both Langmuir and Freundlich equations fitted well to As(III) and As(V) adsorption isotherms and exhibited nonlinear behaviour. In addition, the best-fit parameter values (q_m, K_L, K_F, n) and R^2 for As(V) and As(III) at the equilibrium time and from the previous studies for PS are presented in **Table 5.3**. The marginal differences among the values of Reduced Chi-Sqr and R^2 for both Langmuir and Freundlich models indicated that these models can well describe the adsorption isotherms for PS and LDPE related

to As(III) and As(V). Previous studies showed that Langmuir and Freundlich models were applied for various heavy metals and the goodness of the fitting with the dataset was not very different between these models (Collard et al., 2019; Dong et al., 2020; Holmes et al., 2014; Hosseinpour et al., 2018).

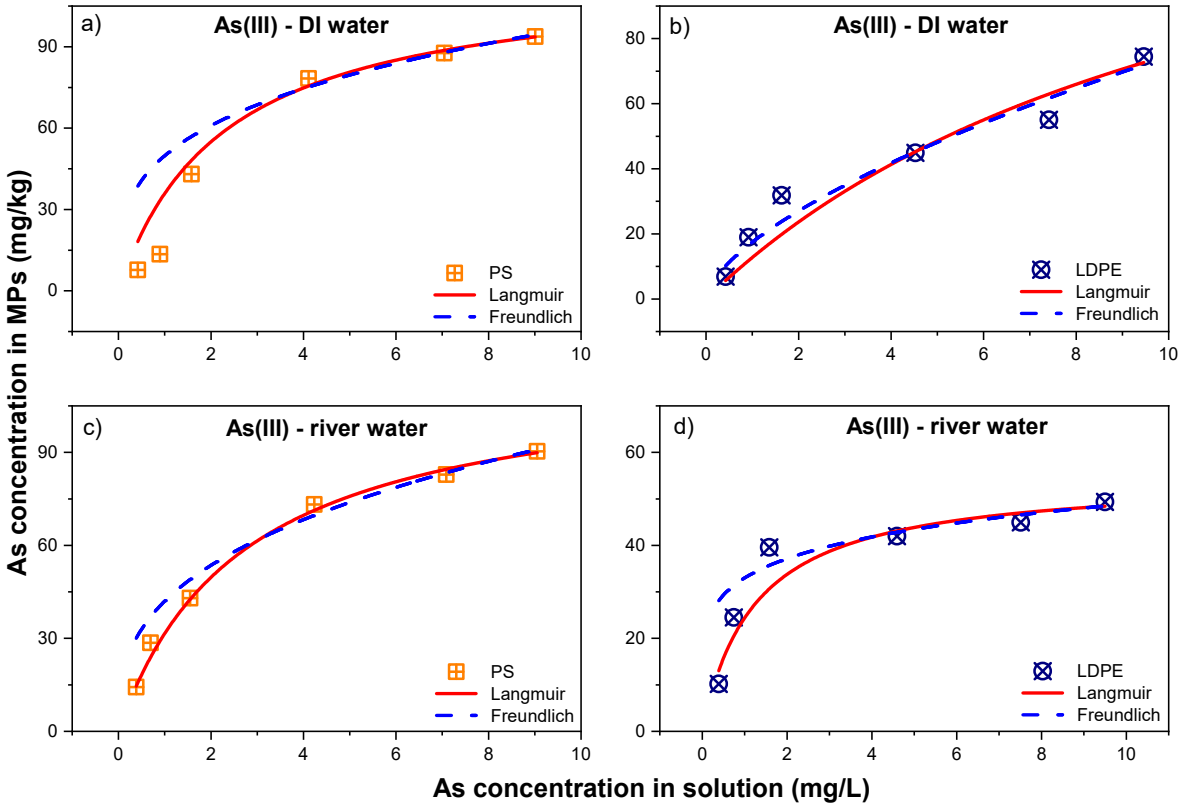

Figure 5.3. The isotherm of As(III) adsorption on PS (a, c) and LDPE (b, d).

In the Langmuir model, the maximum adsorption capacities (q_m), for different conditions (As species, PS, LDPE, DI water and RW) were consistent to the kinetic results. For example, q_m (mg/kg) values for As(III) adsorption on PS (117.18) and on LDPE (163.30) using DI water were higher than those in RW, 116.73 (PS) and 54.78 (LDPE). These q_m values in this study were significantly less than q_m values estimated by Dong et al. (2020), who used the smaller sizes of PS for experiments (**Table 5.3**). Regarding As(V), the q_m values of PS and LDPE related to DI water were 110.26 and 130.70 mg/kg compared to 96.93 and 115.06 mg/kg in RW, respectively, which were accordance with the kinetic results. For river water, the q_m values

were for PS and LDPE, respectively. Moreover, the separation factor (R_L) values given in **Table 5.4** was less than 1 indicated that both PS and LDPE have high adsorption affinity for As(III) and As(V). The favourable sorption processes with high affinity occur when the values of R_L range from 0 to 1 (Rawat et al., 2021). From the Freundlich isotherm parameters, the values of 1/n less than 1 for PS and LDPE regardless of experimental conditions indicated As(III) and As(V) adsorption on PS and LDPE were the non-linear form (**Table 5.3**). Dong et al. (2020) explained that the interactions between adsorbate and adsorbent cause uneven distribution sites. In that way, the pore on the adsorbent surface is filled during the adsorption process.

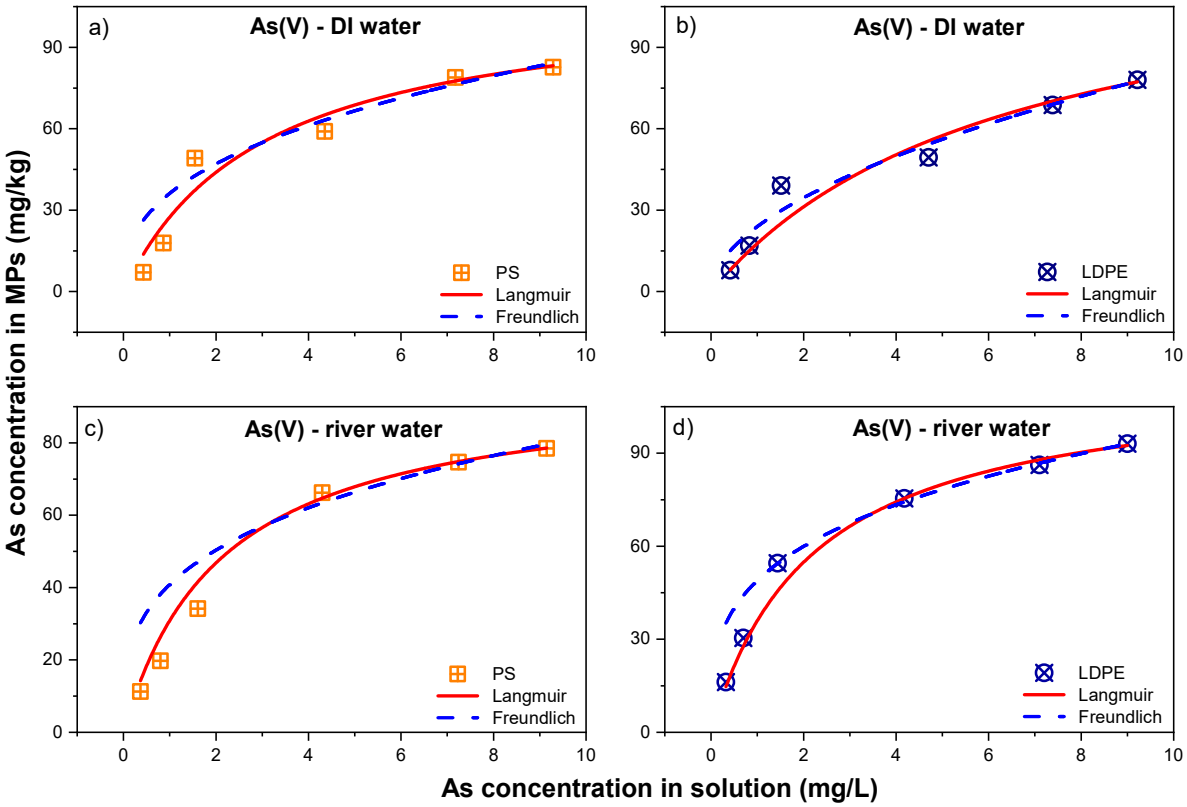

Figure 5.4. The isotherm of As(V) adsorption on PS (a, c) and LDPE (b, d).

In summary, the Langmuir model can describe homogeneous adsorbent surface while Freundlich model is suitable for multi-layers of adsorption. Ma et al. (2015) referred that both types of adsorption processes can be fitted well by the data, however the nonlinear Langmuir model described such data more properly than the nonlinear Freundlich model for both As(III)

and As(V) regardless of adsorbents in this study (**Figures 5.3 and 5.4**). The results were agreement with findings by Ma et al. (2015), indicating monolayer of As onto sediment, in which adsorption occurs at the specific localized sites, '*that are identical and equivalent, with no lateral interaction and steric hindrance between the adsorbed molecules*' (López-Luna et al., 2019, p.13) As a result, As(III) and As(V) adsorbed on selected MPs was suggested as physisorption, with higher adsorption capacity of As(III) than As(V) and more As adsorbed on LDPE than on PS (in DI water and RW), except the adsorption of As(III) and As(V) on LDPE in RW. Furthermore, no significant difference in As(III) and As(V) adsorption between PS and LDPE was found regarding isotherm models.

Table 5.3. Calculated Langmuir and Freundlich equation parameters for As(III) and As(V) adsorption at the equilibrium time in this study and data from the previous studies.

	As(III)				As(V)				Reference
Langmuir	q_m (mg/kg)	K_L (L/mg)	R. Chi-Sqr	R^2	q_m (mg/kg)	K_L (L/mg)	R. Chi-Sqr	R^2	
PS-DI	117.18 ± 5.67	0.441 ± 0.09	0.197	1.000	110.26 ± 9.88	0.331 ± 0.11	0.465	1.000	This study
LDPE-DI	163.30 ± 60.27	0.085 ± 0.05	1.000	0.999	130.70 ± 23.57	0.157 ± 0.06	0.565	0.999	This study
PS-RW	116.73 ± 4.11	0.371 ± 0.05	0.092	1.000	96.93 ± 3.14	0.467 ± 0.07	0.092	1.000	This study
LDPE-RW	54.78 ± 3.68	0.803 ± 0.36	1.382	0.995	115.06 ± 4.20	0.455 ± 0.07	0.158	1.000	This study
PS (0.1-1μm)	1120	0.0006		0.951					Dong et al. (2020)
PS (1-10μm)	1047	0.0013		0.904					Dong et al. (2020)
PS (>10μm)	920	0.0001		0.906					Dong et al. (2020)
Freundlich	K_F	1/n	R. Chi-Sqr	R^2	K_F	n	R. Chi-Sqr	R^2	
PS-DI	49.83 ± 7.42	0.291 ± 0.07	0.579	1.000	36.18 ± 5.13	0.379 ± 0.07	0.556	1.000	This study
LDPE-DI	17.48 ± 3.61	0.630 ± 0.10	0.680	0.999	23.95 ± 3.87	0.529 ± 0.08	0.443	0.999	This study
PS-RW	42.01 ± 4.05	0.351 ± 0.05	0.227	1.000	40.85 ± 6.77	0.302 ± 0.08	0.586	0.999	This study
LDPE-RW	33.00 ± 2.85	0.171 ± 0.04	0.938	0.997	48.98 ± 2.46	0.292 ± 0.02	0.103	1.000	This study
PS (0.1-1μm)	0.017	0.887		0.875					Dong et al. (2020)
PS (1-10μm)	0.017	0.903		0.901					Dong et al. (2020)
PS (>10μm)	0.015	0.907		0.950					Dong et al. (2020)

Table 5.4. R_L factor As(III) and As(V) adsorption on MPs.

R_L factor for As(III)				R_L factor for As(V)			
PS + DI	LDPE + DI	PS + RW	LDPE + RW	PS + DI	LDPE + DI	PS + RW	LDPE + RW
0.845	0.965	0.875	0.762	0.876	0.939	0.853	0.119
0.716	0.928	0.795	0.625	0.778	0.885	0.728	0.067
0.590	0.878	0.635	0.440	0.661	0.808	0.571	0.039
0.355	0.723	0.389	0.213	0.410	0.575	0.332	0.028
0.243	0.614	0.276	0.142	0.296	0.463	0.228	0.025
0.201	0.555	0.230	0.116	0.245	0.409	0.190	0.023

5.3.4. Sorption mechanisms

The Langmuir and Freundlich isotherm results indicated that both chemisorption and physisorption were participated in the adsorption process of As(III) and As(V) on PS and LDPE. The binding sites on the adsorbent surface were supported by FTIR results (**Figure 5.1a** and **b**). It was reported that the H atoms on the carboxyl group for PS and hydroxyl group for PTFE have the large positive electrostatic potential, at +56.60 and +82.37 kcal/mol, respectively (Dong et al., 2020, 2019). The O–H bond length was shortened due to the O atom participated in the complexation of As(III) or As(V) during the adsorption process (Dong et al., 2020). This study revealed that adsorption of As metal ion is related to nitrogen and oxygen functional groups of material surface (Gordon et al., 2015). Based on the surface electrostatic potential analysis of PS and PTFE (Dong et al., 2020, 2019), the key mechanisms for As(III) adsorption onto PS and PTFE are electrostatic force and non-covalent interaction. Sharing the similar FTIR results with Dong et al. (2020) for PS adsorbed As(III), it was suggested that electrostatic force and non-covalent interaction are the main factors affecting adsorption mechanism of As(III) and As(V) on PS and LDPE.

5.4. Conclusions

The adsorption of As(III) and As(V) on PS and LDPE in this chapter related to cleaned-fresh water (DI water) and simulated river conditions (RW) was investigated by using pre-production bead MPs. The adsorption rate was higher within the first 24h, followed by slow stage for all experimental conditions. The PSO model could provide better exhibition of kinetic adsorption related to higher R^2 and q_e values. Langmuir and Freundlich isotherm models were well fitted with experimental data indicating both chemisorption and physisorption were involved in the adsorption processes. The q_m values estimated by Langmuir model of PS (117.18 mg/kg) were lower than LDPE (163.30 mg/kg) for As(III) in DI water, but higher than in RW (116.73 and 54.78 mg/kg, respectively). The q_m values for As(V) adsorbed on LDPE were higher than PS by using both DI water and river water, 130.70 and 115.06 mg/kg compared to 110.26 and 96.93 mg/kg. The degrees of As adsorbed on PS and LDPE varied in different aqueous environments (DI water and RW) referred that environmental factor contributed major influence on the adsorption of As species on MPs, thus this factor need to be comprehensively investigated further. Furthermore, the interactions between As species and PS and LDPE mainly occur on the carboxyl and hydroxyl groups of adsorbent surface, whilst electrostatic force and non-covalent interaction significantly contributed to the adsorption mechanism of As(III) and As(V) on PS and LDPE.

CHAPTER SIX:

ADSORPTION-DESORPTION OF ARSENIC SPECIES ON RIVER SEDIMENT AND MICROPLASTICS

6. CHAPTER SIX: ADSORPTION-DESORPTION OF ARSENIC SPECIES ON RIVER SEDIMENT AND MICROPLASTICS

Adsorption-desorption of arsenic species on river sediment in this chapter covers the contents of a published review paper: **Kien Thanh Nguyen**, Amir Navidpour, Mohammad Boshir Ahmed, Amin Mojiri, Yuhan Huang, John L. Zhou (2022) Behaviour and mechanism of arsenite and arsenate adsorption and desorption at river sediment-water interface. *Journal of Environmental Management.* (Accepted 6 June 2022).

6.1. Introduction

Highly toxic element, As presences in the biota such as fresh water and sediments in various concentrations (Chen et al., 2016; Goldberg and Suarez, 2013; Osuna-Martínez et al., 2021). Natural processes (i.e. weathering and biological activity) and anthropogenic activities (e.g. mining, industrial processes and agricultural activities) have been reported as the main sources of As releasing into the environments (Hua, 2018; Osuna-Martínez et al., 2021; Xie et al., 2018b). In terrestrial and aquatic environments, As predominantly occurs as As(III) and As(V), which have higher toxic levels than organic forms (Wang et al., 2018; Xie et al., 2018b). In surface waters such as river water, As pollution is considered as an environmental problem (Hua, 2018). Recently, Osuna-Martínez et al. (2021) reported the level of As contamination in river water was high as 8684 µg/L in Matehuala, Mexico. As concentrations in sediments were significantly higher than in water bodies, with the highest value up to 28600 mg/kg (Osuna-Martínez et al., 2021). In Australia, high As polluted degree in Sydney harbour estuary sediments was 29 mg/kg (Jahan and Strezov, 2018), but this level was still lower than

Australian Water Quality Guidelines for Freshwater (AWQG, 1992). Sediments can observe significant amount of As from high As concentrations in waters under favourable hydraulic conditions (Chen et al., 2016; Jahan and Strezov, 2018). The sedimentary environmental conditions such as grain size and organic matter influenced the chemical fraction of As, its concentration and distribution in sediment (Wang et al., 2019), resulting in the degrees of As toxicity and bioavailability (Ma et al., 2015). In another way, As may return into the water column under the changes in physical and chemical factors or under variable hydraulic conditions (Jahan and Strezov, 2018; Nematollahi et al., 2021). As a result, contaminated sediments are a secondary As polluted source (Chen et al., 2016; Nematollahi et al., 2021). Thus, study the transport and fate of As in the solid and aqueous environments is necessary (Wang et al., 2018).

Adsorption and desorption studies of As have been widely investigated for predicting the fate and behaviour of As in soils and sediments as well as the part of these components such as Al and Fe oxides, clay minerals, organic matter, particle size and natural fulvic acids (Dousova et al., 2012; Goldberg and Suarez, 2013; Li et al., 2018; Wang and Mulligan, 2006a; Yang et al., 2006; Zhang and Selim, 2005). Other controlling factors such as pH, competitive anions, cations, bacterial activity, concentrations of As in solution, reaction time and amount of adsorbent dosages have been reported to explore the ratio of adsorption and maximum adsorption capacities of soils and sediments (Huang et al., 2013; Xie et al., 2018b). Adsorption and release processes involved two stages including a rapid rate and then a slow rate (Huang et al., 2013; Xie et al., 2018b). Additionally, adsorption behaviour of As under various pH levels has been widely investigated. As(III) and As(V) adsorption on sediments increased with increase in pH degrees between 3-7 (Chen et al., 2016; Ma et al., 2015). In contrast, Yean et al. (2005) reported that both As(III) and As(V) totally desorbed from sorbents in alkaline conditions, of which increase in pH led to higher desorption rates. Studies revealed that iron

oxide, the presence of other cations and bacterial activity enhanced the adsorption rates of As(III) and As(V), while anions and organic matter caused decrease in adsorption rate (Huang et al., 2013; Wang and Mulligan, 2006a; Xie et al., 2018b). Regarding the desorption rate, Sharma and Kappler (2011) found that no clear trend was observed for the release of As (III) and As(V) from the humic acid-coated clay regardless of initial concentrations of As or the presence of phosphate and silicate. Interactions between As(III) or As(V) with clay minerals or iron oxides indicated that the inner-sphere complex, hydroxide corrosion of zerovalent iron, ternary complex formation with Ca^{2+} functioning (outer-sphere complex) and aggregating with amine groups from humic molecules involved in the sorption of As species on the clay surface (Sharma and Kappler, 2011; Yean et al., 2005). Additionally, As(V) adsorption on sediment is strongly related to smectite clays rather than high content of quartz or elite mineral (Borgnino et al., 2012; Goldberg and Suarez, 2013).

MPs contamination in biota systems such as river water and sediments are a hot topic due to their environmental persistence and ecological effects (Shen et al., 2021). MPs have been detected in river water bodies in various shapes (fragments, pellets, fibers, films and foam) and colours (white, transparent, black, red, yellow and green). MPs have been recorded and classified as major groups including PE, PP, PVC, PS and PET (Andrady and Neal, 2009). MP abundance in river waters and sediments was reported as high as $4.7x10^6$ particles/m^3 and 11917 particles/kg, respectively (Liu et al., 2021; Sankoda and Yamada, 2021). Another concern related to MPs is that they can adsorb and convey metal ions in river and marine systems. Al, Cr, Cu, Fe, Mn, Ti and Zn on natural-aged MPs have been reported (He et al., 2020b; Vedolin et al., 2018; Wang et al., 2017). Moreover, studies on the kinetic and isotherm adsorption of As onto different types of MPs have been conducted in the laboratory (Dong et al., 2020, 2019). Controlling factors including pH, temperature, interfering NO_3^- and PO_4^{3-} ions influencing As(III) adsorption on polytetrafluoroethylene (PTFE) and PS were reported. SSA,

pH, NO_3^- and PO_4^{3-} showed the similar effects on adsorption of As(III) on MPs as on soils. Polarity, morphology and organic polymer composition also enhanced heavy metals adsorption on MPs (Ahmed et al., 2021; Ashton et al., 2010). The adsorption of As(III) on surface of MPs primarily occurs via hydrogen bond of carboxyl group, while electrostatics forces and non-covalent are the main interactions of adsorption mechanisms (Dong et al., 2020). However, one question is that how As interacts with both sediments and MPs, particularly in RW. Sediment is a vital compartment in river systems, and works as a sink of metals, MPs and other pollutants (Jahan and Strezov, 2018; Nematollahi et al., 2021). This chapter, thus, aims to (1) investigate the adsorption and desorption behaviours of As(III) and As(V) in RS by using RW as the feeding solution; (2) assess the adsorption and release capacities of As(III) and As(V) in the mixed-environments of RS with PS or LDPE by using DI water and RW; and (3) study the adsorption and desorption mechanisms of As(III) and As(V) on RS, PS and LDPE via the analysis of surface functional groups.

6.2. Methodology

The detailed descriptions about the components and preparation of RS are in **Chapter 4** (**Table 4.1**). Information related to RW, PS and LDPE is described in **Chapter 5.2**.

The adsorption of As(III)/As(V) was assessed by using various adsorbents including RS, RS-PS, and RS-LDPE. The stock solution of 100 mg/L of As(III)/As(V) was diluted by DI water or RW to obtain the solutions of 10 As mg/L. The adsorption experiments were conducted by mixing 200-mL of As(III) or As(V) (0.5-10.0 mg/L) with either 2.0 g of sorbents (i.e. 2.0 g sediment, or 2.0 g of sediment with 2.0 g of PS, or 2.0 g of sediment with 2.0 g of LDPE). The adsorption and desorption experimental investigations were given in **Chapter 3**.

To assess the adsorption and desorption of As(III) and As(V) onto different adsorbents, a series of experiments were conducted (**Table 6.1**). Firstly, the sorbent of RS was carried out

in RW solution to evaluate the adsorption and desorption behaviours. After that, the mixture of sediment with PS or LDPE as an adsorbent was conducted in both DI water and RW. The experiments using 10.0 mg/L of As(III) or As(V) and the adsorbent of sediment with PS or LDPE were performed in triplicate, and the averaged results were calculated (Dousova et al., 2012). The functional groups of the sediment, PS and LDPE were detected by the FTIR spectrometer before and after adsorption process. The kinetic sorption, isotherm sorption and partition coefficient analysis are described in **Chapter 3**.

Table 6.1. Sorption experiment conditions.

As species	Adsorbent type	DI water		RW	
		Kinetic	Isotherm	Kinetic	Isotherm
As(III)	RS			✓	✓
	RS+PS	✓	✓	✓	✓
	RS+LDPE	✓	✓	✓	✓
As(V)	RS			✓	✓
	RS+PS	✓	✓	✓	✓
	RS+LDPE	✓	✓	✓	✓

As(III) and As(V) adsorption on RS by using DI water was conducted in **Chapter 4**.

6.3. Results and discussion

6.3.1. FTIR results of sediment, PS and LDPE

Figure 6.1(a and **b)** illustrate the FTIR spectra results of the interactions between As(III) and As(V) with RS particles after adsorption and desorption using RW solution. The results showed no difference between As(III) and As(V) after both adsorption and desorption, indicating that the same functional groups of RS interacted with As species during the adsorption process.

Compared to the surface of RS particles before adsorption, the main functional groups involved in the interactions with As species were phenolic hydroxyl, carboxyl, quartz and goethite groups (**Figure 6.1(a** and **b**)). The similar results were found for RS particles after As(III) and As(V) adsorption in the mix of RS with PS or LDPE in both DI water and RW solutions (**Figure 6.1(c** and **d**)). In the phenolic hydroxyl group, a new band of 3865 cm^{-1} appeared after adsorption. The new peak at 2307 cm^{-1} was attributed to C–O molecular vibrations in calcite (Hahn et al., 2018). In the carboxyl group, two new peaks of 1651.07 and 1705.07 cm^{-1} were assigned to amine C=O stretching (Yu et al., 2015). Moreover, the FTIR bands at 795 and 1088 cm^{-1} attributed to Si–O symmetrical stretching vibrations and Si(Al)–O vibration or antisymmetric stretching vibrations of Si–O tetrahedron of quartz (Hahn et al., 2018), while the peak of 694 cm^{-1} was associated with Fe–O/Fe–OH vibration of the magnetite phase (Luo et al., 2012; Rawat et al., 2021).

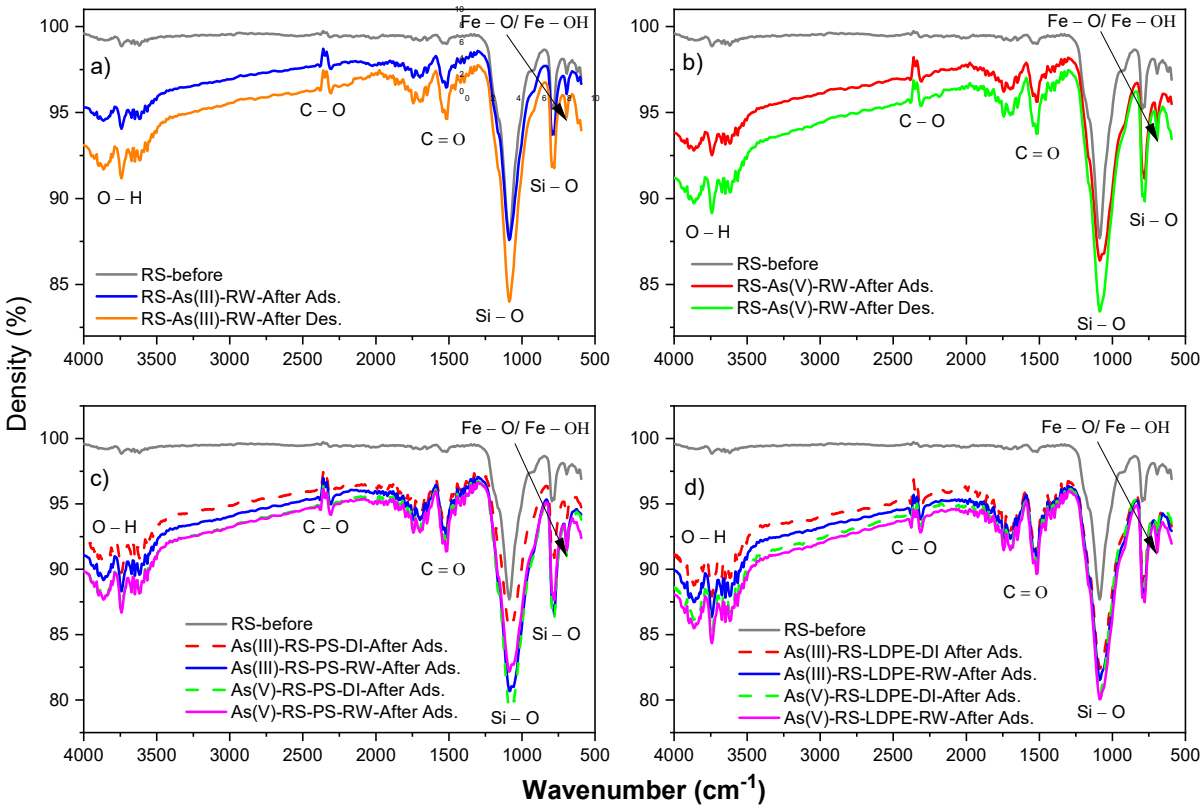

Figure 6.1. FTIR spectra of RS for As(III) and As(V). a) As(III) adsorption/desorption – RS-RW, b) As(V) adsorption/desorption – RS-RW, c) As(III)/As(V) adsorption – RS-PS-DI/RW, and d) As(III)/As(V) adsorption – RS-LDPE-DI/RW.

Furthermore, **Figure 6.2a** shows the FTIR results of PS beads before and after As(III) and As(V) adsorption under DI water and RW solutions. The peaks at 748 and 2847 cm^{-1} slightly shifted to 756 and 2855 cm^{-1} after adsorption of As(III) in both DI and RW, which were assigned to the presence of CH_2 chain (Dong et al., 2020). Regarding As(V) species, FTIR peaks were changed after adsorption of As(V) in RW solution. New bands at the centre of 3742 cm^{-1} was assigned to O–H functional groups, whilst the peaks of 1681-1744 cm^{-1}, 2315 and 2855 cm^{-1} were associated with C–N, C–O and O–H groups, respectively (Dong et al., 2020; Misra et al., 2006). Three main functional groups including C–H, C=O and O–H before and after As(III) and As(V) adsorption can be seen at LDPE surface (**Figure 6.2b**). There was a

slightly change at the peak of 3194 cm^{-1} before adsorption which shifted to 3186 cm^{-1} after the adsorption of As(III) in RW and As(V) in DI water, which was attributed to the involvement of C–H functional group in the binding of As species.

Furthermore, **Figure 6.3** showed lower Al contents was detected for As(V) adsorption on RS, indicating SEM-EDS revealed the results higher enrichment of As(V) on RS than As(III) (Matera et al., 2003). Another suggestion was that rich contents of Al and Si in RS particles resulted in overestimation of As signal after adsorption of both As(III) and As(V). In addition, **The Figure 6.3c** showed two distinctive fitted peaks at 1329 and 1327 eV corresponding to the As(III) and As(V), respectively, for RS particles after adsorption of As(III). However, **Figure 6.3d** showed not detective result for (As3d) (Gomes et al., 2007), though higher adsorption of As(V) on RS was calculated at the equilibrium time. As a result, the concentration of As on RS particles after adsorption of As(V) was low to detect. It is suggested that not all RS particles adsorbed the same amount of As. Moreover, the % atomic of As(V) and As(III) on RS particles after adsorption of As(III) were 0.03% and 0.04%, respectively, indicating some of As(III) on RS particles being oxidised to As(V).

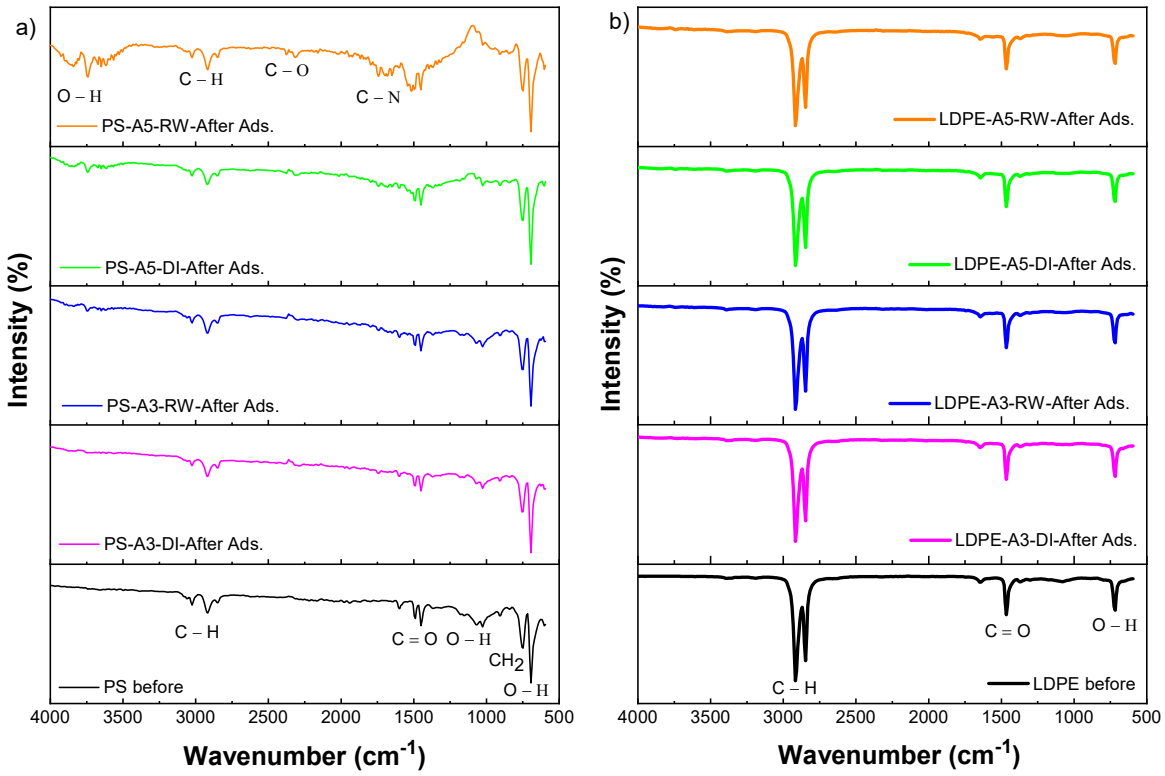

Figure 6.2. FTIR spectra of PS (a) and LDPE (b) before and after As(III) and As(V) adsorption on RS-PS or RS-LDPE under DI and RW conditions.

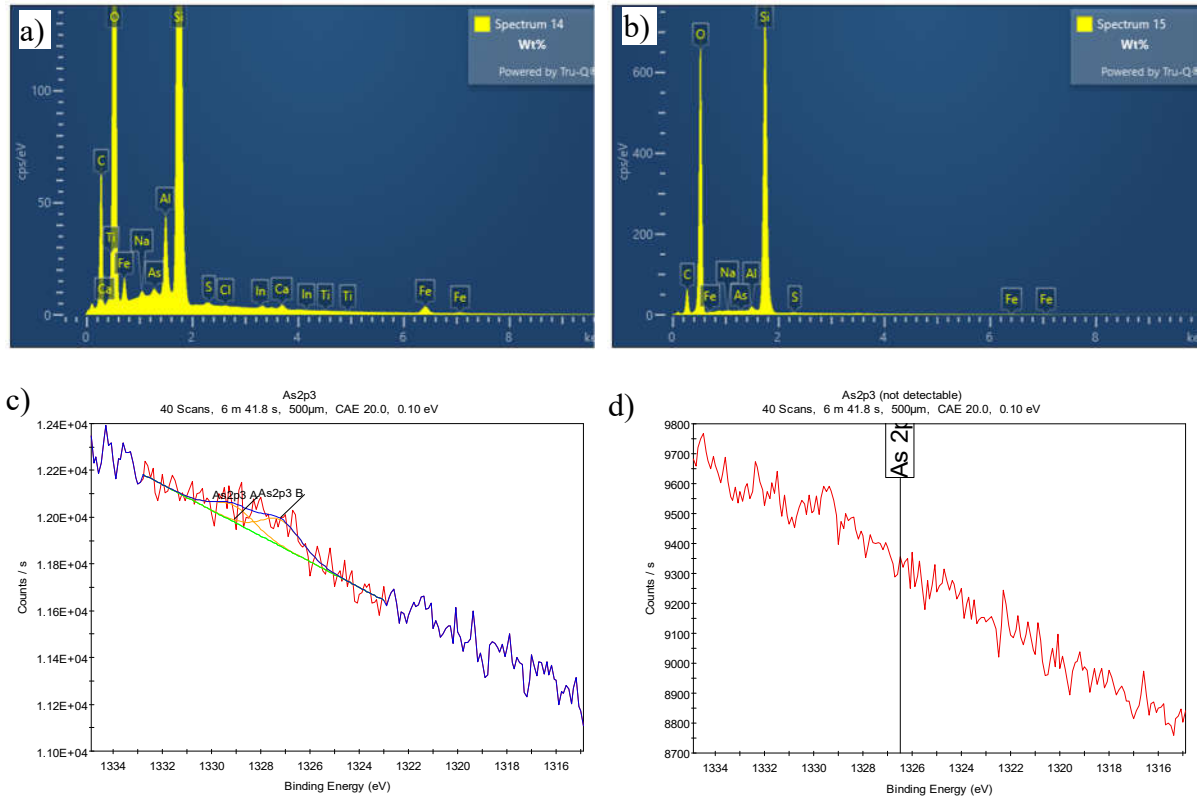

Figure 6.3. SEM-EDS analysis of RS after adsorption of (a) As(III) and (b) As(V); and XPS analysis of RS after adsorption of (c) As(III) and (d) As(V) by using RW.

6.3.2. Sorption kinetics

Kinetic experimental data was simulated by PFO and PSO models to illustrate the changes in amounts of As(III) and As(V) in adsorbents versus time (**Figures 6.3** and **6.4**). The rates of As(III) and As(V) retention for all experiments were rapid during the first 24 h of reaction, followed by slow reactions, depicting the correlation between As(III) and As(V) concentrations in solution versus time. The concurrence of kinetic models with experimental data illustrated the time dependence of both As(III) and As(V) sorption. This biphasic arsenic adsorption behaviour was observed on sediments over different time scales from minutes (Ma et al., 2015), 24 h (Dousova et al., 2012) to days (Xie et al., 2018b). According to Zhang and Selim (2005), the non-equilibrium conditions of As(V) adsorption could occur in heterogeneous soil systems. Without significant differences of adsorption behaviours for As(III) and As(V) in this study, this phenomenon may be suggested for heterogeneous sediment systems due to three hypotheses, namely: 1) the heterogeneity of sorption sites, 2) *three-dimensional growth of a arsenic solid phase caused by slow precipitation at the mineral surface, and 3) slow accessible sites with variable degrees of affinities to As(III) or As(V) caused by slow diffusion to sites within the sediment matrix* (Zhang and Selim, 2005).

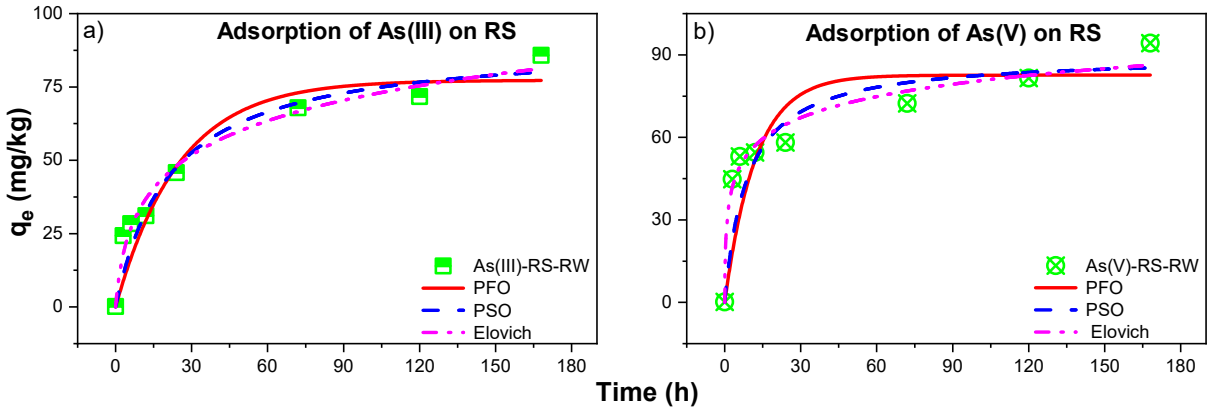

Figure 6.4. PFO, PSO and Elovich kinetic models of As(III) (a) and As(V) (b) adsorption on RS by using RW. Symbols are experimental data.

Figure 6.4 illustrates that As(V) had higher adsorption affinity than As(III) on RS under the RW condition. As shown in **Table 6.2**, the equilibrium data (q_e) for As(III) on RS under RW condition estimated by PFO was 77.28 mg/kg, which was lower than that of experimental data (85.81 mg/kg) whilst the PSO predicted a higher value of 90.35 mg/kg. In contrast, both PFO and PSO models estimated lower q_e degrees than experimental value, 82.62 and 89.78 mg/kg compared to 94.25 mg/kg, respectively. Xie et al. (2018b) reported that the amounts of As(V) adsorbed on three sediments were higher than that of As(III) regardless of bacterial activity.

Additionally, the results of PFO and PSO models for As(III) and As(V) adsorption on different adsorbents of RS-PS and RS-LDPE under DI water and RW were well fitted with experimental data (**Figure 6.5**). The kinetic parameters of the PFO and PSO models for these experiments are presented in **Table 6.2**. The PSO provided better results of q_e than PFO, which were closer to the experimental data. The experimental q_e (mg/kg) values for As(III) and As(V) were decreased in the order of: As(V)-RS-LDPE-RW > As(V)-RS-PS-RW > As(III)-RS-PS-DI > As(III)-RS-LDPE-DI > As(III)-RS-PS-RW > As(V)-RS-LDPE-DI > As(III)-RS-LDPE-RW > As(V)-RS-PS-DI. As a result, there was higher adsorption affinity of As(III) in DI water than in

RW, whilst the opposite trend was observed for As(V). Finally, compared to PFO and PSO models, Elovich model provided the best the adsorption of both As(III) and As(V) regardless of experimental conditions (RS, RS-PS, RS-LDPE, DI water and RS). It was revealed that the chemisorption mechanism was favour for all these conditions (Alkurdi et al., 2021; Nguyen et al., 2020). The Elovich adsorption rate (α) of As(V) on RS was higher than that of As(III), indicating higher adsorption rate at the initial phase for As(V). In contrast, the adsorption rates for first adsorption phase of As(III) on RS-PS and RS-LDPE were higher than As(V) in both DI water and RW due to higher values of α for As(III) except for adsorbent of RS-LDPE using RW.

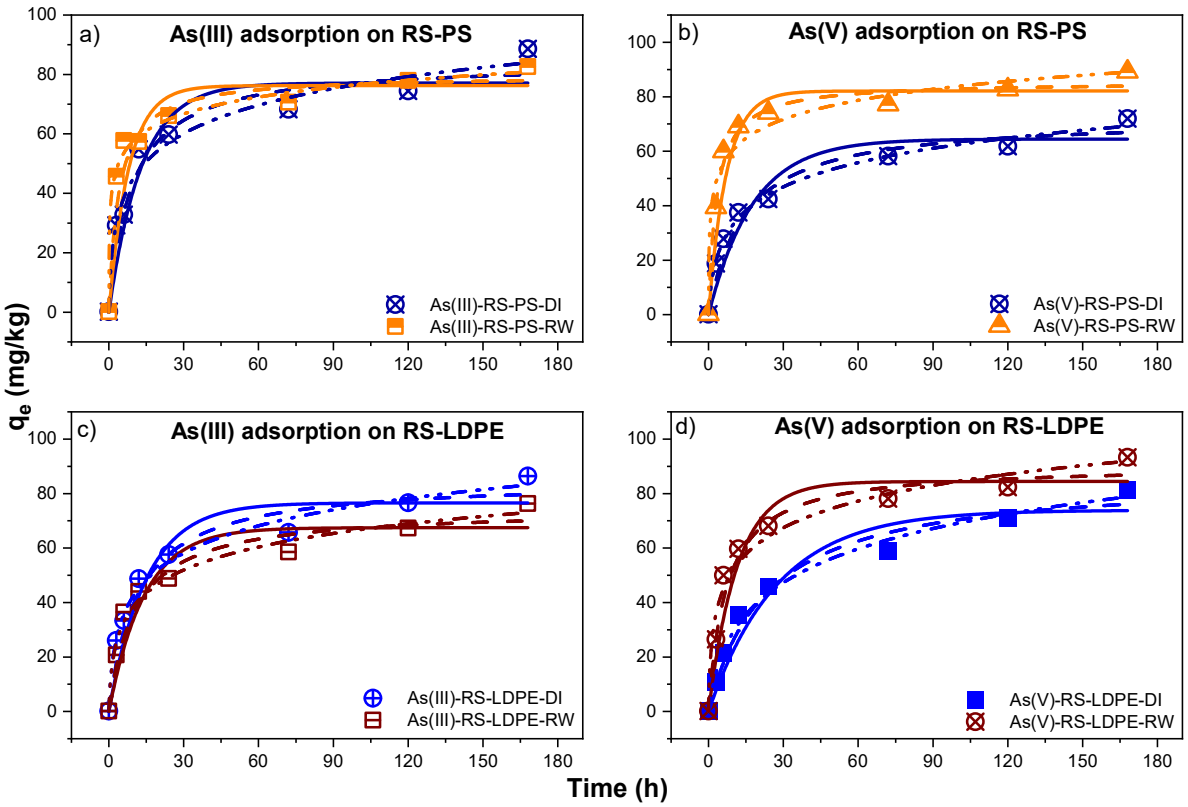

Figure 6.5. PFO, PSO and Elovich kinetic models of As(III) (a) and (c); As(V) (b) and (d) adsorption on RS and PS/LDPE. Symbols are experimental data; solid, dash and dash dot dot curves depict results of curve-fitting with the PFO, PSO and Elovich equations, respectively.

Table 6.2. PFO and PSO kinetic parameters, equilibrium adsorption and desorption capacities.

As	Exp. conditions	PFO			PSO			q_e[c] (mg/kg)	Elovich		
		R^2	K_1 (1/h)	q_e[a] (mg/kg)	R^2	K_2 (kg/mg-h)	q_e[b] (mg/kg)		R^2	α (mg/kg min)	β (kg/mg)
	Adsorption										
As(III)	RS-RW-Ads.	0.995	0.040	77.28	0.997	0.001	90.35	85.81	0.980	10.50	0.057
	RS-PS-DI-Ads.	0.993	0.077	77.12	0.996	0001	84.27	88.64	0.974	34.44	0.072
	RS-PS-RW-Ads.	0.996	0.126	76.24	0.998	0.003	79.79	82.67	0.991	955.54	0.122
	RS-LDPE-DI-Ads.	0.993	0.067	76.58	0.997	0.001	85.11	86.42	0.989	25.59	0.068
	RS-LDPE-RW-Ads.	0.994	0.070	67.47	0.997	0.001	74.35	76.32	0.983	27.31	0.081
As(V)	RS-RW-Ads.	0.989	0.082	82.62	0.993	0.001	89.78	94.25	0.972	156.25	0.090
	RS-PS-DI-Ads.	0.996	0.056	64.46	0.998	0.001	72.51	71.97	0.994	15.30	0.076
	RS-PS-RW-Ads.	0.997	0.139	82.11	0.998	0.004	85.53	89.18	0.968	421.90	0.100
	RS-LDPE-DI-Ads.	0.995	0.036	73.90	0.998	0.001	86.55	81.24	0.991	6.95	0.052
	RS-LDPE-RW-Ads.	0.995	0.087	84.43	0.998	0.002	90.48	93.33	0.974	53.88	0.070
	Desorption										
As(III)	RS-RW-Des.	1.000	0.090	75.84	1.000	0.011	74.92	75.22			
	RS-PS-DI-Des.	1.000	0.152	80.96	1.000	0.028	80.40	80.30			
	RS-PS-RW-Des.	1.000	0.088	73.60	1.000	0.012	72.69	72.38			

	RS-LDPE-DI-Des.	1.000	0.165	79.14	1.000	0.033	78.66	78.51
	RS-LDPE-RW-Des.	1.000	0.150	69.29	1.000	0.003	68.78	68.64
As(V)	RS-RW-Des.	1.000	0.059	86.27	1.000	0.007	85.15	85.44
	RS-PS-DI-Des.	1.000	0.116	65.85	1.000	0.025	65.37	65.35
	RS-PS-RW-Des.	1.000	0.100	81.66	1.000	0.017	80.99	80.64
	RS-LDPE-DI-Des.	1.000	0.175	74.53	1.000	0.036	74.05	73.67
	RS-LDPE-RW-Des.	1.000	0.072	84.72	1.000	0.010	83.82	84.08

[a.] estimated equilibrium adsorption capacity from the PFO model.

[b.] estimated equilibrium adsorption capacity from the PSO model.

[c.] estimated equilibrium adsorption capacity in the experiments.

6.3.3. Desorption kinetics

The desorption kinetics for As(III) and As(V) from RS under RW condition are shown in **Figure 6.6**. Both PFO and PSO models successfully described these desorption phases with better results for PSO. Moreover, higher q_e values were estimated from PFO for As(III) (75.84 mg/kg) and As(V) (86.27 mg/kg) in comparison to 74.92 and 85.15 mg/kg estimated from PSO, respectively (**Table 6.2**). The rate of release from RS were rapid within 24h, followed by stable rate during the remaining time. These results agreed with the findings by Xie et al. (2018b) that the desorption rate was fast during the initial 24 h, then decreased in up to 28 days. At the equilibrium time (7 d), 12.3% of As(III) released from RS in RW was higher than 9.3% for As(V). Xie et al. (2018b) reported the similar trend for all experiments regardless of bacterial activity. The average rates of As(V) released from three sediments with and without the presence of bacteria were 38.2% and 31.5%, compared to 60.3% and 53.1% for As(III), respectively (Xie et al., 2018b). The results indicated stronger binding between As(V) with sediment than As(III) in various aqueous environments.

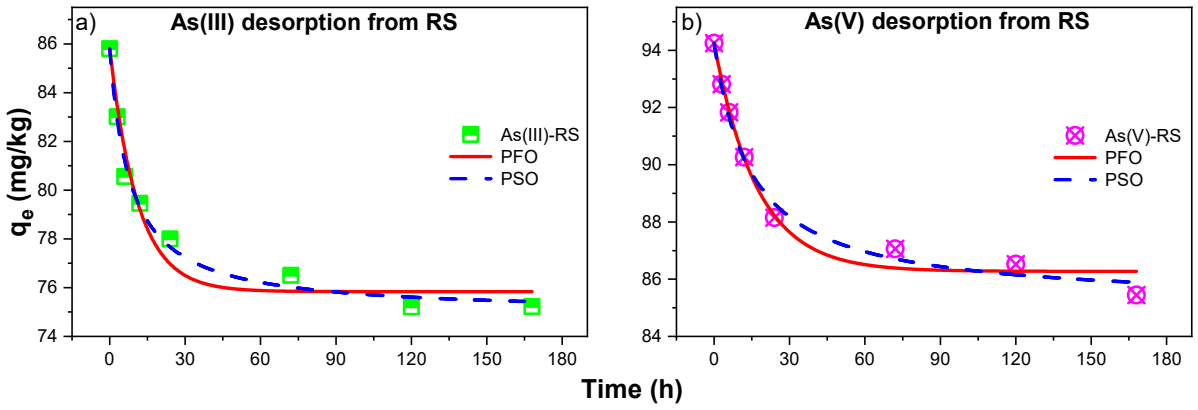

Figure 6.6. PFO and PSO kinetic models of As(III) (a) and As(V) (b) desorption from RS by using RW. Symbols are experimental data.

The results for desorption kinetics of As(III) and As(V) from RS-PS and RS-LDPE simulated by PFO and PSO models are presented in **Figure 6.7** to illustrate the changes in

amounts of As(III) and As(V) in adsorbents versus time. The rates of desorption for these conditions were similar to desorption behaviour of As(III) and As(V) from the RS above and Xie et al. (2018b). PSO provided better q_e values in comparison to experimental data, while PFO estimated higher q_e values for all conditions (**Table 6.2**). The rates of As(V) released from RS-PS (DI: 9.2%, RW: 9.6%) and RS-LDPE (DI: 9.3%, RW: 9.9%) were lower than As(III) desorbing from RS-PS (DI: 9.4%, RW: 12.4%) and RS-LDPE (DI: 9.1%, RW: 10.1%) at the equilibrium, except the experiment of RS-LDPE in DI water. Higher release rates of both As(III) and As(V) from adsorbents in RW than in DI water indicated that RW enhanced the release of As into the water phase. In addition, these polymers has insignificant effects on the desorption behaviours of As(III) and As(V).

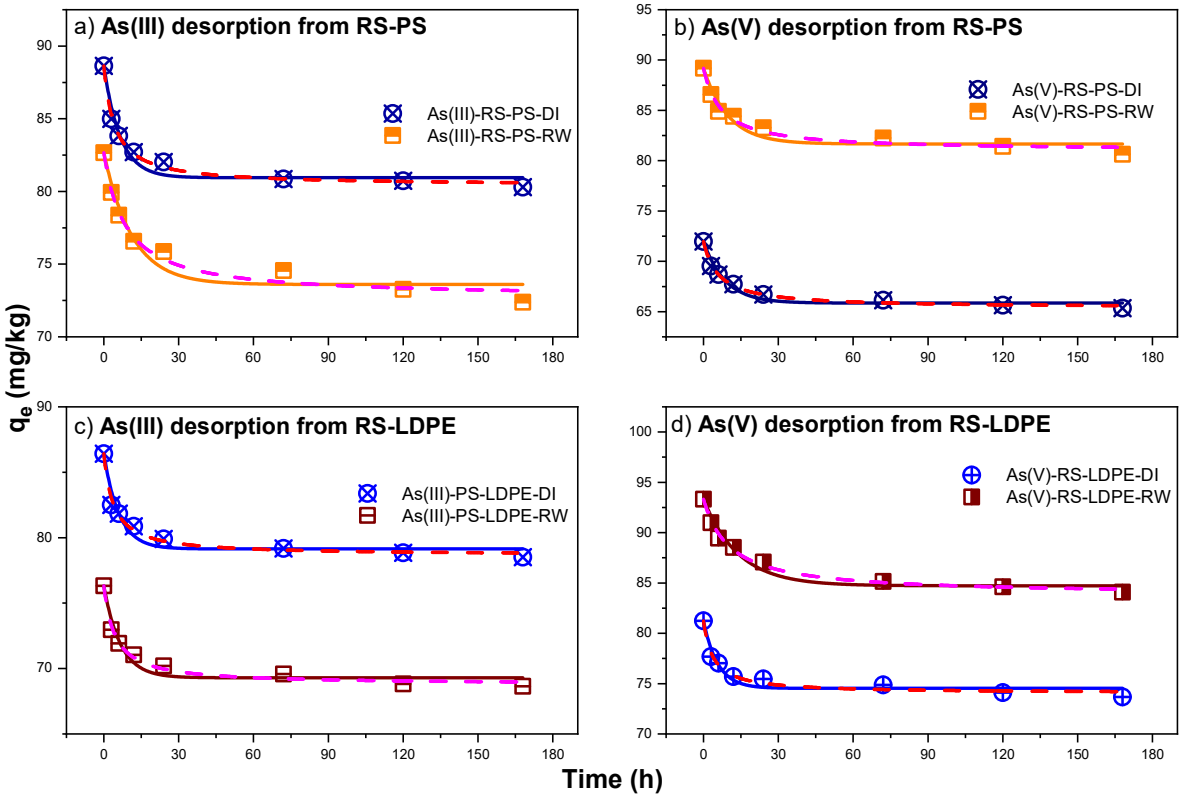

Figure 6.7. PFO and PSO kinetic models of As(III) (a) and (c); As(V) (b) and (d) desorption on RS- PS/LDPE by using DI water and RW. Symbols are experimental data; solid and dash curves depict results of curve-fitting with the PFO and PSO equations, respectively.

6.3.4. Non-linear sorption isotherms

Three isotherm models (Langmuir, Freundlich and Sips) exhibited the adsorption and desorption isotherms of As(III) and As(V) for RS in RW, as shown in **Figure 6.8**. The isotherms of As(III) and As(V) clearly exhibited non-linear forms by Langmuir and Freundlich models, while only As(V) adsorption was fitted with Sips model. According to Zhang and Selim (2005), a Freundlich parameter N value much smaller than 1 represented the adsorption behaviour of As was concentration-dependent. This parameter was used to measure the extent of the sorption site's heterogeneity, providing different adsorption affinities on matrix surfaces for retention. Higher N values from the Freundlich models (0.778 and 0.678 for As(III) and As(V)) were found in this study than those from Zhang and Selim (2005), varying from 0.087-0.368 for As(V) adsorption on different soils, and 0.476-0.556 for As(III) and 0.435-0.625 for As(V) adsorption on lake and river sediments (Ma et al., 2015). Higher N values in this study indicated a low heterogeneity of sorption sites for SOM. Langmuir model reported higher adsorption maxima (q_m) of As(III) (264.85 mg/kg) than that of As(V) (205.92 mg/kg), which showed the opposite result from the fore-mentioned kinetic calculations. The maximum adsorption capacity estimated by Sips model for As(V) adsorption (287.05 mg/kg) was significantly higher than two-parameter Langmuir model although the data was fitted with both of them. The adsorptions of As(III) and As(V) on RS-PS and PS-LDPE were well fitted with Langmuir and Freundlich models (**Figure 6.9**). The q_m values for As(III) were higher than those for As(V), except the figures of RS-LDPE-RW, 117.33 mg/kg for As(III) compared to 127.70 mg/kg for As(V). R_L factors (**Table 6.4**) for adsorption phase of As(III) and As(V) on RS were less than 1 for all experimental conditions, which indicated that the sorption isotherms were favourable. Regarding the three-parameter Sips model, the adsorption of As(III) and As(V) on RS-LDPE-RW as well as the adsorption of As(V) on RS-PS in both DI and RW were claimed successfully while other scenarios were not fitted. However, the Sips q_m values for

As(III) and As(V) adsorption were lower than those from Langmuir model, except As(V) adsorption on RS-LDPE-RW, which were disagreed with findings from Simsek and Beker (2014).

Regarding desorption phase, **Figures 6.8 c** and **d** show that experimental data of As(III) and As(V) desorption on RS by using RW was fitted with the Langmuir, Freundlich and Sips models. The N values of 0.947 and 0.833 for As(III) and As(V) indicated favourable desorption from RS in RW condition (Ma et al., 2015). The desorption data was not well fitted with Langmuir and Freundlich models, supporting by the R_L factors (**Table 6.4**). The R_L values for the desorption phase were closed to 1 for both As(III) and As(V). As(III) desorbing from RS-RW, RS-PS-RW, and As(V) releasing from RS-RW, RS-LDPE-DI and RS-LDPE-RW, indicated linear desorption from the surface of RS (Rawat et al., 2021) or a well-balanced system of solid-water interface (Dousova et al., 2012). The Sips model claimed successfully and was well fitted with As(III) and As(V) desorption process regardless of experimental conditions (**Figure 6.8 c&d, Figure 6.10**). The Sips q_e values were significantly lower than those estimated by Langmuir isotherm model (**Table 6.3**). The maximum desorption capacity of As(V) on RS was higher than that of As(III), 133.39 mg/kg compared to 82.86 mg/kg. Similar trend was found for As(V) desorption on RS-LDPE in both DI water and RS, while the opposite trend can be seen for the adsorbent of RS-PS.

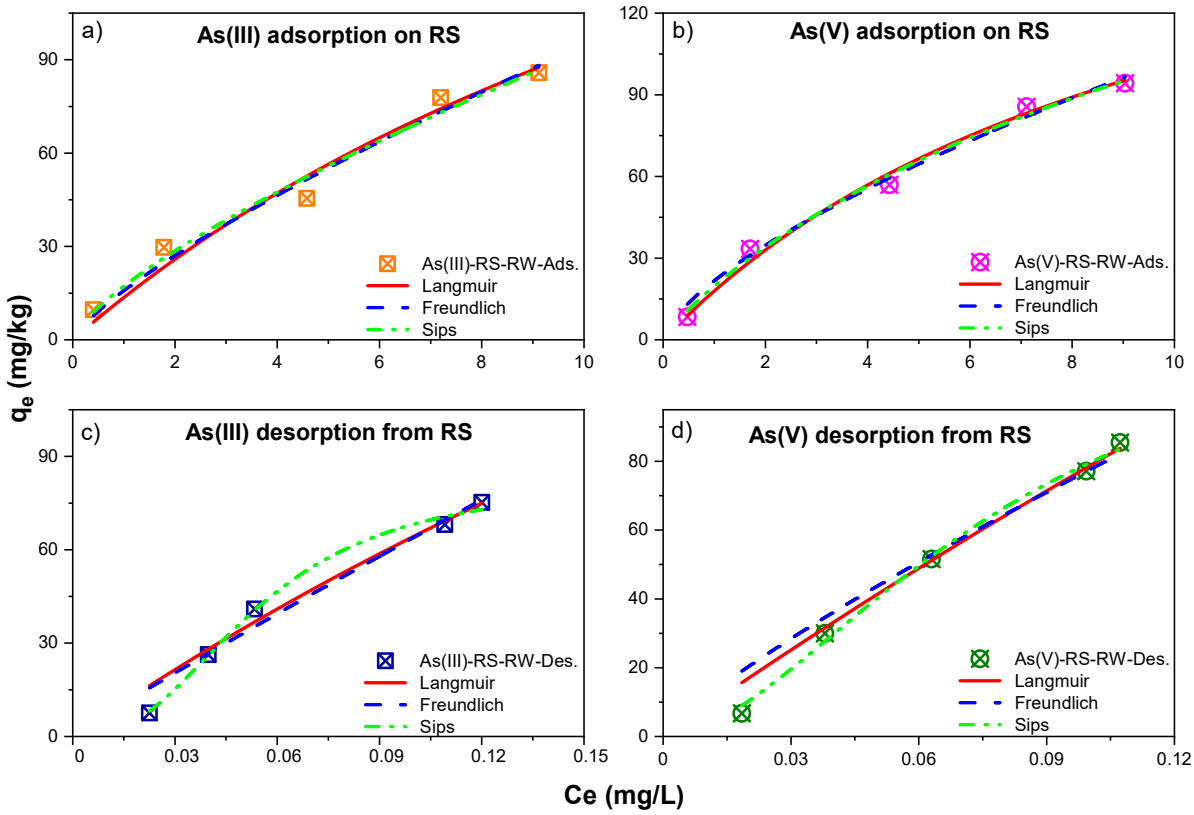

Figure 6.8. Adsorption and desorption isotherms of As(III) and As(V). a) adsorption of As(III), b) adsorption of As(V), c) desorption of As(III), d) desorption of As(V). Symbols are

experimental data, solid, dash and dash dot dot curves depict results of curve-fitting with the Langmuir, Freundlich and Sips equations, respectively.

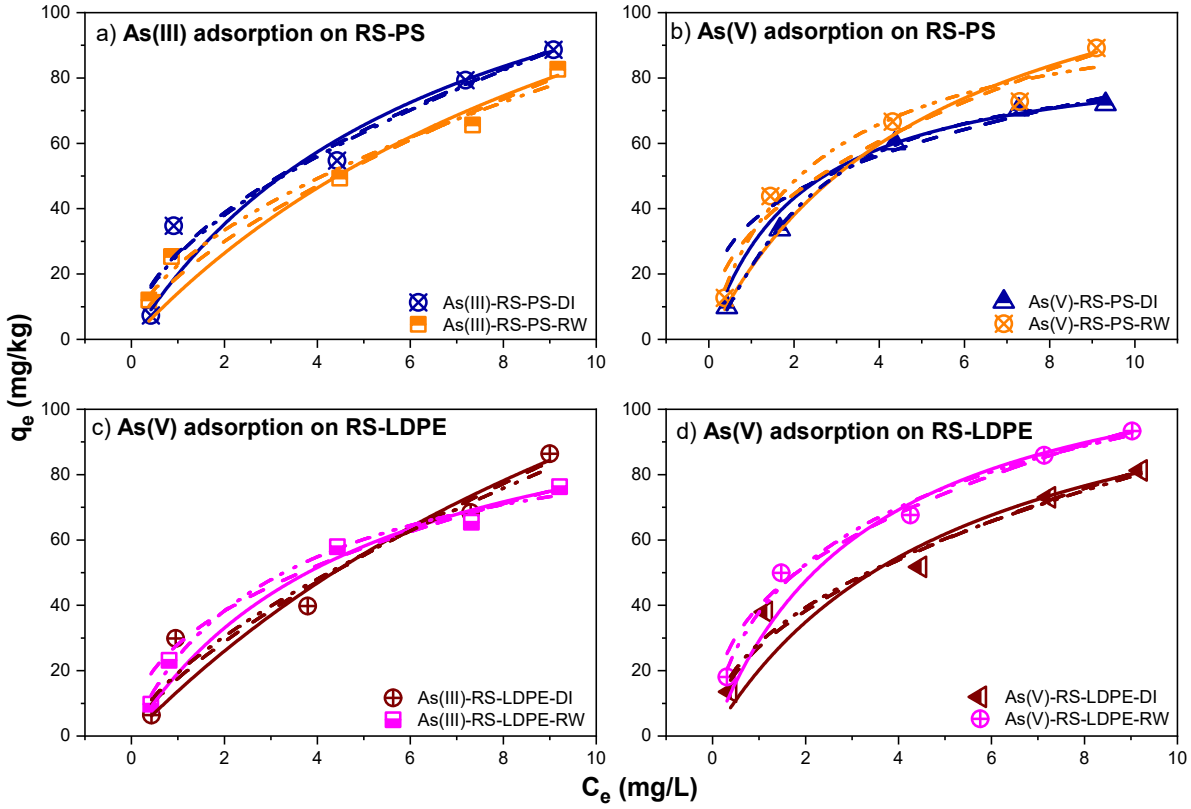

Figure 6.9. Adsorption isotherm of As(III) (a) and (c); As(V) (b) and (d) on RS-PS/LDPE by using DI water and RW solution. Symbols are experimental data, solid, dash and dash dot dot

curves depict results of curve-fitting with the Langmuir, Freundlich and Sips equations, respectively.

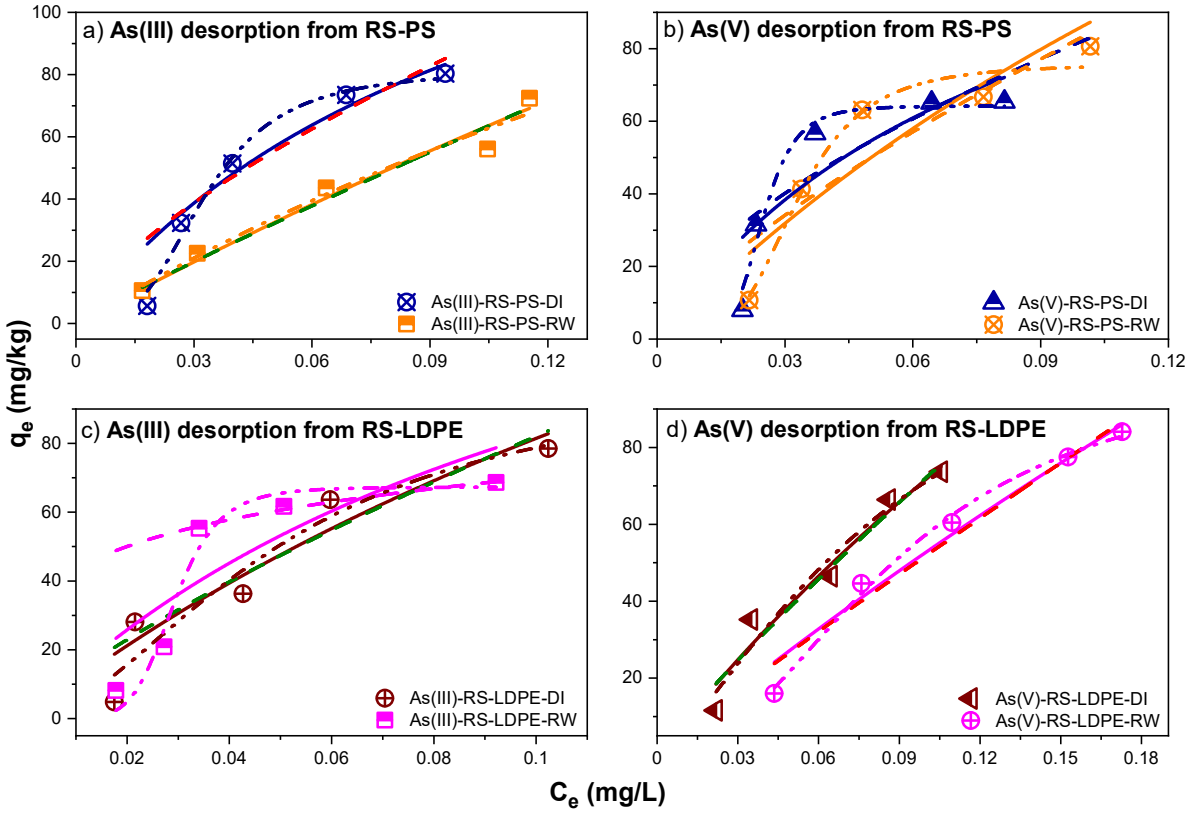

Figure 6.10. Desorption isotherm of As(III) (a) and (c); As(V) (b) and (d) on RS-PS/LDPE by using DI water and RW solution. Symbols are experimental data, solid, dash and dash dot dot curves depict results of curve-fitting with the Langmuir, Freundlich and Sips equations, respectively.

Table 6.3. The Langmuir and Freundlich equation parameters for As(III) and As(V) adsorption and desorption at the equilibrium time.

	As(III)			As(V)		
Langmuir	q_m (mg/kg)	K_L (L/mg)	R^2	q_m (mg/kg)	K_L (L/mg)	R^2
RS-RW-Ads.	264.85 ± 141.76	0.05 ± 0.04	1.000	205.92 ± 38.10	0.10 ± 0.03	1.000
RS-PS-DI-Ads.	153.43 ± 32.84	0.15 ± 0.07	1.000	89.40 ± 4.61	0.47 ± 0.11	1.000
RS-PS-RW-Ads.	190.28 ± 74.09	0.08 ± 0.05	0.999	139.36 ± 30.14	0.19 ± 0.10	0.999
RS-LDPE-DI-Ads.	236.15 ± 144.38	0.06 ± 0.06	0.999	127.27 ± 22.26	0.49 ± 0.08	0.999
RS-LDPE-RW-Ads.	117.33 ± 16.58	0.20 ± 0.07	1.000	127.70 ± 9.35	0.30 ± 0.07	1.000
RS-RW-Des.	443.36 ± 511.85	1.70 ± 2.31	1.000	891.47 ± 1743.98	0.97 ± 2.07	1.000
RS-PS-DI-Des.	181.40 ± 94.73	9.03 ± 7.98	1.000	147.65 ± 161.36	11.70 ± 22.17	1.000
RS-PS-RW-Des.	562.09 ± 1000.09	1.22 ± 2.43	1.000	320.98 ± 587.34	3.67 ± 8.61	1.000
RS-LDPE-DI-Des.	282.72 ± 320.70	4.05 ± 6.08	1.000	384.91 ± 219.78	2.29 ± 3.15	0.952
RS-LDPE-RW-Des.	182.79 ± 351.35	8.21 ± 24.08	1.000	624.69 ± 835.91	0.92 ± 1.40	0.969
Freundlich	K_F	N (1/n)	R^2	K_F	N (1/n)	R^2
RS-RW-Ads.	15.80 ± 3.63	0.778 ± 0.11	1.000	21.69 ± 3.01	0.678 ± 0.07	1.000
RS-PS-DI-Ads.	26.52 ± 4.58	0.547 ± 0.08	1.000	35.89 ± 6.58	0.325 ± 0.09	0.999
RS-PS-RW-Ads.	19.15 ± 3.47	0.647 ± 0.09	1.000	32.64 ± 6.34	0.447 ± 0.10	0.999
RS-LDPE-DI-Ads.	17.62 ± 4.93	0.711 ± 0.14	0.999	27.24 ± 4.33	0.492 ± 0.08	1.000

RS-LDPE-RW-Ads.	28.09 ± 4.34	0.447 ± 0.08		1.000	39.73 ± 2.32	0.389 ± 0.03		1.000
RS-RW-Des.	566.32 ± 195.63	**0.947 ± 0.15**		1.000	527.26 ± 185.66	**0.833 ± 0.15**		1.000
RS-PS-DI-Des.	435.03 ± 246.64	0.689 ± 0.21		1.000	326.49 ± 39.91	0.597 ± 0.37		1.000
RS-PS-RW-Des.	516.08 ± 181.50	**0.929 ± 0.15**		1.000	323.75 ± 186.51	0.595 ± 0.22		1.000
RS-LDPE-DI-Des.	508.57 ± 303.34	0.792 ± 0.23		1.000	564.86 ± 219.78	**0.894 ± 0.15**		1.000
RS-LDPE-RW-Des.	113.50 ± 32.28	0.209 ± 0.11		1.000	452.41 ± 122.12	**0.940 ± 0.14**		1.000
Sips	q_{ms} (mg/kg)	Ks (L/mg)	n_s	R^2	q_{ms} (mg/kg)	K_s (L/mg)	n_s	R^2
RS-RW-Ads.	155601.08 ± 2.81	0.001 ± 0.4	0.73 ± 0.45	0.979	287.05 ± 349.03	0.074 ± 0.09	0.87 ± 0.28	0.992
RS-PS-DI-Ads.	25935.40 ± 10^7	0.001 ± 0.5	0.56 ± 0.54	0.954	84.86 ± 4.17	0.35 ± 0.03	1.28 ± 0.11	0.999
RS-PS-RW-Ads.	205472 ± 5.5*10^8	10^{-4} ± 0.30	0.56 ± 0.33	0.981	107.40 ± 38.80	0.42 ± 0.24	0.95 ± 0.44	0.973
RS-LDPE-DI-Ads.	315964.93 ± 2*10^9	6*10^{-5} ± 0.6	0.66 ± 0.66	0.945	45924.75 ± 4*10^7	6*10^{-4} ± 0.6	0.47 ± 0.45	0.962
RS-LDPE-RW-Ads.	104.02 ± 35.13	0.30 ± 0.15	0.94 ± 0.28	0.990	171.86 ± 104.07	0.28 ± 0.22	0.64 ± 0.22	0.989
RS-RW-Des.	82.86 ± 7.24	1524 ± 2601	2.5 ± 0.5	0.996	133.39 ± 40.32	90.52 ± 155	1.79 ± 0.42	0.996
RS-PS-DI-Des.	81.27 ± 6.32	7*10^5	3.26 ± 0.96	0.986	64.21 ± 4.45	1.5*10^{10}	6.33 ± 5.92	0.971
RS-PS-RW-Des.	274.18 ± 1113.4	2.93 ± 20.44	1.02 ± 0.76	0.970	75.70 ± 5.73	10^7	4.05 ± 1.61	0.974
RS-LDPE-DI-Des.	100.03 ± 48.30	268 ± 1229	1.86 ± 1.16	0.928	130.97 ± 144.09	29.46 ± 132.4	1.39 ± 0.94	0.959
RS-LDPE-RW-Des.	67.28 ± 6.31	1.9*10^{10}	6.7 ± 7.76	0.962	102.66 ± 12.29	196.66 ± 244	2.19 ± 0.40	0.995

Table 6.4. R_L factor As(III) and As(V) adsorption and desorption from RS+PS/LDPE.

	As(III)					As(V)				
	RS-RW	RS-PS-DI	RS-PS-RW	RS-LDPE-DI	RS-LDPE-RW	RS-RW	RS-PS-DI	RS-PS-RW	RS-LDPE-DI	RS-LDPE-RW
Adsorption	0.979	0.941	0.971	0.974	0.924	0.957	0.834	0.934	0.932	0.916
	0.912	0.881	0.935	0.915	0.863	0.861	0.561	0.786	0.822	0.696
	0.801	0.602	0.735	0.729	0.535	0.704	0.328	0.553	0.542	0.443
	0.720	0.482	0.629	0.583	0.411	0.597	0.227	0.422	0.422	0.321
	0.670	0.424	0.575	0.532	0.356	0.538	0.187	0.369	0.365	0.272
Desorption	0.979	0.859	0.980	0.934	0.872	0.998	0.810	0.926	0.952	0.961
	0.963	0.806	0.964	0.920	0.817	0.996	0.786	0.889	0.926	0.935
	0.951	0.736	0.928	0.853	0.781	0.994	0.697	0.850	0.871	0.908
	0.904	0.617	0.887	0.805	0.706	0.991	0.570	0.780	0.835	0.876
	0.896	0.541	0.877	0.707	0.569	0.990	0.512	0.728	0.805	0.862

6.3.5. Interaction of As(III) and As(V) with adsorbents

The FTIR results (**Figure 6.1**) of RS particles after As(III) and As(V) adsorption illustrated that several surface functional groups participated in the interactions between As(III) or As(V) with sediment particles. The new peaks of 1651, 1705, 2307 and 3865 cm^{-1} on the surface of sediment associated with As(III) or As(V) are related to amine C=O stretching, C–O molecular vibrations and phenolic hydroxyl functional groups (Hahn et al., 2018; Yu et al., 2015). According to Rawat et al. (2021), As(V) can assigned with organic-Si or with SiO_2 in the presence of OM to create the As–O–Si form. In addition, the carboxyl group was involved in binding As(V) probably via transferring the inorganic As(V) into its organic compound (Rawat et al., 2021). The presence of Fe–O surface groups in As(III) and As(V) adsorption possibly form the immobilization As(V) of bidentate complex $(\text{-Fe})_2HAsO_4^{2-}$ or monodentate complex $(\text{-Fe})H_2AsO_4^-$ (Rawat et al., 2021; Sun et al., 2009). This process occurred via surface complexation or coordination (Sun et al., 2018), and transformation from As(III) to As(V) was finding via XPS analysis. There were no differences among functional groups of RS after As(III) and As(V) adsorption, suggesting that As(V) may share these sorption mechanisms to As(III).

In addition, the surface functional groups of PS and LDPE also contributed to the interactions with As(III) and As(V) during the adsorption process. The FTIR results for PS after adsorption of As(V) revealed that nitrogen and oxygen functional groups of an adsorbent participated in the adsorption of metal ions (Darnall et al., 1986). Regarding As(III), Dong et al. (2020) reported that As(III) adsorbed on PS via chemisorption, in which hydrogen bonds were produced when trivalent arsenic interacted with carboxyl group. The FTIR results for LDPE pellets revealed that As(III) and As(V) adsorption occurred on the functional groups of -COOH and -OH (Irani et al., 2015). The previous findings indicated that electrostatic

attraction and chelation were the physisorption and complexation mechanisms for metal ion adsorption beside the ion exchange (Irani et al., 2015).

6.4. Conclusions

This chapter found that the adsorption and desorption kinetics were well displayed by the PFO, PSO and Elovich kinetic models when As(III) and As(V) were adsorbed on or released from RS, RS-PS and PS-LDPE in both DI water and RW conditions. The Elovich model provides the best fitting with the experimental data for the adsorption process. However, As(III) and As(V) adsorption processes were more favourable with non-linear Langmuir and Sips isotherm model than Freundlich models in this experimental condition. Higher adsorption affinity (q_e) of As(V) than As(III) was found at the equilibrium in all conditions, while the Langmuir model showed lower adsorption maximum (q_m) of As(V) than that of As(III). The lower q_e values for RS-PS and RS-LDPE after adsorption of As(III) and As(V) than only RS as the adsorbent suggested that the presence of PS and LDPE in the solution may prevent the sorption of As(III) and As(V) on RS. Moreover, adsorption affinity of As(III) on RS-PS and RS-LDPE in DI water was higher than that in RW, while the result of As(V) was opposite, indicating that RW has significant roles in adsorption of As. Regarding desorption process, RW plays a positive role in enhancement of As(III) and As(V) release into the water phase. The Sips models estimated better q_e results for both adsorption and desorption process, maybe it uses three parameters compared two parameters were used by Langmuir and Freundlich models. The surface complexation or coordination of As(III) or As(V) interacted with sediment surface functional groups was the main sorption mechanism. The SEM-EDS revealed more As(V) adsorbed on RS than As(III), while XPS showed the oxidation from As(III) to As(V) after adsorption. Moreover, the adsorption of As species on PS mainly occurred via nitrogen and oxygen

functional groups, while COO- and OH- functional groups contributed to the adsorption mechanism of As species on LDPE.

CHAPTER SEVEN:

CONCLUSIONS AND FUTURE RESEARCH

7. CHAPTER SEVEN: CONCLUSIONS AND FUTURE RESEARCH

7.1. Conclusions

This study focused on understanding the sorption behaviours and mechanisms of As(III) and As(V) using three types of adsorbents including RS, PS and LDPE. The batch experiments showed that adsorption affinities of RS, PS and LDPE for As(III) and As(V) in DI water were higher than those in RW. In the first stage of experiments, this study revealed that both As(III) and As(V) adsorption was favourable in acidic to neutral conditions and smaller sediment sizes. However, organic matter slightly inhibited the adsorption affinity. In acidic environment (pH 4), q_e values of As(III) and As(V) were 20.8% and 45.4% higher than alkaline environment, whilst q_e values of As(III) and As(V) adsorbed on RS only reduced by 7.9% and 1.2% in comparison to adsorption on RS-NOM. Sediment fraction sizes had the largest influence on adsorption affinity of RS, and higher effect on the adsorption of As(III) than As(V). The adsorption of As(III) on the smallest fraction size (S_4) was nearly double as 94.25% and 100.79% as adsorption capacity of As(III) on RS and on the largest fraction size (S_1), respectively. The adsorption of As(V) on S_4 was 71.83% and 89.11% greater than that on RS and S_1. However, the adsorption affinity of RS and all fraction sizes (S_1, S_2, S_3, S_4) for As(V) was higher than As(III). RS particles analysis indicates that higher amount of As(V) adsorbed on RS which reduces to As(III) form in DI water after adsorption.

The next step of experiments focused on adsorption of As(III) and As(V) on PS and LDPE. LDPE had higher adsorption affinity for both As(III) and As(V) than PS, except for the results of As(III) adsorbed on PS and LDPE in RW. The FTIR analysis revealed the results that ─COOH, COO- and OH- were the predominately functional groups of PS and LDPE participated in the interactions between As(III)/As(V) and these selected MP pellets.

In the final experimental target, As(III) adsorption on RS-PS at the equilibrium was higher than that on RS-LDPE by using either DI water or RW, whilst the opposite trend was seen for As(V). The highest q_e values was the adsorption of As(V) on PS-LDPE-RW (93.33 mg/kg) followed by adsorption of As(III) on RS-PS-DI (88.64 mg/kg). However, the Langmuir model provided various results of q_m values for both RS-PS and RS-LDPE, with higher estimated adsorption capacities for As(III) than As(V). In contrast, Sips isotherm model was the best fit for both adsorption and desorption phases of As(III) and As(V) and provided more reasonable q_e values when the regression was successful carried out. The desorption processes of As(III) and As(V) on DI water and RW indicated that RW enhanced the release of As(III) and As(V) into the aquatic system. As a result, higher amounts of As(III) and As(V) were desorbed from RS, RS-PS and RS-LDPE into RW than into DI water at the equilibrium. In addition, As(III) and As(V) desorption on the mixture of RS-PS and RS-LDPE showed that a higher amount of As(III) was released into the water from adsorbents than As(V), indicating the impact of PS or LDPE on desorption behaviour of As(III). The study on the adsorption mechanism of As(III) and As(V) on these adsorbents provided the information that As interacts RS surface via the functional groups of Fe–O/Fe–OH, Si(Al)–O, hydroxyl (O─H) and carboxyl (─COOH). Additionally, the oxidation from As(III) to As(V) on RS by using RW was observed after As(III) adsorption.

Overall, this study demonstrates that As(V) has higher adsorption affinity than As(III), resulting in stronger binding with adsorbents than As(III). This means that As(III) releases into water phase more efficiently. Sediment characterisations, solution pH, MPs and river water have effects on adsorption and desorption of As(III) and As(V) by various degrees. Specifically, RW is considered as a medium that partly inhibits the adsorption of As(III) but promotes the adsorption of As(V) on sediment-polymers, and enhances the desorption of both

As(III) and As(V) into water phase. The transformation between two forms of As are found after adsorption of As(III) and As(V) on RS depending on the conditions of feeding solution as DI water or RW. However, no desorption experiments for As(III) and As(V) on the selected MPs were conducted as well as the comprehensive understanding the mechanism and transformation between these As species due to lack of SEM-EDS and XPS analysis for PS and LDPE are the major limitations in this study.

7.2. Recommendations for Further Research

Based on the experimental, kinetic and isotherm modelling results of this research, the following recommendations are proposed for future study:

- Since RW had a negative impact on As adsorption and a positive effect on As desorption, further research should be conducted to clarify which compounds of RW may lead to these results and the causes.
- Most of the anthropogenic activities caused serious contamination in the RW and RS for not only inorganic As species but also other heavy metals and pollutants. Therefore, the sorption behaviour and mechanism of As should be carried out in the presence of other metals.
- One of the important environmental factors that was not determined in this study is the change in hydraulic conditions of rivers. This factor changes other parameters in RW such as pH, temperature, concentrations of pollutants and the status of RS. Therefore, designing sorption experiments in continuous flows would provide results on sorption breakthrough behaviour and in predicting the change of As in river systems.
- Most current studies used virgin MPs for experiments on MPs' fate and interactions with other pollutants. Future studies should concentrate in using aged MPs which better represent the natural changes of MPs through different environmental processes.

- Furthermore, environmental fate model should be developed to simulate MP-As interactions in river systems, incorporating pollutant sources, pollutant properties, pollution processes, and hydrodynamics in rivers.

REFERENCES

ABS, 2020. Waste Account, Australia, Experimental Estimates, 2018-19 financial year | Australian Bureau of Statistics. Aust. Bur. Stat. URL https://www.abs.gov.au/statistics/environment/environmental-management/waste-account-australia-experimental-estimates/latest-release (accessed 10.24.21).

AGI, 2019. Toxicant default guideline values for sediment quality. Aust. Gov. Initiat. URL https://www.waterquality.gov.au/anz-guidelines/guideline-values/default/sediment-quality-toxicants.

Ahmed, M.B., Rahman, M.S., Alom, J., Hasan, M.S., Johir, M.A.H., Mondal, M.I.H., Lee, D.Y., Park, J., Zhou, J.L., Yoon, M.H., 2021. Microplastic particles in the aquatic environment: A systematic review. Sci. Total Environ. 775, 145793.

Akdogan, Z., Guven, B., 2019. Microplastics in the environment: A critical review of current understanding and identification of future research needs. Environ. Pollut. 254, 113011.

Aksentijevi´c, S., Jelena, A. ·, Milica, K. ·, Vučini´c, V., Vasi´c, V., Aksentijevi´caksentijevi´c, S., Kiurski, J., Vasi´cvasi´c, · M V, 2012. Arsenic distribution in water/sediment system of Sevojno. Env. Monit Assess 184, 335–341.

Akter, K.F., Owens, G., Davey, D.E., Naidu, R., 2006. Arsenic speciation and toxicity in biological systems. Rev. Environ. Contam. Toxicol. 184.

Alam, F.C., Sembiring, E., Muntalif, B.S., Suendo, V., 2019. Microplastic distribution in surface water and sediment river around slum and industrial area (case study: Ciwalengke River, Majalaya district, Indonesia). Chemosphere 224, 637–645.

Ali, M.M., Ali, M.L., Islam, M.S., Rahman, M.Z., 2016. Preliminary assessment of heavy metals in water and sediment of Karnaphuli River, Bangladesh. Environ. Nanotechnology, Monit. Manag. 5, 27–35.

Alkurdi, S.S.A., Al-Juboori, R.A., Bundschuh, J., Bowtell, L., Marchuk, A., 2021. Inorganic arsenic species removal from water using bone char: A detailed study on adsorption kinetic and isotherm models using error functions analysis. J. Hazard. Mater. 405, 124112.

Allen, S., Allen, D., Allen, S., Allen, D., Phoenix, V.R., Le Roux, G., Durántez Jiménez, P., Simonneau, A., Binet, S., Galop, D., 2019. Atmospheric transport and deposition of microplastics in a remote mountain catchment. Nat. Geosci. 339–344.

Alloway, B., 2012. Heavy metals in soils: trace metals and metalloids in soils and their bioavailability.

Álvarez-Benedí, J., Bolado, S., Cancillo, I., Calvo, C., García-Sinovas, D., 2005. Adsorption-Desorption of Arsenate in Three Spanish Soils. Vadose Zo. J. 4.

Andrady, A.L., 2011. Microplastics in the marine environment. Mar. Pollut. Bull. 62, 1596–1605.

Andrady, A.L., Neal, M.A., 2009. Applications and societal benefits of plastics. Philos. Trans. R. Soc. B 364, 1977–1984.

Antelo, J., Avena, M., Fiol, S., López, R., 2005. Effects of pH and ionic strength on the adsorption of phosphate and arsenate at the goethite–water interface. J. Colloid Interface Sci. 285, 476–486.

Arco-Lázaro, E., Agudo, I., Clemente, R., Bernal, M.P., 2016. Arsenic(V) adsorption-desorption in agricultural and mine soils: Effects of organic matter addition and phosphate competition. Environ. Pollut. 216, 71–79.

Ashley, P.M., Lottermoser, B.G., 1999. Arsenic contamination at the Mole River mine, northern New South Wales. Aust. J. Earth Sci. 46.

Ashton, K., Holmes, L., Turner, A., 2010. Association of metals with plastic production pellets in the marine environment. Mar. Pollut. Bull. 60.

AWQG, 1992. Australian Water Quality Guidelines for Fresh and Marine Waters National

Water Quality Management Strategy.

Azizian, S., 2004. Kinetic models of sorption: a theoretical analysis. J. Colloid Interface Sci. 276, 47–52.

Ballent, A., Corcoran, P.L., Madden, O., Helm, P.A., Longstaffe, F.J., 2016. Sources and sinks of microplastics in Canadian Lake Ontario nearshore, tributary and beach sediments. Mar. Pollut. Bull. 110, 383–395.

Barcelo, D., Pico, Y., 2020. Case studies of macro- and microplastics pollution in coastal waters and rivers: Is there a solution with new removal technologies and policy actions? Case Stud. Chem. Environ. Eng. 2, 100019.

Barrows, A.P.W., Christiansen, K.S., Bode, E.T., Hoellein, T.J., 2018. A watershed-scale, citizen science approach to quantifying microplastic concentration in a mixed land-use river. Water Res. 147.

Basu, A., Saha, D., Saha, R., Ghosh, T., Saha, B., 2014. A review on sources, toxicity and remediation technologies for removing arsenic from drinking water. Res. Chem. Intermed.

Baviskar, S., Choudhury, R., Mahanta, C., 2015. Dissolved and solid-phase arsenic fate in an arsenic-enriched aquifer in the river Brahmaputra alluvial plain. Environ. Monit. Assess. 187.

Bhattacharya, S., Sharma, P., Mitra, S., Mallick, I., Ghosh, A., 2021. Arsenic uptake and bioaccumulation in plants: A review on remediation and socio-economic perspective in Southeast Asia. Environ. Nanotechnology, Monit. Manag. 15, 100430.

Blair, R.M., Waldron, S., Phoenix, V.R., Gauchotte-Lindsay, C., 2019. Microscopy and elemental analysis characterisation of microplastics in sediment of a freshwater urban river in Scotland, UK. Environ. Sci. Pollut. Res. 26, 12491–12504.

Borgnino, L., de Pauli, C.P., Depetris, P.J., 2012. Arsenate adsorption at the sediment-water interface: Sorption experiments and modelling. Environ. Earth Sci. 65, 441–451.

Browne, M.A., Crump, P., Niven, S.J., Teuten, E., Tonkin, A., Galloway, T., Thompson, R., 2011. Accumulation of Microplastic on Shorelines Woldwide: Sources and Sinks. Environ. Sci. Technol 45, 9175–9179.

Browne, M.A., Galloway, T., Thompson, R., 2007. Microplastic--an emerging contaminant of potential concern? Integr. Environ. Assess. Manag. 3.

Campanale, C., Stock, F., Massarelli, C., Kochleus, C., Bagnuolo, G., Reifferscheid, G., Uricchio, V.F., 2020. Microplastics and their possible sources: The example of Ofanto river in southeast Italy. Environ. Pollut. 258, 113284.

Campbell, K., Mineralogy, D.N.-R. in, 2014, undefined, 2014. Arsenic Speciation and Sorption in Natural Environments. Rev. Mineral. Geochemistry 79, 185–216.

Cao, X., Gao, X., Zeng, X., Ma, Y., Gao, Y., Baeyens, W., Jia, Y., Liu, J., Wu, C., Su, S., 2021. Seeking for an optimal strategy to avoid arsenic and cadmium over-accumulation in crops: Soil management vs cultivar selection in a case study with maize. Chemosphere 272.

Caporale, A., Pigna, M., Azam, S., … A.S.-C.E., 2013, undefined, 2013. Effect of competing ligands on the sorption/desorption of arsenite on/from Mg–Fe layered double hydroxides (Mg–Fe-LDH). Chem. Eng. J. 225, 704–709.

Carlin, D.J., Naujokas, M.F., Bradham, K.D., Cowden, J., Heacock, M., Henry, H.F., Lee, J.S., Thomas, D.J., Thompson, C., Tokar, E.J., Waalkes, M.P., Birnbaum, L.S., Suk, W.A., 2016. Arsenic and environmental health: State of the science and future research opportunities. Environ. Health Perspect.

Carrillo-Chávez, A., Salas-Megchún, E., Levresse, G., Muñoz-Torres, C., Pérez-Arvizu, O., Gerke, T., 2014. Geochemistry and mineralogy of mine-waste material from a “skarn-type” deposit in central Mexico: Modeling geochemical controls of metals in the surface environment. J. Geochemical Explor. 144, 28–36.

Casado, M., Anawar, H.M., Garcia-Sanchez, A., Regina, I.S., 2007. Antimony and arsenic

uptake by plants in an abandoned mining area. Commun. Soil Sci. Plant Anal. 38, 1255–1275.

Casiot, C., Ujevic, M., Munoz, M., Seidel, J.L., Elbaz-Poulichet, F., 2007. Antimony and arsenic mobility in a creek draining an antimony mine abandoned 85 years ago (upper Orb basin, France). Appl. Geochemistry 22, 788–798.

Chen, G., Liu, S., Chen, S., Qi, Z., 2001. FTIR Spectra, Thermal Properties, and Dispersibility of a Polystyrene/Montmorillonite Nanocomposite, Macromol. Chem. Phys.

Chen, X., Sun, Q., Ding, S., Chen, M., Fan, X., Zhang, L., Zhang, C., 2016. Mobile Arsenic Distribution and Release Kinetics in Sediment Profiles under Varying pH Conditions. Water. Air. Soil Pollut. 228, 1–12.

Christensen, N.D., Wisinger, C.E., Maynard, L.A., Chauhan, N., Schubert, J.T., Czuba, J.A., Barone, J.R., 2020. Transport and characterization of microplastics in inland waterways. J. Water Process Eng. 38, 2214–7144.

Cole, M., Lindeque, P., Halsband, C., Galloway, T.S., 2011. Microplastics as contaminants in the marine environment: A review. Mar. Pollut. Bull.

Cole, M., Lindeque, P.K., Fileman, E., Clark, J., Lewis, C., Halsband, C., Galloway, T.S., 2016. Microplastics Alter the Properties and Sinking Rates of Zooplankton Faecal Pellets. Environ. Sci. Technol. 50, 3239–3246.

Collard, F., Gasperi, J., Gabrielsen, G.W., Tassin, B., Guo, X., Wang, J., Dong, Y., Gao, M., Qiu, W., Song, Z., Fu, Q., Tan, X., Ye, S., Ma, L., Gu, Y., Zhang, P., Chen, Q., Yang, Y., Tang, Y., Adomat, Y., Grischek, T., Adu-Boahen, K., Dadson, I.Y., Mensah, D.K.D., Kyeremeh, S., Akdogan, Z., Guven, B., Andrady, A.L., Neal, M.A., Antunes, J.C., Frias, J.G.L., Micaelo, A.C., Sobral, P., Carretero, O., Gago, J., Viñas, L., Cera, A., Cesarini, G., Scalici, M., Dong, Y., Gao, M., Song, Z., Qiu, W., Fries, E., Zarfl, C., Galafassi, S., Nizzetto, L., Volta, P., Guerranti, C., Cannas, S., Scopetani, C., Fastelli, P., Cincinelli, A.,

Renzi, M., Hale, R.C., Seeley, M.E., Guardia, M.J. La, Mai, L., Zeng, E.Y., 2019. As(III) adsorption onto different-sized polystyrene microplastic particles and its mechanism. Mar. Pollut. Bull. 254, 1296–1304.

Constant, M., Ludwig, W., Kerhervé, P., Sola, J., Charrière, B., Sanchez-Vidal, A., Canals, M., Heussner, S., 2020. Microplastic fluxes in a large and a small Mediterranean river catchments: The Têt and the Rhône, Northwestern Mediterranean Sea. Sci. Total Environ. 716, 136984.

Crew, A., Gregory-Eaves, I., Ricciardi, A., 2020. Distribution, abundance, and diversity of microplastics in the upper St. Lawrence River. Environ. Pollut. 260, 113994.

Culioli, J.L., Fouquoire, A., Calendini, S., Mori, C., Orsini, A., 2009. Trophic transfer of arsenic and antimony in a freshwater ecosystem: A field study. Aquat. Toxicol. 94, 286–293.

Cullen, W.R., Reimer, K.J., 1989. Arsenic Speciation in the Environment. Chem. Rev. 89.

Darnall, D.W., Greene, B., Henzl, M.T., Hosea, J.M., McPherson, R.A., Sneddon, J., Alexander, M.D., 1986. Selective Recovery of Gold and Other Metal Ions from an Algal Biomass. Environ. Sci. Technol. 20, 206–208.

De Brouwere, K., Smolders, E., Merckx, R., 2004. Soil properties affecting solid-liquid distribution of As(V) in soils. Eur. J. Soil Sci. 55, 165–173.

De Felice, B., Sabatini, V., Antenucci, S., Gattoni, G., Santo, N., Bacchetta, R., Ortenzi, M.A., Parolini, M., 2019. Polystyrene microplastics ingestion induced behavioral effects to the cladoceran Daphnia magna. Chemosphere 231.

De Jonge, M., Teuchies, J., Meire, P., Blust, R., Bervoets, L., 2012. The impact of increased oxygen conditions on metal-contaminated sediments part I: Effects on redox status, sediment geochemistry and metal bioavailability. Water Res. 46, 2205–2214.

Deng, Y., Li, Y., Li, X., Sun, Y., Ma, J., Lei, M., Weng, L., 2018. Influence of calcium and

phosphate on pH dependency of arsenite and arsenate adsorption to goethite. Chemosphere 199, 617–624.

Dias, F.F., Allen, H.E., Guimarães, J.R., Taddei, M.H.T., Nascimento, M.R., Guilherme, L.R.G., 2009. Environmental behavior of arsenic(III) and (V) in soils. J. Environ. Monit. 11, 1412–1420.

Ding, L., Mao, R. fan, Guo, X., Yang, X., Zhang, Q., Yang, C., 2019. Microplastics in surface waters and sediments of the Wei River, in the northwest of China. Sci. Total Environ. 667, 427–434.

Dong, G., Han, R., Pan, Y., Zhang, C., Liu, Y., Wang, H., Ji, X., Dahlgren, R.A., Shang, X., Chen, Z., Zhang, M., 2021. Role of MnO2 in controlling iron and arsenic mobilization from illuminated flooded arsenic-enriched soils. J. Hazard. Mater. 401.

Dong, Y., Gao, M., Song, Z., Qiu, W., 2020. As(III) adsorption onto different-sized polystyrene microplastic particles and its mechanism. Chemosphere 239.

Dong, Y., Gao, M., Song, Z., Qiu, W., 2019. Adsorption mechanism of As(III) on polytetrafluoroethylene particles of different size. Environ. Pollut. 254, 112950.

Donoso, J.M., Rios-Touma, B., 2020. Microplastics in tropical Andean rivers: A perspective from a highly populated Ecuadorian basin without wastewater treatment. Heliyon 6, e04302.

Dousova, B., Buzek, F., Rothwell, J., Krejcova, S., Lhotka, M., 2012. Adsorption behavior of arsenic relating to different natural solids: Soils, stream sediments and peats. Sci. Total Environ. 433, 456–461.

Dris, R., Gasperi, J., Rocher, V., Saad, M., Renault, N., Tassin, B., 2015a. Microplastic contamination in an urban area: A case study in Greater Paris. Environ. Chem. 12, 592–599.

Dris, R., Gasperi, J., Rocher, V., Tassin, B., 2018. Synthetic and non-synthetic anthropogenic

fibers in a river under the impact of Paris Megacity: Sampling methodological aspects and flux estimations. Sci. Total Environ. 618, 157–164.

Dris, R., Imhof, H., Sanchez, W., Gasperi, J., Galgani, F., Tassin, B., Laforsch, C., 2015b. Beyond the ocean: Contamination of freshwater ecosystems with (micro-)plastic particles. Environ. Chem. 12, 539–550.

Eerkes-Medrano, D., Thompson, R.C., Aldridge, D.C., 2015. Review Microplastics in freshwater systems: A review of the emerging threats, identification of knowledge gaps and prioritisation of research needs. Water Res. 75, 63–82.

Ellwood, M.J., Maher, W.A., 2003. Measurement of arsenic species in marine sediments by high-performance liquid chromatography–inductively coupled plasma mass spectrometry. Anal. Chim. Acta 477, 279–291.

Eo, S., Hong, S.H., Song, Y.K., Han, M., Shim, J., 2019. Spatiotemporal distribution and annual load of microplastics in the Nakdong River, South Korea. Water Res. 160, 228–237.

Estahbanati, S., Fahrenfeld, N.L., 2016. Influence of wastewater treatment plant discharges on microplastic concentrations in surface water. Chemosphere 162.

Europe, P., 2019. Plastics - the Facts 2019.

Even, E., Masuda, H., Shibata, T., Nojima, A., Sakamoto, Y., Murasaki, Y., Chiba, H., 2017. Geochemical distribution and fate of arsenic in water and sediments of rivers from the Hokusetsu area, Japan. J. Hydrol. Reg. Stud. 9.

Fan, Y., Zheng, C., Liu, H., He, C., Shen, Z., Zhang, T.C., 2020. Effect of pH on the adsorption of arsenic(V) and antimony(V) by the black soil in three systems: Performance and mechanism. Ecotoxicol. Environ. Saf. 191, 110145.

Fan, Y., Zheng, K., Zhu, Z., Chen, G., Peng, X., 2019. Distribution, sedimentary record, and persistence of microplastics in the Pearl River catchment, China +. Environ. Pollut. 251,

862–870.

Fang, Z., Wang, Y., Xie, D., Wang, D., 2021. Potential Ecological Risk of Heavy Metals in a Typical Tributary of the Three Gorges Reservoir. Bull. Environ. Contam. Toxicol. 106.

Farrell, J., 2017. Tridentate arsenate complexation with ferric hydroxide and its effect on the kinetics of arsenate adsorption and desorption. Chemosphere 184, 1209–1214.

Faure, F., Demars, C., Wieser, O., Kunz, M., De Alencastro, L.F., 2015. Plastic pollution in Swiss surface waters: Nature and concentrations, interaction with pollutants. Environ. Chem. 12.

Fendall, L.S., Sewell, M.A., 2009. Contributing to marine pollution by washing your face: Microplastics in facial cleansers. Mar. Pollut. Bull. 58, 1225–1228.

Fendorf, S., Nico, P.S., Kocar, B.D., Masue, Y., Tufano, K.J., 2010. Arsenic chemistry in soils and sediments. Dev. Soil Sci. 34, 357–378.

Feng, Q., Zhang, Z., Chen, Y., Liu, L., Zhang, Z., Chen, C., 2013. Adsorption and Desorption Characteristics of Arsenic on Soils: Kinetics, Equilibrium, and Effect of Fe(OH)3 Colloid, H2SiO3 Colloid and Phosphate. Procedia Environ. Sci. 18, 26–36.

Fleck, A.T., Mattusch, J., Schenk, M.K., 2013. Silicon decreases the arsenic level in rice grain by limiting arsenite transport. J. Plant Nutr. Soil Sci. 176, 785–794.

Fleming, C., Morrison, K., Robba, L., Reynolds, J., Wright, I.A., 2021. 14-Month Water Quality Investigation of Coal Mine Discharge on Two Rivers in NSW, Australia: Implications for Environmental Regulation. Water. Air. Soil Pollut. 232.

Foo, K.Y., Hameed, B.H., 2010. Insights into the modeling of adsorption isotherm systems. Chem. Eng. J. 156, 2–10.

Foroutan, R., Mohammadi, R., Adeleye, A.S., Farjadfard, S., Esvandi, Z., Arfaeinia, H., Sorial, G.A., Ramavandi, B., Sahebi, S., 2019. Efficient arsenic(V) removal from contaminated water using natural clay and clay composite adsorbents. Environ. Sci. Pollut. Res. 26,

29748–29762.

Fu, Q., Tan, X., Ye, S., Ma, L., Gu, Y., Zhang, P., Chen, Q., Yang, Y., Tang, Y., 2021. Mechanism analysis of heavy metal lead captured by natural-aged microplastics. Chemosphere 270, 128624.

Galafassi, S., Nizzetto, L., Volta, P., 2019. Plastic sources: A survey across scientific and grey literature for their inventory and relative contribution to microplastics pollution in natural environments, with an emphasis on surface water. Sci. Total Environ.

Gallitelli, L., Cesarini, G., Cera, A., Sighicelli, M., Lecce, F., Menegoni, P., Scalici, M., 2020. Transport and Deposition of Microplastics and Mesoplastics along the River Course: A Case Study of a Small River in Central Italy. Hydrology 7, 90.

Gao, Z., 2018. Evaluation of heavy metal pollution and its ecological risk in one river reach of a gold mine in Inner Mongolia, Northern China. Int. Biodeterior. Biodegrad. 128, 94–99.

García-Gaines, R.A., Frankenstein, S., 2015. USCS and the USDA Soil Classification System, Development of a Mapping Scheme. UPRM ERDC Educ. Res. Internsh. Progr.

Garneau, C., Sauvage, S., Probst, A., Sánchez-Pérez, J.M., 2015. Modelling of trace metal transfer in a large river under different hydrological conditions (the Garonne River in southwest France). Ecol. Modell. 306, 195–204.

Gedik, K., Kongchum, M., Boran, M., Delaune, R.D., 2016. Adsorption and desorption of arsenate in Louisiana rice soils. Arch. Agron. Soil Sci. 0340, 856–864.

Gemici, Ü., Tarcan, G., 2007. Assessment of the pollutants in farming soils and waters around untreated abandoned Türkönü mercury mine (Turkey). Bull. Environ. Contam. Toxicol. 79, 20–24.

Gemici, Ü., Tarcan, G., Helvaci, C., Somay, A.M., 2008. High arsenic and boron concentrations in groundwaters related to mining activity in the Bigadiç borate deposits (Western Turkey). Appl. Geochemistry 23, 2462–2476.

Gerdelidani, A.F., Towfighi, H., Shahbazi, K., Lamb, D.T., Choppala, G., Abbasi, S., Bari, A.S.M.F., Naidu, R., Rahman, M.M., 2021. Arsenic geochemistry and mineralogy as a function of particle-size in naturally arsenic-enriched soils. J. Hazard. Mater. 403, 123931.

Gerolin, C.R., Pupim, N., Oliveira Sawakuchi, A., Grohmann, C.H., Labuto, G., Semensatto, D., 2020. Short Communication Microplastics in sediments from Amazon rivers, Brazil. Sci. Total Environ. 749, 141604.

Geyer, R., Jambeck, J.R., Law, K.L., 2017. Production, use, and fate of all plastics ever made. Sci. Adv. 3, e1700782.

Ghosal, P.S., Gupta, A.K., 2017. Development of a generalized adsorption isotherm model at solid-liquid interface: A novel approach. J. Mol. Liq. 240, 21–24.

Gitari, M.W., Mudzielwana, R., 2018. Mineralogical and Chemical Characteristics of Raw and Modified Clays and Their Application in Arsenic and Fluoride Removal: Review. Curr. Top. Util. Clay Ind. Med. Appl.

Godoy, V., Blázquez, G., Calero, M., Quesada, L., Martín-Lara, M.A., 2019. The potential of microplastics as carriers of metals. Environ. Pollut. 255.

Goh, K.H., Lim, T.T., 2004. Geochemistry of inorganic arsenic and selenium in a tropical soil: Effect of reaction time, pH, and competitive anions on arsenic and selenium adsorption. Chemosphere 55, 849–859.

Goldberg, S., 2000. Competitive adsorption of inorganic arsenicspecies on oxides and clay minerals. ACS Div. Environ. Chem. Prepr. 40, 512–515.

Goldberg, S., Lesch, S.M., Suarez, D.L., 2005. Predicting selenite adsorption by soils using soil chemical parameters in the constant capacitance model. Geochim. Cosmochim. Acta 71, 5750–5762.

Goldberg, S., Suarez, D.L., 2013. Arsenate Adsorption by Unsaturated Alluvial Sediments. Soil Sci. Soc. Am. J. 77, 782–791.

Gordon, S.H., Mohamed, A.A., Harry-Okuru, R.E., Biresaw, G., 2015. Identification and Measurement of Intermolecular Interaction in Polyester/Polystyrene Blends by FTIR-Photoacoustic Spectrometry. J. Polym. Environ. 23, 459–469.

Gorny, J., Billon, G., Noiriel, C., Dumoulin, D., Lesven, L., Madé, B., 2018. Redox behaviour of arsenic in the surface sediments of the Marque River (Northern France). J. Geochemical Explor. 188.

Grafe, M., Eick, M.J., Grossl, P.R., 2001. Adsorption of Arsenate (V) and Arsenite (III) on Goethite in the Presence and Absence of Dissolved Organic Carbon; Adsorption of Arsenate (V) and Arsenite (III) on Goethite in the Presence and Absence of Dissolved Organic Carbon, Soil Sci. Soc. Am. J.

Guerranti, C., Cannas, S., Scopetani, C., Fastelli, P., Cincinelli, A., Renzi, M., 2017. Plastic litter in aquatic environments of Maremma Regional Park (Tyrrhenian Sea, Italy): Contribution by the Ombrone river and levels in marine sediments. Mar. Pollut. Bull. 117, 366–370.

Guo, H., Stüben, D., Berner, Z., 2007. Adsorption of arsenic(III) and arsenic(V) from groundwater using natural siderite as the adsorbent. J. Colloid Interface Sci. 315, 47–53.

Hahn, A., Vogel, H., Andó, S., Garzanti, E., Kuhn, G., Lantzsch, H., Schüürman, J., Vogt, C., Zabel, M., 2018. Using Fourier transform infrared spectroscopy to determine mineral phases in sediments. Sediment. Geol. 375, 27–35.

Han, M., Niu, X., Tang, M., Zhang, B.-T., Wang, G., Yue, W., Kong, X., Zhu, J., 2020. Distribution of microplastics in surface water of the lower Yellow River near estuary. Sci. Total Environ. 707, 135601.

Hao, L., Wang, N., Wang, C., Li, G., 2018. Arsenic removal from water and river water by the combined adsorption - UF membrane process. Chemosphere 202.

Hayat, K., Menhas, S., Bundschuh, J., Chaudhary, H.J., 2017. Microbial biotechnology as an

emerging industrial wastewater treatment process for arsenic mitigationA critical review. J. Clean. Prod. 151, 427–438.

He, B., Goonetilleke, A., Ayoko, G.A., Rintoul, L., 2020a. Abundance, distribution patterns, and identification of microplastics in Brisbane River sediments, Australia. Sci. Total Environ. 700, 134467.

He, B., Wijesiri, B., Ayoko, G.A., Egodawatta, P., Rintoul, L., Goonetilleke, A., 2020b. Influential factors on microplastics occurrence in river sediments. Sci. Total Environ. 738, 139901.

Hettiarachchi, S.R., Maher, W.A., Krikowa, F., Ubrihien, R., 2017. Factors influencing arsenic concentrations and species in mangrove surface sediments from south-east NSW, Australia. Environ. Geochem. Health 39, 209–219.

Hidalgo-Ruz, V., Gutow, L., Thompson, R.C., Thiel, M., 2012. Microplastics in the marine environment: A review of the methods used for identification and quantification. Environ. Sci. Technol. 46, 3060–3075.

Ho, Y.S., McKay, G., 1999. Pseudo-second order model for sorption processes. Process Biochem. 34, 451–465.

Hoellein, T.J., McCormick, A.R., Hittie, J., London, M.G., Scott, J.W., Kelly, J.J., 2017. Longitudinal patterns of microplastic concentration and bacterial assemblages in surface and benthic habitats of an urban river. Freshw. Sci. 36, 491–507.

Holmes, L.A., Turner, A., Thompson, R.C., 2014. Interactions between trace metals and plastic production pellets under estuarine conditions. Mar. Chem. 167, 25–32.

Holmes, L.A., Turner, A., Thompson, R.C., 2012. Adsorption of trace metals to plastic resin pellets in the marine environment. Environ. Pollut. 160.

Hoogsteen, M.J.J., Lantinga, E.A., Bakker, E.J., Tittonell, P.A., 2018. Communications in Soil Science and Plant Analysis An Evaluation of the Loss-on-Ignition Method for

Determining the Soil Organic Matter Content of Calcareous Soils An Evaluation of the Loss-on-Ignition Method for Determining the Soil Organic Matter Content. Commun. Soil Sci. Plant Anal. 49, 1541–1552.

Horton, A.A., Svendsen, C., Williams, R.J., Spurgeon, D.J., Lahive, E., 2017. Large microplastic particles in sediments of tributaries of the River Thames, UK-Abundance, sources and methods for effective quantification. Mar. Pollut. Bull. 114, 218–226.

Horton, A.A., Walton, A., Spurgeon, D.J., Lahive, E., Svendsen, C., 2017. Microplastics in freshwater and terrestrial environments: Evaluating the current understanding to identify the knowledge gaps and future research priorities. Sci. Total Environ. 586, 127–141.

Hossain Bhuiyan, M.A., Chandra Karmaker, S., Bodrud-Doza, M., Rakib, M.A., Saha, B.B., 2021. Enrichment, sources and ecological risk mapping of heavy metals in agricultural soils of dhaka district employing SOM, PMF and GIS methods. Chemosphere 263.

Hosseinpour, S.A., Karimipour, G., Ghaedi, M., Dashtian, K., 2018. Use of metal composite MOF-5-Ag2O-NPs as an adsorbent for the removal of Auramine O dye under ultrasound energy conditions. Appl. Organomet. Chem. 32.

Hu, L., Chernick, M., Hinton, D.E., Shi, H., 2018. Microplastics in Small Waterbodies and Tadpoles from Yangtze River Delta, China. Environ. Sci. Technol. 52, 8885–8893.

Hua, J., 2018. Adsorption of low-concentration arsenic from water by co-modified bentonite with manganese oxides and poly(dimethyldiallylammonium chloride). J. Environ. Chem. Eng. 6, 156–168.

Huang, D., Li, X., Ouyang, Z., Zhao, X., Wu, R., Zhang, C., Lin, C., Li, Y., Guo, X., 2021. The occurrence and abundance of microplastics in surface water and sediment of the West River downstream, in the south of China. Sci. Total Environ. 756, 143857.

Huang, G., Chen, Z., Wang, J., Sun, J., Liu, J., Zhang, Y., 2013. Adsorption of arsenite onto a soil irrigated by sewage. J. Geochemical Explor. 132, 164–172.

Huang, J.H., 2018. Characterising microbial reduction of arsenate sorbed to ferrihydrite and its concurrence with iron reduction. Chemosphere 194, 49–56.

Huang, R.Q., Gao, S.F., Wang, W.L., Staunton, S., Wang, G., 2006. Soil arsenic availability and the transfer of soil arsenic to crops in suburban areas in Fujian Province, southeast China. Sci. Total Environ. 368, 531–541.

Huling, J.R., Huling, S.G., Ludwig, R., 2017. Enhanced adsorption of arsenic through the oxidative treatment of reduced aquifer solids. Water Res. 123, 183–191.

Irani, M., Ismail, H., Ahmad, Z., Fan, M., 2015. Synthesis of linear low-density polyethylene-g-poly (acrylic acid)-co-starch/organo-montmorillonite hydrogel composite as an adsorbent for removal of Pb(II) from aqueous solutions. J. Environ. Sci. (China) 27, 9–20.

Islam, M.S., Ahmed, M.K., Raknuzzaman, M., Habibullah -Al- Mamun, M., Islam, M.K., 2015. Heavy metal pollution in surface water and sediment: A preliminary assessment of an urban river in a developing country. Ecol. Indic. 48, 282–291.

Ivar Do Sul, J.A., Costa, M.F., 2014. The present and future of microplastic pollution in the marine environment. Environ. Pollut. 185, 352–364.Jahan, S., Strezov, V., 2018. Comparison of pollution indices for the assessment of heavy metals in the sediments of seaports of NSW, Australia. Mar. Pollut. Bull. 128, 295–306.

Jana, U., Chassany, V., Bertrand, G., Castrec-Rouelle, M., Aubry, E., Boudsocq, S., Laffray, D., Repellin, A., 2012. Analysis of arsenic and antimony distribution within plants growing at an old mine site in Ouche (Cantal, France) and identification of species suitable for site revegetation. J. Environ. Manage. 110, 188–193.

Jeppu, G.P., Clement, T.P., 2012. A modified Langmuir-Freundlich isotherm model for simulating pH-dependent adsorption effects. J. Contam. Hydrol. 129–130, 46–53.

Jia, X., Cao, Y., O'Connor, D., Zhu, J., Tsang, D.C.W., Zou, B., Hou, D., 2021. Mapping soil

pollution by using drone image recognition and machine learning at an arsenic-contaminated agricultural field. Environ. Pollut. 270.

Jiang, C., Yin, L., Li, Z., Wen, X., Luo, X., Hu, S., Yang, H., Long, Y., Deng, B., Huang, L., Liu, Y., 2019. Microplastic pollution in the rivers of the Tibet Plateau. Environ. Pollut. 249, 91–98.

Jiang, J., Dai, Z., Sun, R., Zhao, Z., Dong, Y., Hong, Z., Xu, R., 2017. Evaluation of ferrolysis in arsenate adsorption on the paddy soil derived from an Oxisol. Chemosphere 179, 232–241.

Jiang, W., Zhang, S., Shan, X., Feng, M., Zhu, Y.-G., McLaren, R.G., 2005a. Adsorption of arsenate on soils. Part 1: Laboratory batch experiments using 16 Chinese soils with different physiochemical properties. Environ. Pollut. 138, 278–284.

Jiang, W., Zhang, S., Shan, X., Feng, M., Zhu, Y.-G., McLaren, R.G., 2005b. Adsorption of arsenate on soils. Part 2: Modeling the relationship between adsorption capacity and soil physiochemical properties using 16 Chinese soils. Environ. Pollut. 138, 285–289.

Jiang, Z., Li, P., Tu, J., Wei, D., Zhang, R., Wang, Y., Dai, X., 2018. Arsenic in geothermal systems of Tengchong, China: Potential contamination on freshwater resources. Int. Biodeterior. Biodegrad. 128.

Jlassi, K., Krupa, I., Chehimi, M.M., 2017. Overview: Clay Preparation, Properties, Modification, in: Clay-Polymer Nanocomposites.

Johnston, S.G., Bennett, W.W., Doriean, N., Hockmann, K., Karimian, N., Burton, E.D., 2020. Antimony and arsenic speciation, redox-cycling and contrasting mobility in a mining-impacted river system. Sci. Total Environ. 710, 136354.

Kabir, A.H.M.E., Sekine, M., Imai, T., Yamamoto, K., Kanno, A., Higuchi, T., 2021. Assessing small-scale freshwater microplastics pollution, land-use, source-to-sink conduits, and pollution risks: Perspectives from Japanese rivers polluted with microplastics. Sci. Total

Environ. 768, 144655.

Kadokami, K., Li, X., Pan, S., Ueda, N., Hamada, K., Jinya, D., Iwamura, T., 2013. Screening analysis of hundreds of sediment pollutants and evaluation of their effects on benthic organisms in Dokai Bay, Japan. Chemosphere 90, 721–728.

Kapp, K.J., Yeatman, E., 2018. Microplastic hotspots in the Snake and Lower Columbia rivers: A journey from the Greater Yellowstone Ecosystem to the Pacific Ocean. Environ. Pollut. 241.

Karczewska, A., Bogda, A., Krysiak, A., 2007. Arsenic in soils in the areas of former mining and mineral processing in Lower Silesia, southwestern Poland. Trace Met. other Contam. Environ.

Kaufhold, S., Hein, M., Dohrmann, R., Ufer, K., 2012. Quantification of the mineralogical composition of clays using FTIR spectroscopy. Vib. Spectrosc. 59, 29–39.

Ke, X., Bao, Q., Qi, Y., Huang, X., Zhang, H., 2018. Toxicity assessment of sediments from the Liaohe River Protected Area (China) under the influence of ammonia nitrogen, heavy metals and organic contaminants. Environ. Toxicol. Pharmacol. 59, 34–42.

Kebonye, N.M., John, K., Chakraborty, S., Agyeman, P.C., Ahado, S.K., Eze, P.N., Němeček, K., Drábek, O., Borůvka, L., 2021. Comparison of multivariate methods for arsenic estimation and mapping in floodplain soil via portable X-ray fluorescence spectroscopy. Geoderma 384.

Klein, S., Worch, E., Knepper, T.P., 2015. Occurrence and Spatial Distribution of Microplastics in River Shore Sediments of the Rhine-Main Area in Germany. Environ. Sci. Technol. 49, 6070–6076.

Kolařík, J., Prucek, R., Tuček, J., Filip, J., Sharma, V.K., Zbořil, R., 2018. Impact of inorganic ions and natural organic matter on arsenates removal by ferrate(VI): Understanding a complex effect of phosphates ions. Water Res. 141.

Kumar, R.R., Kumar, R.R., Mittal, S., Arora, M., Babu, J.N., 2016. Role of soil physicochemical characteristics on the present state of arsenic and its adsorption in alluvial soils of two agri-intensive region of Bathinda, Punjab, India. J. Soils Sediments 16, 605–620.

Kundu, S., Gupta, A.K., 2006. Arsenic adsorption onto iron oxide-coated cement (IOCC): Regression analysis of equilibrium data with several isotherm models and their optimization. Chem. Eng. J. 122, 93–106.

Lagarde, F., Olivier, O., Zanella, M., Daniel, P., Hiard, S., Caruso, A., 2016. Microplastic interactions with freshwater microalgae: Hetero-aggregation and changes in plastic density appear strongly dependent on polymer type. Environ. Pollut. 215, 331–339.

Lahens, L., Strady, E., Kieu-Le, T.-C., Dris, R., Boukerma, K., Rinnert, E., Gasperi, J., Tassin, B., 2018. Macroplastic and microplastic contamination assessment of a tropical river (Saigon River, Vietnam) transversed by a developing megacity. Environ. Pollut. 236, 661–671.

Larrose, A., Coynel, A., Schäfer, J., Blanc, G., Massé, L., Maneux, E., 2010. Assessing the current state of the Gironde Estuary by mapping priority contaminant distribution and risk potential in surface sediment. Appl. Geochemistry 25, 1912–1923.

Lebreton, L.C.M., Van Der Zwet, J., Damsteeg, J.W., Slat, B., Andrady, A., Reisser, J., 2017. River plastic emissions to the world's oceans. Nat. Commun. 8.

Lebrun, M., Van Poucke, R., Miard, F., Scippa, G.S., Bourgerie, S., Morabito, D., Tack, F.M.G., 2021. Effects of carbon-based materials and redmuds on metal(loid) immobilization and growth of Salix dasyclados Wimm. on a former mine Technosol contaminated by arsenic and lead. L. Degrad. Dev. 32.

Li, H., Wang, J., Zhao, B., Gao, M., Shi, W., Zhou, H., Xie, Z., Zhou, B., Lü, C., He, J., 2018. The role of major functional groups: Multi-evidence from the binding experiments of

heavy metals on natural fulvic acids extracted from lake sediments. Ecotoxicol. Environ. Saf. 162, 514–520.

Li, J., Ouyang, Z., Liu, P., Zhao, X., Wu, R., Zhang, C., Lin, C., Li, Y., Guo, X., 2021. Distribution and characteristics of microplastics in the basin of Chishui River in Renhuai, China. Sci. Total Environ. 773, 145591.

Li, J., Zhang, K., Zhang, H., 2018. Adsorption of antibiotics on microplastics. Environ. Pollut. 237.

Li, S., Yang, C., Peng, C., Li, H., Liu, B., Chen, C., Chen, B., Bai, J., Lin, C., 2018. Effects of elevated sulfate concentration on the mobility of arsenic in the sediment–water interface. Ecotoxicol. Environ. Saf. 154.

Li, Y., Shao, L., Wang, W., Zhang, M., Feng, X., Li, W., Zhang, D., 2020. Airborne fiber particles: Types, size and concentration observed in Beijing. Sci. Total Environ. 705, 135967.

Li, Z., Liu, X., Jin, W., Hu, Q., Zhao, Y., 2019. Adsorption behavior of arsenicals on MIL-101(Fe): The role of arsenic chemical structures. J. Colloid Interface Sci. 554.

Liao, J., Ru, X., Xie, B., Zhang, W., Wu, H., Wu, C., Wei, C., 2017. Multi-phase distribution and comprehensive ecological risk assessment of heavy metal pollutants in a river affected by acid mine drainage. Ecotoxicol. Environ. Saf. 141, 75–84.

LibreTexts, 2021. 11.5: Infrared Spectra of Some Common Functional Groups - Chemistry LibreTexts [WWW Document]. Chemistry (Easton). URL https://chem.libretexts.org/Bookshelves/Organic_Chemistry/Map%3A_Organic_Chemistry_(Wade)/11%3A_Infrared_Spectroscopy_and_Mass_Spectrometry/11.05%3A_Infrared_Spectra_of_Some_Common_Functional_Groups (accessed 11.4.21).

Lin, L., Zuo, L.Z., Peng, J.P., Cai, L.Q., Fok, L., Yan, Y., Li, H.X., Xu, X.R., 2018. Occurrence and distribution of microplastics in an urban river: A case study in the Pearl River along

Guangzhou City, China. Sci. Total Environ. 644, 375–381.

Lithner, D., Larsson, A., Dave, G., 2011. Environmental and health hazard ranking and assessment of plastic polymers based on chemical composition. Sci. Total Environ. 409.

Liu, P., Zhan, X., Wu, X., Li, J., Wang, H., Gao, S., 2020. Effect of weathering on environmental behavior of microplastics: Properties, sorption and potential risks. Chemosphere.

Liu, Y., Zhang, J., Cai, C., He, Y., Chen, L., Xiong, X., Huang, H., Tao, S., Liu, W., 2020. Occurrence and characteristics of microplastics in the Haihe River: An investigation of a seagoing river flowing through a megacity in northern China. Environ. Pollut. 262, 114261.

Liu, Y., Zhang, J., Tang, Y., He, Y., Li, Y., You, J., Breider, F., Tao, S., Liu, W., 2021. Effects of anthropogenic discharge and hydraulic deposition on the distribution and accumulation of microplastics in surface sediments of a typical seagoing river: The Haihe River. J. Hazard. Mater. 404, 124180.

Lombi, E., Holm, P.E., 2010. Metalloids, soil chemistry and the environment. Adv. Exp. Med. Biol.

Long, M., Moriceau, B., Gallinari, M., Lambert, C., Huvet, A., Raffray, J., Soudant, P., 2015. Interactions between microplastics and phytoplankton aggregates: Impact on their respective fates. Mar. Chem. 175, 39–46.

López-Luna, J., Ramírez-Montes, L. E., Martinez-Vargas, S., Martínez, A. I., Mijangos-Ricardez, O. F., González-Chávez, M. del C. A., Carrillo-González, R., Solís-Domínguez, F. A., Cuevas-Díaz, M. del C., Vázquez-Hipólito, V., 2019. Linear and nonlinear kinetic and isotherm adsorption models for arsenic removal by manganese ferrite nanoparticles. SN Applied Sciences. 1, 8.

Luo, T., Sun, J., Liu, Y., Cui, L., Fu, Q., 2019. Adsorption and transport behavior of arsenate

on saline-alkali soils of tidal flat of Yellow Sea, Eastern China. Environ. Pollut. Bioavailab. 31, 166–173.

Luo, W., Su, L., Craig, N.J., Du, F., Wu, C., Shi, H., 2018. Comparison of microplastic pollution in different water bodies from urban creeks to coastal waters. Environ. Pollut. 246, 174–182.

Luo, X., Wang, C., Luo, S., Dong, R., Tu, X., Zeng, G., 2012. Adsorption of As (III) and As (V) from water using magnetite Fe3O4-reduced graphite oxide–MnO2 nanocomposites. Chem. Eng. J. 187, 45–52.

Ma, J., Guo, H., Lei, M., Zhou, X., Li, F., Yu, T., Wei, R., Zhang, H., Zhang, X., Wu, Y., 2015. Arsenic Adsorption and its Fractions on Aquifer Sediment: Effect of pH, Arsenic Species, and Iron/Manganese Minerals. Water Air Soil Pollut. 226, 260.

Macht, F., Eusterhues, K., Pronk, G.J., Totsche, K.U., 2011. Specific surface area of clay minerals: Comparison between atomic force microscopy measurements and bulk-gas (N2) and -liquid (EGME) adsorption methods. Appl. Clay Sci. 53, 20–26.

Maity, S.K., Maiti, R., 2016. Understanding the sediment sources from mineral composition at the lower reach of Rupnarayan River, West Bengal, India – XRD-based analysis. GeoResJ 9–12.

Maji, S.K., Pal, A., Pal, T., Adak, A., 2007. Modeling and fixed bed column adsorption of As(III) on laterite soil. Sep. Purif. Technol. 56, 284–290.

Malvandi, H., 2017. Preliminary evaluation of heavy metal contamination in the Zarrin-Gol River sediments, Iran. Mar. Pollut. Bull. 117, 547–553.

Mamindy-Pajany, Y., Hurel, C., Marmier, N., Roméo, M., 2011. Arsenic (V) adsorption from aqueous solution onto goethite, hematite, magnetite and zero-valent iron: Effects of pH, concentration and reversibility. Desalination 281, 93–99.

Mani, T., Primpke, S., Lorenz, C., Gerdts, G., Burkhardt-Holm, P., 2019. Microplastic

Pollution in Benthic Midstream Sediments of the Rhine River. Environ. Sci. Technol. 53, 6053–6062.

Martin, M., Violante, A., Ajmone-Marsan, F., Barberis, E., 2014. Surface Interactions of Arsenite and Arsenate on Soil Colloids. Soil Sci. Soc. Am. J. 78, 157–170.

Masri, S., Lebrón, A.M.W., Logue, M.D., Valencia, E., Ruiz, A., Reyes, A., Wu, J., 2021. Risk assessment of soil heavy metal contamination at the census tract level in the city of Santa Ana, CA: Implications for health and environmental justice. Environ. Sci. Process. Impacts 23, 812–830.

Matouq, M., Jildeh, N., Qtaishat, M., Hindiyeh, M., Al Syouf, M.Q., 2015. The adsorption kinetics and modeling for heavy metals removal from wastewater by Moringa pods. J. Environ. Chem. Eng. 3, 775–784.

McCormick, A., Hoellein, T.J., Mason, S.A., Schluep, J., Kelly, J.J., 2014. Microplastic is an Abundant and Distinct Microbial Habitat in an Urban River. Environ. Sci. Technol. 48, 11863–11871.

Meeker, J.D., Sathyanarayana, S., Swan, S.H., 2009. Phthalates and other additives in plastics: human exposure and associated health outcomes. Philos. Trans. R. Soc. Lond. B. Biol. Sci. 364, 2097–2113.

Mihaljevcič, M., Sisr, L., Ettler, V., Šebec, O., Pruša, J., 2004. Oxidation of As-bearing gold ore - A comparison of batch and column experiments. J. Geochemical Explor. 81.

Miller, R.Z., Watts, A.J.R., Winslow, B.O., Galloway, T.S., Barrows, A.P.W., 2017. Mountains to the sea: River study of plastic and non-plastic microfiber pollution in the northeast USA. Mar. Pollut. Bull. 124, 245–251.

Mishra, A.K., Ramaprabhu, S., 2012. Ultrahigh arsenic sorption using iron oxide-graphene nanocomposite supercapacitor assembly. J. Appl. Phys. 112, 1–7.

Misra, A., Tyagi, P.K., Singh, M.K., Misra, D.S., 2006. FTIR studies of nitrogen doped carbon

nanotubes. Diam. Relat. Mater. 15, 385–388.

Mohan, D., Pittman, C.U., 2007. Arsenic removal from water/wastewater using adsorbents-A critical review. J. Hazard. Mater. 142, 1–53.

Mondal, P., Balomajumder, C., Mohanty, B., 2007. A laboratory study for the treatment of arsenic, iron, and manganese bearing ground water using Fe3+ impregnated activated carbon: Effects of shaking time, pH and temperature. J. Hazard. Mater. 144, 420–426.

Moore, C.J., Lattin, G.L., Zellers, A.F., 2011. Quantity and type of plastic debris flowing from two urban rivers to coastal waters and beaches of Southern California. Rev. Gestão Costeira Integr. 11.

Mukhopadhyay, R., Manjaiah, K.M., Datta, S.C., Yadav, R.K., Sarkar, B., 2017. Inorganically modified clay minerals: Preparation, characterization, and arsenic adsorption in contaminated water and soil. Appl. Clay Sci. 147, 1–10.

Murphy, F., Ewins, C., Carbonnier, F., Quinn, B., 2016. Wastewater Treatment Works (WwTW) as a Source of Microplastics in the Aquatic Environment. Environ. Sci. Technol. 50, 5800–5808.

Napper, I.E., Baroth, A., Barrett, A.C., Bhola, S., Chowdhury, G.W., Davies, F.R., Duncan, E.M., Kumar, S., Nelms, S.E., Niloy, N.H., Nishat, B., Maddalene, T., Thompson, R.C., Koldewey, H., 2021. Road-15 (new) 28 (old), Dhanmondi R/A, Dhaka 1209. Bangladesh Environ. Pollut. 274, 116348.

Naqash, N., Prakash, S., Dhriti Kapoor, ·, Singh, R., 2020. Interaction of freshwater microplastics with biota and heavy metals: a review. Environ. Chem. Lett. 18, 1813–1824.

Nasrabadi, T., 2015. An index approach to metallic pollution in river waters. Int. J. Environ. Res. 9.

Neidhardt, H., Kramar, U., Tang, X., Guo, H., Norra, S., 2015. Arsenic accumulation in the roots of Helianthus annuus and Zea mays by irrigation with arsenic-rich groundwater:

Insights from synchrotron X-ray fluorescence imaging. Chemie der Erde 75, 261–270.

Nel, H.A., Dalu, T., Wasserman, R.J., 2018. Sinks and sources: Assessing microplastic abundance in river sediment and deposit feeders in an Austral temperate urban river system. Sci. Total Environ. 612, 950–956.

Nematollahi, M.J., Keshavarzi, B., Moore, F., Vogt, R.D., Nasrollahzadeh Saravi, H., 2021. Trace elements in the shoreline and seabed sediments of the southern Caspian Sea: investigation of contamination level, distribution, ecological and human health risks, and elemental partition coefficient. Environ. Sci. Pollut. Res.

Nguyen, K.T., Ahmed, M.B., Mojiri, A., Huang, Y., Zhou, J.L., Li, D., 2021. Advances in As contamination and adsorption in soil for effective management. J. Environ. Manage. 296, 113274.

Nguyen, K.T., Nguyen, H.M., Truong, C.K., Ahmed, M.B., Huang, Y., Zhou, J.L., 2019. Chemical and microbiological risk assessment of urban river water quality in Vietnam. Environ. Geochem. Health 41, 2559–2575.

Nguyen, T.T.H., Zhang, W., Li, Z., Li, J., Ge, C., Liu, J., Bai, X., Feng, H., Yu, L., 2016. Assessment of heavy metal pollution in Red River surface sediments, Vietnam. Mar. Pollut. Bull. 113.

Nguyen, T. T. Q., Loganathan, P., Nguyen, T. V., Vigneswaran, S., 2020. Removing arsenic from water with an original and modified natural manganese oxide ore: batch kinetic and equilibrium adsorption studies. Environ. Sci. Pollut. Res. 27, 5.

Nizzetto, L., Bussi, G., Futter, M.N., Butterfield, D., Whitehead, P.G., 2016. A theoretical assessment of microplastic transport in river catchments and their retention by soils and river sediments. Environ. Sci. Process. Impacts 18, 1050–1059.

O'Brine, T., Thompson, R.C., 2010. Degradation of plastic carrier bags in the marine environment. Mar. Pollut. Bull. 60, 2279–2283.

Orosun, M.M., 2021. Assessment of arsenic and its associated health risks due to mining activities in parts of North-central Nigeria: Probabilistic approach using Monte Carlo. J. Hazard. Mater. 412, 125262.

Osuna-Martínez, C.C., Armienta, M.A., Bergés-Tiznado, M.E., Páez-Osuna, F., 2021. Arsenic in waters, soils, sediments, and biota from Mexico: An environmental review. Sci. Total Environ. 752, 142062.

Park, T.-J., Lee, S.-H., Lee, M.-S., Lee, J.-K., Lee, S.-H., Zoh, K.-D., 2020. Occurrence of microplastics in the Han River and riverine fish in South Korea. Sci. Total Environ. 708, 134535.

Patel, K.S., Shrivas, K., Brandt, R., Jakubowski, N., Corns, W., Hoffmann, P., 2005. Arsenic contamination in water, soil, sediment and rice of central India. Environ. Geochem. Health 27. https://doi.org/10.1007/s10653-005-0120-9

Peng, G., Xu, P., Zhu, B., Bai, M., Li, D., 2018. Microplastics in freshwater river sediments in Shanghai, China: A case study of risk assessment in mega-cities. Environ. Pollut. 234, 448–456.

Phuong, N.N., Zalouk-Vergnoux, A., Poirier, L., Kamari, A., Châtel, A., Mouneyrac, C., Lagarde, F., 2016. Is there any consistency between the microplastics found in the field and those used in laboratory experiments? Environ. Pollut. 211, 111–123.

Plant, J., Kinniburg, D., Smedley, Fordyce, F., Klinck, B., 2005. Arsenic and Selenium, in: British Geological Survey.

Plazinski, W., Rudzinski, W., Plazinska, A., 2009. Theoretical models of sorption kinetics including a surface reaction mechanism: A review. Adv. Colloid Interface Sci. 152, 1–2.

Plasctic Europe, 2020. Plastics – the Facts 2020. PlasticEurope 1–64.

Polizzotto, M.L., Kocar, B.D., Benner, S.G., Sampson, M., Fendorf, S., 2008. Near-surface wetland sediments as a source of arsenic release to ground water in Asia. Nature 454.

Postma, D., Jessen, S., Hue, N.T.M., Duc, M.T., Koch, C.B., Viet, P.H., Nhan, P.Q., Larsen, F., 2010. Mobilization of arsenic and iron from Red River floodplain sediments, Vietnam. Geochim. Cosmochim. Acta 74.

Qiu, G., Gao, T., Hong, J., Luo, Y., Liu, L., Tan, W., Liu, F., 2018. Mechanisms of interaction between arsenian pyrite and aqueous arsenite under anoxic and oxic conditions. Geochim. Cosmochim. Acta 228, 205–219.

Rao, Z., Niu, S., Zhan, N., Wang, X., Song, · Xiaolong, 2020. Microplastics in Sediments of River Yongfeng from Maanshan City, Anhui Province, China. Bull. Environ. Contam. Toxicol. 104, 166–172.

Rapant, S., Dietzová, Z., Cicmanová, S., 2006. Environmental and health risk assessment in abandoned mining area, Zlata Idka, Slovakia. Environ. Geol. 51, 387–397.

Ravenscroft, P., Brammer, H., Richards, K., 2009. Arsenic Pollution: A Global Synthesis, Arsenic Pollution: A Global Synthesis.

Rawat, A.P., Kumar, V., Singh, P., Shukla, A.C., Singh, D.P., 2021. Soil and Sediment Contamination: An International Journal ISSN: (Print) (Online) Journal homepage: https://www.tandfonline.com/loi/bssc20 Kinetic Behavior and Mechanism of Arsenate Adsorption by Loam and Sandy Loam Soil Kinetic Behavior and Mechanism of Arsenate Adsorption by Loam and Sandy Loam Soil. Soil Sediment Contam. An Int. J.

Reid, M.S., Hoy, K.S., Schofield, J.R.M., Uppal, J.S., Lin, Y., Lu, X., Peng, H., Le, X.C., 2020. Arsenic speciation analysis: A review with an emphasis on chromatographic separations. TrAC - Trends Anal. Chem. 123.

Rezaei, H., Mehrabi, B., Khanmirzaee, A., Shahbazi, K., 2019. Arsenic heavy metal mapping in agricultural soils of Alborz province, Iran. Int. J. Environ. Anal. Chem. 101, 127–139.

Ritchie, V.J., Ilgen, A.G., Mueller, S.H., Trainor, T.P., Goldfarb, R.J., 2013. Mobility and chemical fate of antimony and arsenic in historic mining environments of the Kantishna

Hills district, Denali National Park and Preserve, Alaska. Chem. Geol. 335, 172–188.

Rodrigues, M.O., Abrantes, N., Gonçalves, F.J.M., Nogueira, H., Marques, J.C., Gonçalves, A.M.M., 2018. Spatial and temporal distribution of microplastics in water and sediments of a freshwater system (Antuã River, Portugal). Sci. Total Environ. 633, 1549–1559.

Rowley, K.H., Cucknell, A.-C., Smith, B.D., Clark, P.F., Morritt, D., 2020. London's river of plastic: High levels of microplastics in the Thames water column. Sci. Total Environ.

Sankoda, K., Yamada, Y., 2021. Occurrence, distribution, and possible sources of microplastics in the surface river water in the Arakawa River watershed. Environ. Sci. Pollut. Res. 28, 27474–27480.

Sarkar, D.J., Das Sarkar, S., Das, B.K., Manna, R.K., Behera, B.K., Samanta, S., 2019. Spatial distribution of meso and microplastics in the sediments of river Ganga at eastern India. Sci. Total Environ. 694, 1–7.

Scherer, C., Weber, A., Stock, F., Vurusic, S., Egerci, H., Kochleus, C., Arendt, N., Foeldi, C., Dierkes, G., Wagner, M., Brennholt, N., Reifferscheid, G., 2020. Comparative assessment of microplastics in water and sediment of a large European river. Sci. Total Environ. 738, 139866.

Scircle, A., Cizdziel, J. V., Missling, K., Li, L., Vianello, A., 2020. Single-Pot Method for the Collection and Preparation of Natural Water for Microplastic Analyses: Microplastics in the Mississippi River System during and after Historic Flooding. Environ. Toxicol. Chem. 39.

Selim, H.M., 2013. Competitive sorption and transport of heavy metals in soils and geological media, Competitive Sorption and Transport of Heavy Metals in Soils and Geological Media.

Sharma, P., Kappler, A., 2011. Desorption of arsenic from clay and humic acid-coated clay by dissolved phosphate and silicate. J. Contam. Hydrol. 126, 216–225.

Shen, M., Song, B., Zeng, G., Zhang, Y., Teng, F., Zhou, C., 2021. Surfactant changes lead adsorption behaviors and mechanisms on microplastics. Chem. Eng. J. 405, 126989.

SIMEC, 2021. Monthly Water Record. SIMEC. URL http://www.simec.com/media/7195/monthly-water_sept-2021.pdf (accessed 10.28.21).

Simon-Sánchez, L., Grelaud, M., Garcia-Orellana, J., Ziveri, P., 2019. River Deltas as hotspots of microplastic accumulation: The case study of the Ebro River (NW Mediterranean). Sci. Total Environ. 687, 1186–1196.

Simpson, B.S.L., Batley, G.E., Chariton, A. a, Stauber, J.L., King, C.K., Chapman, J.C., Hyne, R. V, Gale, S. a, Roach, A.C., Maher, W. a, Simpson, S.L., 2005. Handbook for Sediment Quality Assessment Quality Assessment. Design.

Singh, K.P., Mohan, D., Singh, V.K., Malik, A., 2005. Studies on distribution and fractionation of heavy metals in Gomti river sediments - A tributary of the Ganges, India. J. Hydrol. 312, 14–27.

Singh, R., Singh, S., Parihar, P., Singh, V.P., Prasad, S.M., 2015. Arsenic contamination, consequences and remediation techniques: A review. Ecotoxicol. Environ. Saf.

Smedley, P.L., Kinniburgh, D.G., 2002. A review of the source, behaviour and distribution of arsenic in natural waters. Appl. Geochemistry.

Smith, E., Naidu, R., Alston, A.M., 2002. Chemistry of Inorganic Arsenic in Soils. J. Environ. Qual. 31, 557–563.

Smith, E., Naidu, R., Alston, A.M., 1998. Arsenic in the Soil Environment: A Review, in: Advances in Agronomy.

Smith, E., Smith, J., Naidu, R., 2006. Distribution and nature of arsenic along former railway corridors of South Australia. Sci. Total Environ. 363, 175–182.

Sosa, N.N., Kulkarni, H. V., Datta, S., Beilinson, E., Porfido, C., Spagnuolo, M., Zárate, M.A., Surber, J., 2019. Occurrence and distribution of high arsenic in sediments and

groundwater of the Claromecó fluvial basin, southern Pampean plain (Argentina). Sci. Total Environ. 695.

Stafilov, T., Šajn, R., Pančevski, Z., Boev, B., Frontasyeva, M. V., Strelkova, L.P., 2010. Heavy metal contamination of topsoils around a lead and zinc smelter in the Republic of Macedonia. J. Hazard. Mater. 175.

Stollenwerk, K.G., 2005. Geochemical Processes Controlling Transport of Arsenic in Groundwater: A Review of Adsorption. Arsen. Gr. Water 67–100.

Štrbac, S., Kašanin Grubin, M., Vasić, N., 2017. Importance of background values in assessing the impact of heavy metals in river ecosystems: Case study of Tisza River, Serbia. Environ. Geochem. Health 40.

Sun, T., Zhao, Z., Liang, Z., Liu, J., Shi, W., Cui, F., 2018. Efficient degradation of p-arsanilic acid with arsenic adsorption by magnetic CuO-Fe3O4 nanoparticles under visible light irradiation. Chem. Eng. J. 334, 1527–1536.

Sun, W., Sierra-Alvarez, R., Milner, L., Oremland, R., Field, J.A., 2009. Arsenite and ferrous iron oxidation linked to chemolithotrophic denitrification for the immobilization of arsenic in anoxic environments. Environ. Sci. Technol. 43, 6585–6591.

Szopka, K., Gruss, I., Gruszka, D., Karczewska, A., Gediga, K., Gałka, B., Dradrach, A., 2021. The effects of forest litter and waterlogging on the ecotoxicity of soils strongly enriched in arsenic in a historical mining site. Forests 12, 7–11.

Tahira, S., Khan, S., Samrana, S., Shahi, L., Ali, I., Murad, W., Rehman, Z. ur, Azizullah, A., 2019. Bio-assessment and remediation of arsenic (arsenite As-III) in water by Euglena gracilis. J. Appl. Phycol. 31.

Tang, L., Feng, H., Tang, J., Zeng, G., Deng, Y., Wang, J., Liu, Y., Zhou, Y., 2017. Treatment of arsenic in acid wastewater and river sediment by Fe@Fe2O3 nanobunches: The effect of environmental conditions and reaction mechanism. Water Res. 117, 175–186.

Tapia, J., Murray, J., Ormachea, M., Tirado, N., Nordstrom, D.K., 2019. Origin, distribution, and geochemistry of arsenic in the Altiplano-Puna plateau of Argentina, Bolivia, Chile, and Perú. Sci. Total Environ. 678, 309–325.

Thompson, R.C., Moore, C.J., vom Saal, F.S., Swan, S.H., 2009. Plastics, the environment and human health: current consensus and future trends. Philos. Trans. R. Soc. Lond. B. Biol. Sci. 364, 2153–2166.

Thuong, N.T., Yoneda, M., Ikegami, M., Takakura, M., 2013. Source discrimination of heavy metals in sediment and water of to Lich River in Hanoi City using multivariate statistical approaches. Environ. Monit. Assess. 185.

Tien, C.-J., Wang, Z.-X., Chen, C.S., 2020. Microplastics in water, sediment and fish from the Fengshan River system: Relationship to aquatic factors and accumulation of polycyclic aromatic hydrocarbons by fish. Environ. Pollut. 265, 114962.

Tseng, J.Y., Chang, C.Y., Chang, C.F., Chen, Y.H., Chang, C.C., Ji, D.R., Chiu, C.Y., Chiang, P.C., 2009. Kinetics and equilibrium of desorption removal of copper from magnetic polymer adsorbent. J. Hazard. Mater. 171. https://doi.org/10.1016/j.jhazmat.2009.06.030

Ungureanu, G., Santos, S., Boaventura, R., Botelho, C., 2015. Arsenic and antimony in water and wastewater: Overview of removal techniques with special reference to latest advances in adsorption. J. Environ. Manage. 151, 326–342.

Varol, M., Şen, B., 2012. Assessment of nutrient and heavy metal contamination in surface water and sediments of the upper Tigris River, Turkey. Catena 92, 1–10.

Varsányi, I., Kovács, L.Ó., 2006. Arsenic, iron and organic matter in sediments and groundwater in the Pannonian Basin, Hungary. Appl. Geochemistry 21, 949–963.

Vedolin, M.C., Teophilo, C.Y.S., Turra, A., Figueira, R.C.L., 2018. Spatial variability in the concentrations of metals in beached microplastics. Mar. Pollut. Bull. 129

Violante, A., Pigna, M., 2002. Competitive Sorption of Arsenate and Phosphate on Different

Clay Minerals and Soils. Soil Sci. Soc. Am. J. 66, 1788–1796.

Wagner, M., Scherer, C., Alvarez-Muñoz, D., Brennholt, N., Bourrain, X., Buchinger, S., Fries, E., Grosbois, C., Klasmeier, J., Marti, T., Rodriguez-Mozaz, S., Urbatzka, R., Vethaak, A.D., Winther-Nielsen, M., Reifferscheid, G., 2014. Microplastics in freshwater ecosystems: what we know and what we need to know. Environ. Sci. Eur. 26, 12.

Wang, F., Shih, K.M., Li, X.Y., 2015. The partition behavior of perfluorooctanesulfonate (PFOS) and perfluorooctanesulfonamide (FOSA) on microplastics. Chemosphere 119.

Wang, G., Lu, J., Li, W., Ning, J., Zhou, L., Tong, Y., Liu, Z., Zhou, H., Xiayihazi, N., 2021. Seasonal variation and risk assessment of microplastics in surface water of the Manas River Basin, China. Ecotoxicol. Environ. Saf. 208, 111477.

Wang, G., Lu, J., Tong, Y., Liu, Z., Zhou, H., Xiayihazi, N., 2020. Occurrence and pollution characteristics of microplastics in surface water of the Manas River Basin, China. Sci. Total Environ. 710, 136099.

Wang, H. bo, Xu, J. ming, Gomez, M.A., Shi, Z. liang, Li, S. feng, Zang, S. yan, 2019. Arsenic concentration, speciation, and risk assessment in sediments of the Xijiang River basin, China. Environ. Monit. Assess. 191.

Wang, J., Peng, J., Tan, Z., Gao, Y., Zhan, Z., Chen, Q., Cai, L., 2017. Microplastics in the surface sediments from the Beijiang River littoral zone: Composition, abundance, surface textures and interaction with heavy metals m-FTIR. Chemposphere 171, 248–258.

Wang, J., Xu, J., Xia, J., Wu, F., Zhang, Y., 2018. A kinetic study of concurrent arsenic adsorption and phosphorus release during sediment resuspension. Chem. Geol. 495, 67–75.

Wang, S., Mulligan, C.N., 2006a. Effect of natural organic matter on arsenic release from soils and sediments into groundwater. Environ. Geochem. Health 28, 197–214.

Wang, S., Mulligan, C.N., 2006b. Natural attenuation processes for remediation of arsenic

contaminated soils and groundwater. J. Hazard. Mater. 138, 459–470.

Wang, Y., Wang, X., Li, Y., Li, J., Wang, F., Xia, S., Zhao, J., 2020. Biofilm alters tetracycline and copper adsorption behaviors onto polyethylene microplastics. Chem. Eng. J. 392, 123808.

Welch, A.H., Stollenwerk, K.G., 2003. Arsenic in ground water: geochemistry and occurrence. Springer Science & Business Media.

Wen, X., Du, C., Xu, P., Zeng, G., Huang, D., Yin, L., Yin, Q., Hu, L., Wan, J., Zhang, J., Tan, S., Deng, R., 2018. Microplastic pollution in surface sediments of urban water areas in Changsha, China: Abundance, composition, surface textures. Mar. Pollut. Bull. 136, 414–423.

Wenzel, W.W., Brandstetter, A., Wutte, H., Lombi, E., Prohaska, T., Stingeder, G., Adriano, D.C., 2002. Arsenic in field-collected soil solutions and extracts of contaminated soils and its implication to soil standards. J. Plant Nutr. Soil Sci. 165, 221–228.

Williams, L.E., Barnett, M.O., Kramer, T.A., Melville, J.G., 2003. Adsorption and Transport of Arsenic(V) in Experimental Subsurface Systems. J. Environ. Qual. 32, 841–850.

Wilson, N.J., Craw, D., Hunter, K., 2004. Antimony distribution and environmental mobility at an historic antimony smelter site, New Zealand. Environ. Pollut. 129, 257–266.

Wilson, S.C., Lockwood, P. V., Ashley, P.M., Tighe, M., 2010. The chemistry and behaviour of antimony in the soil environment with comparisons to arsenic: A critical review. Environ. Pollut. 158, 1169–1181.

Woitke, P., Wellmitz, J., Helm, D., Kube, P., Lepom, P., Litheraty, P., 2003. Analysis and assessment of heavy metal pollution in suspended solids and sediments of the river Danube. Chemosphere 51, 633–642.

Wong, G., Owemark, L.L.€, Kunz, A., 2020. Microplastic pollution of the Tamsui River and its tributaries in northern Taiwan: Spatial heterogeneity and correlation with precipitation

*. Environ. Pollut. 260, 113935.

Wu, P., Tang, Y., Dang, M., Wang, S., Jin, H., Liu, Y., Jing, H., Zheng, C., Yi, S., Cai, Z., 2020. Spatial-temporal distribution of microplastics in surface water and sediments of Maozhou River within Guangdong-Hong Kong-Macao Greater Bay Area. Sci. Total Environ. 717, 135187.

Xie, Y., Lu, G., Yang, C., Qu, L., Chen, M., Guo, C., Dang, Z., 2018a. Mineralogical characteristics of sediments and heavy metal mobilization along a river watershed affected by acid mine drainage. PLoS One 13, 1–17.

Xie, Z., Wang, J., Wei, X., Li, F., Chen, M., Wang, J., Gao, B., 2018b. Interactions between arsenic adsorption/desorption and indigenous bacterial activity in shallow high arsenic aquifer sediments from the Jianghan Plain, Central China. Sci. Total Environ. 644, 382–388.

Xie, Z., Zhou, Y., Wang, Y., Luo, Y., Sun, X., 2013. Influence of Arsenate on Lipid Peroxidation Levels and Antioxidant Enzyme Activities in Bacillus cereus Strain XZM002 Isolated from High Arsenic Aquifer Sediments. Geomicrobiol. J. 30, 645–652.

Xu, Q., Xing, R., Sun, M., Gao, Y., An, L., 2020. Microplastics in sediments from an interconnected river-estuary region. Sci. Total Environ. 729, 139025.

Xu, R., WangG, Y., Tiwari, D., Wang, H., 2009. Effect of ionic strength on adsorption of As(III) and As(V) on variable charge soils. J. Environ. Sci. 21, 927–932.

Yang, J.K., Barnett, M.O., Jardine, P.M., Basta, N.T., Casteel, S.W., 2002. Adsorption, sequestration, and bioaccessibility of As(V) in soils. Environ. Sci. Technol. 36, 4562–4569.

Yang, L., Dadwhal, M., Shahrivari, Z., Ostwal, M., Liu, P.K.T., Sahimi, M., Tsotsis, T.T., 2006. Adsorption of arsenic on layered double hydroxides: Effect of the particle size. Ind. Eng. Chem. Res. 45, 4742–4751.

Yang, Z., Wang, Y., Shen, Z., Niu, J., Tang, Z., 2009. Distribution and speciation of heavy metals in sediments from the mainstream, tributaries, and lakes of the Yangtze River catchment of Wuhan, China. J. Hazard. Mater. 166, 1186–1194.

Yean, S., Cong, L., Yavuz, C.T., Mayo, J.T., Yu, W.W., Kan, A.T., Colvin, V.L., Tomson, M.B., 2005. Effect of magnetite particle size on adsorption and desorption of arsenite and arsenate. J. Mater. Res. 20, 3255–3264.

Yin, Z., Lützenkirchen, J., Finck, N., Celaries, N., Dardenne, K., Hansen, H.C.B., 2019. Adsorption of arsenic(V) onto single sheet iron oxide: X-ray absorption fine structure and surface complexation. J. Colloid Interface Sci. 554, 433–443.

Yohai, L., Giraldo, H., Mejía, M., Procaccini, R., Pellice, S., Laxman Kunjali, K., Dutta, J., Uheida, A., 2019. Nanocomposite functionalized membranes based on silica nanoparticles cross-linked to electrospun nanofibrous support for arsenic(V) adsorption from contaminated underground water †. RSC Adv. 9, 8280–8289.

Yolcubal, I., Akyol, N.H., 2008. Adsorption and transport of arsenate in carbonate-rich soils: Coupled effects of nonlinear and rate-limited sorption. Chemosphere 73, 1300–1307.

Yu, Z., Zhou, L., Huang, Y., Song, Z., Qiu, W., 2015. Effects of a manganese oxide-modified biochar composite on adsorption of arsenic in red soil. J. Environ. Manage. 163, 155–162.

Zeng, X., Wu, P., Su, S., Bai, L., Feng, Q., 2012. Phosphate has a differential influence on arsenate adsorption by soils with different properties. Plant, Soil Environ. 58, 405–411.

Zhang, H., Selim, H.M., 2005. Kinetics of arsenate adsorption - desorption in soils. Environ. Sci. Technol. 39, 6101–6108.

Zhang, H.H., Yuan, H.X., Hu, Y.G., Wu, Z.F., Zhu, L.A., Zhu, L., Li, F.B., LI, D.Q., 2006. Spatial distribution and vertical variation of arsenic in Guangdong soil profiles, China. Environ. Pollut. 144, 492–499.

Zhang, K., Gong, W., Lv, J., Xiong, X., Wu, C., 2015. Accumulation of floating microplastics

behind the Three Gorges Dam. Environ. Pollut. 204, 117–123.

Zhang, W., Singh, P., Paling, E., Delides, S., 2004. Arsenic removal from contaminated water by natural iron ores. Miner. Eng. 17, 517–524.

Zhang, W., Zhang, L., Hua, T., Li, Y., Zhou, X., Wang, W., You, Z., Wang, H., Li, M., 2020. The mechanism for adsorption of Cr(VI) ions by PE microplastics in ternary system of natural water environment. Environ. Pollut. 257, 113440.

Zhang, X., Leng, Y., Liu, X., Huang, K., Wang, Jun, 2020. Microplastics' Pollution and Risk Assessment in an Urban River: A Case Study in the Yongjiang River, Nanning City, South China. Expo. Heal. 12, 141–151.

Zhou, G., Wang, Q., Zhang, J., Li, Q., Wang, Y., Wang, M., Huang, X., 2020. Distribution and characteristics of microplastics in urban waters of seven cities in the Tuojiang River basin, China. Environ. Res. 189, 109893.

Zhou, J., Broodbank, N., 2014. Sediment-water interactions of pharmaceutical residues in the river environment. Water Res. 48, 61–70.

Zong, X., Zhang, J., Zhu, J., Zhang, L., Jiang, L., Yin, Y., Guo, H., 2021. Effects of polystyrene microplastic on uptake and toxicity of copper and cadmium in hydroponic wheat seedlings (Triticum aestivum L.). Ecotoxicol. Environ. Saf. 217, 112217.